MODIFICATION OF ETHYLENE VINYL ACETATE COPOLYMER FILM FOR SELECTIVE CO_2 PERMEATION FROM BIOGAS

A THESIS SUBMITTED IN PARTIAL FULFILLMENT OF THE REQUIREMENT FOR THE DEGREE OF MASTER OF SCIENCE IN POLYMER TECHNOLOGY
DEPARTMENT OF CHEMISTRY FACULTY OF SCIENCE
KING MONGKUT'S INSTITUTE OF TECHNOLOGY LADKRABANG
2020
KMITL-2020-SC-M-014-020

MODIFICATION OF ETHYLENE VINYL ACETATE COPOLYMER FILM FOR SELECTIVE CO_2 PERMEATION FROM BIOGAS

PATCHNAKAN WISATSUVAN

A THESIS SUBMITTED IN PARTIAL FULFILLMENT OF THE REQUIREMENT FOR THE DEGREE OF MASTER OF SCIENCE IN POLYMER TECHNOLOGY
DEPARTMENT OF CHEMISTRY FACULTY OF SCIENCE
KING MONGKUT'S INSTITUTE OF TECHNOLOGY LADKRABANG
2020

KMITL-2020-SC-M-014-020

หัวข้อวิทยานิพนธ์	การปรับปรุงฟิล์มโคพอลิเมอร์พอลิเอทิลีน-ไวนิลอะซีเทตเพื่อคัดสรรการซึมผ่านของก๊าซคาร์บอนไดออกไซด์จากก๊าซชีวภาพ
ชื่อนักศึกษา	นางสาวพัชญ์ณกัญญ์ วิเศษสุวรรณ
รหัสประจำตัว	60605056
ปริญญา	วิทยาศาสตรมหาบัณฑิต (เทคโนโลยีพอลิเมอร์)
ภาควิชา	เคมี
พ.ศ.	2563
อาจารย์ที่ปรึกษาวิทยานิพนธ์	ผศ.ดร.ชลลดา ฤตวิรุฬห์
อาจารย์ที่ปรึกษาวิทยานิพนธ์ร่วม	ศ.ดร.ตะวัน สุขน้อย ผศ.ดร.สุภารัตน์ รักชลธี

บทคัดย่อ

งานวิจัยนี้พัฒนาเมมเบรนพอลิเมอร์ผสมจากเอทิลีนไวนิลอะซีเทตโคพอลิเมอร์ที่ถูกไฮโดรไลซิสบางส่วน (p-EVA) กับพอลิเอทิลีนไกลคอล (PEG) และใช้ซิลิกาที่ถูกดัดแปรพื้นผิวด้วยหมู่เอมีน (AFS) ร่วมด้วย เพื่อปรับปรุงสมบัติการเลือกผ่านของก๊าซคาร์บอนไดออกไซด์ต่อก๊าซมีเทน โดยปัจจัยที่ศึกษาในการซึมผ่านก๊าซคาร์บอนไดออกไซด์ ประกอบด้วยการไฮโดรไลซิส EVA ปริมาณการเติมและน้ำหนักโมเลกุลของ PEG และปริมาณการเติม AFS ซึ่ง AFS คือซิลิกาที่มีการปรับปรุงพื้นผิวให้เกิดหมู่เอมีน โดยใช้ 3-อะมิโนโพรพิลไตรเอทอกซีไซเลน (APTES) โดยจากการตรวจสอบพบว่ามีหมู่เอมีนอยู่ 64% ที่สามารถเกิดอันตรกิริยากับโมเลกุลคาร์บอนไดออกไซด์ จากปฏิกิริยาไฮโดรไลซิสพบว่า EVA ถูกไฮโดรไลซ์ 44% ทำให้เมมเบรน p-EVA มีค่าความแข็งแรงดึงและมอดุลัสของยังสูงกว่าเมมเบรน EVA แต่มีค่าการซึมผ่านของก๊าซคาร์บอนไดออกไซด์ต่ำกว่า เนื่องจากพันธะไฮโดรเจนระหว่างโมเลกุลใน p-EVA นอกจากนี้เมื่อผสม p-EVA กับ PEG (ปริมาณ 5-15%wt) พบว่าค่าอุณหภูมิเปลี่ยนสถานะคล้ายแก้ว (T_g) ของ p-EVA และค่าความแข็งแรงดึงของเมมเบรนลดลง เนื่องจาก PEG ทำหน้าที่เป็นพลาสติไซเซอร์ แต่ในทางตรงกันข้ามอุณหภูมิหลอมเหลวและปริมาณผลึกของ p-EVA ไม่มีการเปลี่ยนแปลงอย่างมีนัยสำคัญ แสดงว่า PEG ไม่ได้รบกวนวัฏภาคผลึกของ p-EVA สำหรับการศึกษาลักษณะทางสัณฐานวิทยา พบว่าพื้นที่ตัดขวางของเมมเบรนพอลิเมอร์ผสม p-EVA/PEG เกิดช่องว่างขนาดเล็กกระจายตัวอยู่ทั่วเนื้อเมมเบรน โดยช่องว่างจะมีขนาดใหญ่ขึ้นเมื่อเพิ่มปริมาณ PEG นอกจากนี้ยังพบว่าเมมเบรนผสม p-EVA/PEG นั้นมีค่าการซึมผ่านก๊าซคาร์บอนไดออกไซด์สูงกว่าเมมเบรน p-EVA และ EVA เนื่องจากการเกิดอันตรกิริยาระหว่างหมู่อีเทอร์และโมเลกุลคาร์บอนไดออกไซด์ โดยพบว่าเมมเบรนพอลิเมอร์ผสม PEG ที่น้ำหนักโมเลกุล 1450 g/mol ให้ค่าการซึมผ่านของก๊าซคาร์บอนไดออกไซด์สูงกว่าเมมเบรนพอลิเมอร์ผสม PEG ที่น้ำหนักโมเลกุล 400 g/mol เนื่องจากมีปริมาณหมู่อีเทอร์ที่มากกว่า อย่างไรก็ตามพบว่าการเพิ่มปริมาณ PEG ส่งผลให้ค่าการเลือกผ่านของก๊าซคาร์บอนไดออกไซด์ต่อก๊าซมีเทน (CO_2/CH_4 selectivity) ลดลง ดังนั้น AFS (0.3-0.9 %wt) จึงถูกเติมลงในพอลิเมอร์ผสม p-EVA/PEG ที่ปริมาณ PEG 15%wt (p-EVA/15PEG400 และ p-EVA/15PEG1450) โดยพบว่าเมมเบรนที่เติม AFS มีค่าการเลือกผ่านก๊าซ

คาร์บอนไดออกไซด์ต่อก๊าซมีเทนสูงขึ้นอย่างเห็นได้ชัด และค่าการซึมผ่านก๊าซคาร์บอนไดออกไซด์เพิ่มสูงขึ้น เมื่อเติม AFS ในปริมาณ 0.3-0.6%wt ในเมมเบรนพอลิเมอร์ผสม p-EVA/15PEG400 และมีค่าลดลง เมื่อเติม AFS 0.9%wt ในเมมเบรนดังกล่าว ส่วนการใช้ AFS 0.3-0.9%wt ในเมมเบรน p-EVA/15PEG1450 มีค่าการซึมผ่านก๊าซคาร์บอนไดออกไซด์ลดลงเช่นกัน เนื่องจากการรวมตัวกันเป็นกลุ่มก้อนของอนุภาค AFS ในเนื้อพอลิเมอร์นั้นไปขัดขวางการซึมผ่านของก๊าซ ดังนั้นเมมเบรนพอลิเมอร์ผสม p-EVA/15PEG400-0.6AFS จึงเป็นสูตรที่เหมาะสมที่สุดสำหรับการแยกก๊าซคาร์บอนไดออกไซด์จากมีเทน โดยให้ค่าการซึมผ่านก๊าซคาร์บอนไดออกไซด์และค่าการเลือกผ่านก๊าซคาร์บอนไดออกไซด์ต่อก๊าซมีเทนถึง 1402.34 g/m^2·day และ 22.31 ตามลำดับ

คำสำคัญ : ก๊าซชีวภาพ การแยกก๊าซคาร์บอนไดออกไซด์จากมีเทน พอลิเมอร์ผสม พอลิเอทิลีนไกล-คอล เอทิลีนไวนิลอะซีเทตโคพอลิเมอร์ 3-อะมิโนโพรพิลไตรเอท็อกซีไซเลน

Thesis Title	Modification of ethylene vinyl acetate copolymer film for selective CO_2 permeation from biogas
Student Name	Miss Patchnakan Wisatsuvan
Student ID	60605056
Degree	Master of Science (Polymer Technology)
Department	Chemistry
Year	2020
Thesis Advisor	Asst.Prof.Dr. Chonlada Ritvirulh
Thesis Co-advisors	Prof.Dr. Tawan Sooknoi
	Asst.Prof.Dr. Suparat Rukchonlatee

Abstract

In this research, polymer blend membranes of partially hydrolyzed ethylene vinyl acetate copolymer (p-EVA)/polyethylene glycol (PEG) with amine-modified SiO_2 were developed to improve the CO_2/CH_4 selectivity from biogas. The variants for CO_2 permeability were investigated, including hydrolysis of EVA, PEG molecular weight and loading (5-15%wt) and surface-modified SiO_2 content (0.3-0.9%wt). 3-aminopropyl triethoxy silane (APTES) was employed to modify on the SiO_2 surface in order to generate the interaction between amino groups and CO_2 molecules, and following the modification 64% active amine sites were detected on SiO_2 surface. It was found that EVA was partially hydrolyzed at about 44%, and called as p-EVA. p-EVA membrane possessed greater tensile strength and Young's modulus but lower CO_2 permeation rate than EVA, because of the intermolecular hydrogen bond in p-EVA. In addition, when 5-15%wt PEG was blended with p-EVA, T_g of p-EVA was decreased simultaneously with tensile strength owing to the plasticizer effect of PEG, whereas T_m and X_c were insignificantly changed, implying that PEG could not interfere the crystalline phase of p-EVA. For morphological study, there were some cavities in the cross-sectional area of p-EVA/PEG blend membrane. Besides, the size of cavities was larger with higher amount of PEG loadings. The CO_2 permeation of p-EVA/PEG blended membranes was higher than that of p-EVA and EVA due to strong interaction between ether groups and CO_2 molecules. Moreover, the CO_2 permeation of p-EVA/PEG1450 was greater than that of p-EVA/PEG400 because of the higher ether oxygen concentration in PEG with 1450 g/mol. Furthermore, the CO_2/CH_4 selectivity was decreased with increasing amount of PEG. Therefore, the amino-functionalized SiO_2 (AFS) (0.3-0.9%wt) was added into the membrane with 15%PEG using PEG with M_w of 400 g/mol (p-EVA/15PEG400),

and PEG with M_w of 1450 g/mol (p-EVA/15 PEG1450). It was revealed that the CO_2/CH_4 selectivity was obviously improved with AFS addition. Additionally, it was presented that CO_2 permeation was increased in p-EVA/15PEG400 with 0.3-0.6%wt of AFS. However, p-EVA/15PEG400 at 0.9%wt of AFS and p-EVA/15PEG1450 using 0.3-0.9%wt of AFS lowered CO_2 permeation due to agglomeration of AFS particles in matrix phase. Accordingly, the optimum formula for CO_2 separation is p-EVA/15PEG400 at 0.6%wt of AFS with CO_2 permeability 1402.34 g/m^2·day and 22.31 of CO_2/CH_4 selectivity.

Keywords : Biogas, CO_2/CH_4 separation, Polymer blend, PEG, EVA, APTES

Acknowledgements

The author would like to express my profound gratitude to my advisors, Asst.Prof.Dr. Chonlada Ritvirulh, Prof.Dr. Tawan Sooknoi and Asst.Prof.Dr. Suparat Rukchonlatee for their supervision, helpful suggestions, and encouragement throughout this thesis.

The author is also grateful to Assoc.Prof.Dr. Kalyanee Sirisinha and Assoc.Prof.Dr. Jutarat Prachayawarakorn for serving as the chairperson and the committee, respectively.

Many thanks go to Mr. Nattapong makmeesub and Mr. Prachya Watasit for experimental guidance, and I am gratefully indebted to them for very valuable comments on this thesis.

The author would like to be thankful for all my teachers and friends for their advices, support and encouragement through the process of researching and writing this thesis.

The author would like to extend this cordial appreciation to KEM KOTE Co., Ltd. for donating the chemical substance (PEG).

The author would like to genuinely appreciate to the Faculty of Science, KMITL for Tuition fee scholarship.

Sincere thanks to the Department of Chemistry, Faculty of Science, King Mongkut's Institute of Technology Ladkrabang (KMITL) to support the equipment, chemicals and facilities.

Scholarship from KMITL for participation and presentation in the International Polymer Conference of Thailand 2019 (PCT-9) is also acknowledged.

Finally, the author would like to give special thanks to my parents for providing me with unfailing support and continuous encouragement throughout my years of study in this thesis. This accomplishment would not have been possible without them.

Miss Patchnakan Wisatsuvan

Table of contents

Table of contents (Continued)

Table of contents (Continued)

List of tables

List of figures

List of figures (Continued)

List of figures (Continued)

List of figures (Continued)

Abbreviations

α	Selectivity
A_{CO2}	Peak area of permeated CO_2
A_{CH4}	Peak area of permeated CH_4
A_S	Peak area of standard CO_2
ABS	Acrylonitrile butadiene styrene
AFS	Amine-functionalized silica
APTES	3-aminopropyltriethoxysilane
ATR	Attenuated total reflection
C.I.	Carbonyl index
DMF	N,N-Dimethylformamide
DP	Dopamine
DSC	Differential scanning calorimetry
EVA	Ethylene vinyl acetate copolymer
EVOH	Ethylene vinyl alcohol
F_f	Flow rate of feed gas
FFV	Fraction free volume
FTIR	Fourier-transform infrared spectroscopy
GO	Graphene oxide
J	Transmission rate of CO_2
M_w	Molecular weight
MMM	Mixed-matrix membrane
P	Permeability, Pressure
p-EVA	Partially hydrolyzed EVA
PEBA	Polyether block amide
PEI	Polyethyleneimine
PEG	Polyethylene glycol
POSS	Polyoctahedral oligomeric silsesquioxanes
PP	Polypropylene
PVC	Poly (vinyl chloride)
Q	Transmission rate of CH_4
R	Ideal gas constant
S_C	Size of permeation cell
SEM	Scanning electron microscope
T_c	Crystallization temperature
T_g	Glass transition temperature
T_m	Melting temperature

Abbreviations (Continued)

TCD	Thermal conductivity detector
UTM	Universal testing machine
VAM	Vinyl acetate monomer
WVP	Water vapor permeability
ZIF	Zeolitic imidazolate framework

Chapter 1
Introduction

1.1 Research motivation

Nowadays, most of the energy around the world comes from burning oil. The contribution of renewable energy is almost negligible. However, it will change in the future due to an increase of oil prices. Thailand is an agricultural country that is the most world-leading manufacturer and exporters of agricultural products each year [1]. Nevertheless, there are many agricultural by-products that are wastes. As mentioned above, it is interesting to reduce the number of those things. Utilization of waste biomass with its conversion to be useful energy by fermentation process that can be treated as the most effective technology for this purpose. Biomass has three main sources, such as solid waste, wastewater sludge, animal and food wastes. Biomass-fed into an anaerobic digester undergoes hydrolysis, acidogenesis, acetogenesis and methanogenesis. During the final stages of methanogenesis, microorganisms convert hydrogen and acetic acid to form CH_4 and CO_2. Normally, a range of 50–75% of CH_4 is expected to be produced in the biogas plant [2].

Biogas contains a mixture of different gasses that consist of methane (CH_4) 50-75%, carbon dioxide (CO_2) 30-45% and may have a small amount of hydrogen sulfide (H_2S), siloxane and moisture [3]. Currently, utilization of CH_4 is so attractive. This is because CH_4 can be used for any heating purpose such as, cooking and electricity. Therefore, CO_2 must be separated from biogas. This is because remaining of CO_2 leads to a decrease of heating value. Thus, purification of CH_4 by removal CO_2 has been investigated [4-5]. Conventional processes for CO_2 capturing are based on reversible chemical or physical adsorption using amine scrubbing and cryogenic distillation. However, these processes are high energy-consuming in terms of solvent regeneration and high operating cost. Therefore, polymeric membranes for separation are the candidates owing to their advantages, for example, simplicity, lower operating costs and low environmental impacts as compared to other conventional technologies.

Generally, most of industrial gas separation processes require high pressure as a driving force. Therefore, engineering polymers with excellent mechanical and thermal properties, such as polyether-block-amide (PEBAX), polyurethane (PU), polyimide (PI), polysulfone (PSU), etc. have been developed for membrane fabrication. On the other hand, this research carries out the permeation system under ambient pressure condition and concentration gradient as the basis for gas permeation. Thus, it is unnecessary to prepare the membrane from an engineering polymer. Consequently,

ethylene vinyl acetate copolymer (EVA), a commercial polymer, was selected to be the membrane.

Mousavi SA. et al. [6] studied effect of preparation conditions on morphology and gas permeation properties of polyethylene (PE) and EVA films. The difference between percentages of vinyl acetate including 18%wt and 28%wt were investigated. PE and EVA films were fabricated by film blowing process and phase inversion method, respectively. In addition, CO_2 and O_2 permeabilities of the films were determined. As compared with PE film, the presence of VA functional group in EVA film resulted in an enhancement of CO_2 permeation due to the polarity of CO_2, which has an interaction with VA polar groups in the copolymer. Besides, adding a higher amount of VA functional groups in EVA (18%VA and 28%VA) leads to a higher CO_2 permeability of the film. In contrast, PE film was fabricated by film blowing process that induces an increase of crystalline phase fraction because of the orientation of polymer chain along with machine direction (MD) and transverse direction (TD) during process. Hence, a decrease in CO_2 permeability of the films were observed. Moreover, the presence of VA functional group gives a higher CO_2/O_2 permselectivity of EVA films as compared to PE films.

Zamiri MA. et. al. [7] studied on effect of polyethylene glycol (PEG) in EVA/PEG blend membranes for CO_2/N_2 separation. The different molecular weight (M_w) of PEGs (200, 1000, and 1500 g/mol), amount of PEG (0-20%wt) and feed pressure (2-8 bar) were evaluated. The pure EVA and blend membranes were prepared by solution blending. The result from DSC revealed that adding PEG in membrane led to a decrease in %crystallinity. However, the permeability of both CO_2 and N_2 were increased by adding PEG to the blend because incorporation of PEG provides more amorphous domains (free volume) in the EVA phase, leading to an increase in diffusion of CO_2 and N_2. Anywise, CO_2 permeability was higher than N_2 owing to strong interaction between CO_2 and ether oxygen in PEG molecule. The blends with lower M_w of PEGs at 10%wt showed better CO_2 permeability and CO_2/N_2 selectivity performance because PEG with lower M_w in blend membrane provides a higher amorphous phase due to the higher segmental mobility and less convenient geometrical alignment. Additionally, an effect of feed pressure showed that increasing the feed pressure (2–8 bar) led to an increase in CO_2 permeability but a decrease in N_2 permeability was observed.

In previous works, EVA was selected to use in membrane technology application because it is a commercially available plastic (cost efficiency) with good properties. In addition, physical and chemical properties of the EVA membranes can be changed because of various percentages of vinyl acetate (%VA). Therefore, this copolymer is selected to use in this research for CO_2 separation because of the strong interaction of polar carbonyl group in vinyl acetate segment and CO_2 gas molecules.

The hydrophilicity of the membrane would enhance a selective CO_2 permeation, hence EVA with 33% VA was chosen because it has greater carbonyl functional groups from higher vinyl acetate content. However, EVA with 33%VA has physical appearances, which are sticky and weak mechanical properties, it was modified to improve the mechanical properties.

1.2 Objectives of the study

1) To improve the mechanical properties of membrane via hydrolysis reaction.

2) To understand the effect of polyethylene glycol (PEG) with various molecular weights on the CO_2 permeability and CO_2/CH_4 selectivity.

3) To study the effect of amine-functionalized silica (AFS) on CO_2/CH_4 selectivity.

1.3 Scopes of the study

1) Modification of EVA copolymer (33%VA) to be the partially hydrolyzed EVA (p-EVA) with KOH solution

2) Modification of partially hydrolyzed EVA (p-EVA) by blending with polyethylene glycol (PEG) at 5, 10 and 15%wt with molecular weights of 400 and 1450 g/mol

3) Surface modification of SiO_2 with 3-Aminopropyltriethoxysilane (APTES)

4) Incorporation of amine functionalized SiO_2 (AFS) into the p-EVA/PEG blend membranes with 0.3, 0.6 and 0.9%wt

5) Fabrication of the membranes using a compression molding technique

6) Examination of functional groups and interaction in the membranes using Fourier-transform infrared spectroscopy in attenuated total reflection mode (ATR-FTIR)

7) Quantification of the elementals on AFS surface with CHNS analysis

8) Quantification of number of amine sites on AFS surface using back titration

9) Determination of the electronic structure of the surface species using X-ray photoelectron spectroscopy (XPS)

10) Investigation of thermal properties of membranes using differential scanning calorimetry (DSC)

11) Morphological characterization of membranes using scanning electron microscopy (SEM)

12) Measurement of the mechanical properties of membranes using universal testing machine (UTM)

13) Study on CO_2 and CH_4 permeabilities of the membranes

1.4 Benefits of the study

The hydrophilicity of modified membranes could improve the CO_2 permeability and also possess an excellent CO_2/CH_4 selectivity. Therefore, CH_4 can also be purified in order to enhance the combustion efficiency of biogas. Moreover, the mechanical properties of modified membranes can be obtained. The received knowledge on gas permeation and separation can be applied for other applications of polymeric membranes.

Chapter 2
Theory and literature reviews

2.1 Biomass

Biomass refers to a non-fossilized and biodegradable organic material that initiates from plants, animals and micro-organism. This shall also include products, by-products, residues and waste from agriculture, forestry and related industries. Biomass also includes only living and recently dead biological species that can be used as fuel or in chemical production. It does not include organic materials that have been transformed by geological processes into substances, such as coal or petroleum. Biomass comes from botanical (plant species), biological (animal waste or carcass) sources, or a combination of these [8]. The common sources of biomass are depicted in Table 2.1.

Table 2.1 Common sources of biomass [8]

Agricultural	Food grain, Bagasse (crushed sugarcane), Corn stalks, Straw, Seed hulls, Nutshells, Manure from cattle, Poultry and Hogs
Forest	Trees, Wood waste, Wood or bark, Sawdust, Timber slash and Mill scrap
Municipal	Sewage sludge, Refuse-derived fuel (RDF), Food waste, Waste paper and Yard clippings
Energy	Poplars, Willows, Switchgrass, Alfalfa, Prairie bluestem, Corn, Soybean, Canola and other plant oils
Biological	Animal waste, Aquatic species and Biological waste

2.1.1 Types of Biomass

Biomass is obtained from a variety of sources as shown in Figure 2.1. It composes of all plants and plant-derived from materials, including livestock manures. Primary or virgin biomass is directly derived from plants or animals. Waste or its derivatives can be produced from different biomass-derived products waste [9]. Biomass may also be divided into two categories as listed in Table 2.2.

Table 2.2 Two major groups of biomasses and their sub classifications [8]

Virgin	Terrestrial biomass	- Forest biomass - Grasses - Energy crops - Cultivated crops
	Aquatic biomass	- Algae - Water plant
Waste	Municipal waste	- Municipal solid waste - Biosolids - Sewage - Landfill gas
	Agricultural solid waste	- Livestock and manures - Agricultural crop residue
	Forestry residues	- Bark, - Leaves - Floor residues
	Industrial waste	- Demolition wood - Sawdust - Waste oil or fat

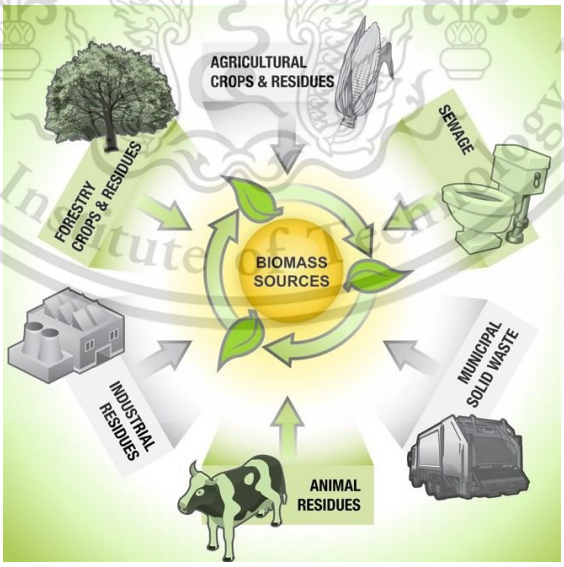

Figure 2.1 Common sources of biomass [10]

2.1.2 Biomass formation [11]

Botanical biomass is formed in the presence of carbon dioxide (CO_2) in the atmosphere, sun light energy, chlorophyll and water in order to produce the carbohydrate. Plants absorb solar energy that was used for the process called photosynthesis. This process may be represented by Figure 2.2 and Equation 2.1:

$$6CO_2 + 6H_2O + \text{Sunlight} \longrightarrow C_6H_{12}O_6 + 6O_2 \qquad (2.1)$$

Metabolic processes in the plant was transformed the following compounds into secondary products.

Carbohydrates: Starch, inulin, cellulose, sugar, pectin
Fat: Fat, fatty acid, oil, phosphatides, waxes, carotene
Protein: Protein, nucleoproteid, phosphoproteid
Vitamin: Vitamins, enzymes, resins, toxins, essential oils.

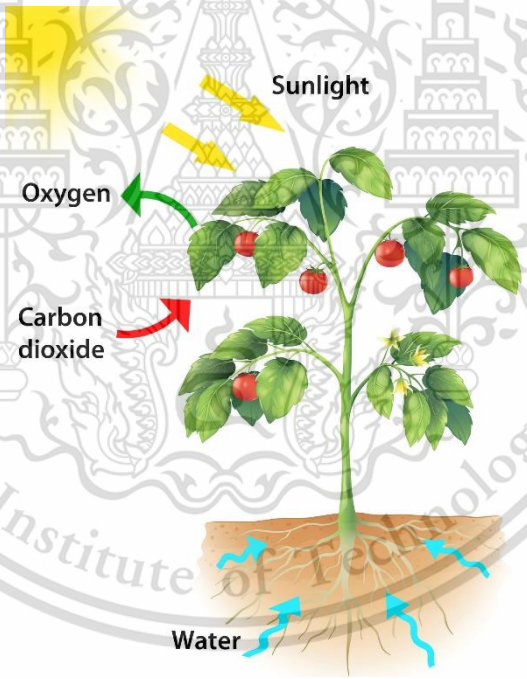

Figure 2.2 Photosynthesis process of plants [12]

2.1.3 Biomass-to-renewable energy [9]

Biomass-to-renewable energy process involves the synthesis or breakdown of organic compounds that constitute different types of biomasses. These organic compounds range in their complexity and contain numerous functional groups that influence the ultimate structure and chemistry of biomass. There are several processes to transform biomass into solid, liquid or gaseous secondary energy carriers. These

products can be generated from combustion, thermo-chemical, physical-chemical and biochemical transformation. The schematic of transformation of biomass to secondary energy source is illustrated in Figure 2.3

2.2 Anaerobic process for biogas production

Biogas mainly composes of methane and carbon dioxide and contains several impurities. However, biogas with a methane content higher than 45% is flammable [11].

Biological conversion of biomass to renewable energy products involves biochemical reactions that convert organic substrates into products for energy production. For example, organic wastes can be changed to methane or hydrogen through anaerobic digestion. In an anaerobic digestion, a consortium of anaerobic bacteria converts the organic compounds into biogas under oxygen-free environmental conditions. The process can be divided into four main steps: hydrolysis, acidogenesis, acetogenesis and methanogenesis. Each of the four steps involves different biochemical reactions with different substrates and microorganisms [13].

2.2.1 Hydrolysis

Original organic waste materials usually contain large-molecules compounds, such as carbohydrates, proteins, lipids and celluloses. These organic compounds are hydrolyzed and cracked into monomer by exoenzymes (hydrolase) of facultative bacteria (active in both environments with and without oxygen) and obligate anaerobic bacteria (active only in the environment without oxygen). The facultative anaerobic microorganisms consume the oxygen dissolving in the water and thus causes the low redox potential necessary for obligatorily anaerobic microorganisms. Actually, the covalent bonds are destroyed in the chemical reaction with water.

The hydrolysis of carbohydrates takes place within a few hours but the hydrolysis of proteins and lipids occurs within a few days. Lignocellulose and lignin were slowly and incompletely degraded.

2.2.2 Acidogenesis

The monomers (sugars, fatty acid, amino acid and peptides) formed in the hydrolytic phase are fermented by the anaerobic bacteria to volatile fatty acid (short-chain organic acid), such as propionic and butyric acid during the acidogenesis. Similar to the hydrolysis process, acidogenesis also produces a small amount of acetic acid, hydrogen and carbon dioxide.

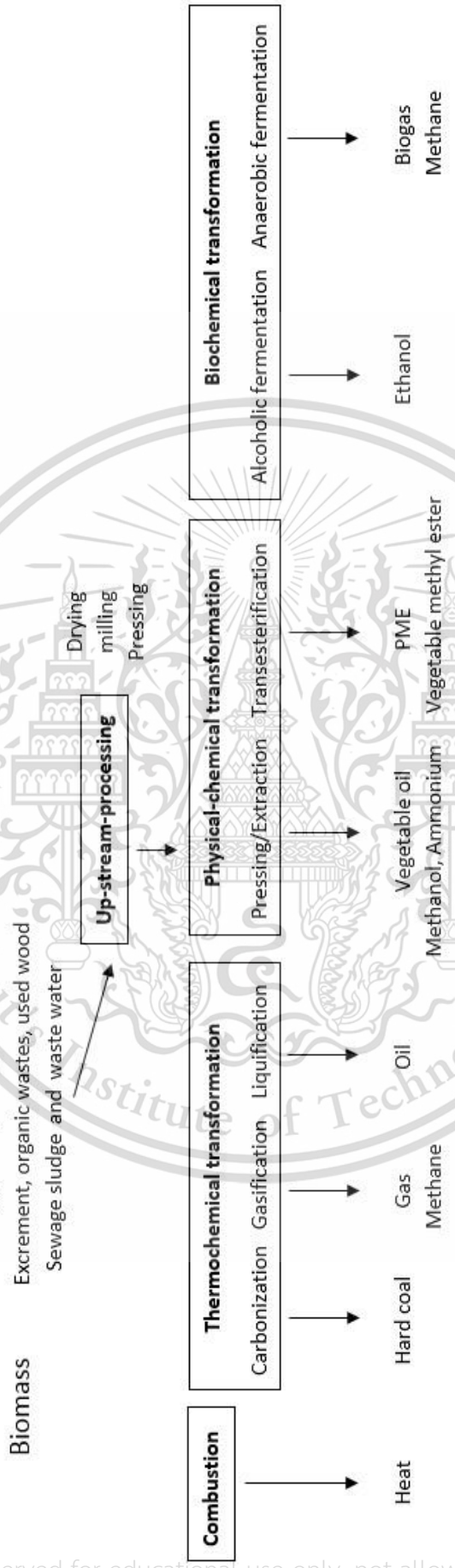

Figure 2.3 Technologies to transform biomass to secondary energy source [9]

2.2.3 Acetogenesis

In the acetogenic phase, the volatile fatty acids and alcohol were degraded into acetic acid by acetogenic bacteria. Limitation of degradation rate in the final stage depends on acetogenic phase. Thus, the quantity and the composition of biogas can rely on the activity of the acetogenic bacteria.

2.2.4 Methanogenesis

In the fourth stage, the methane formation takes place under strictly anaerobic conditions. The pathway for the formation of methane from acetate and/or CO_2 in microorganism is shown in Figure 2.4.

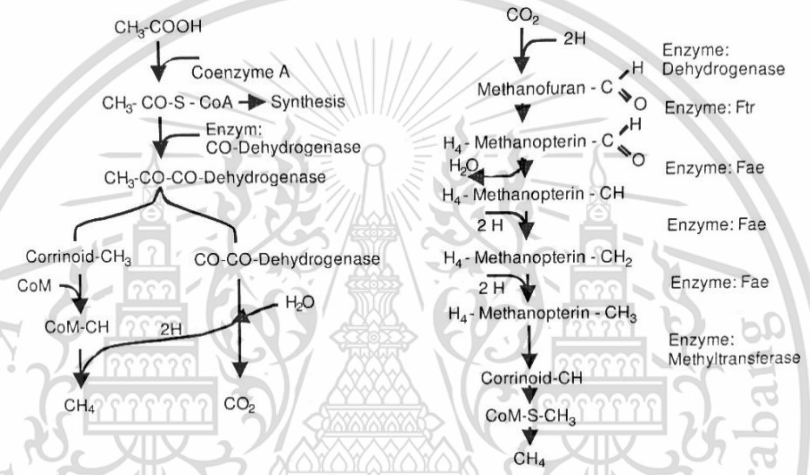

Figure 2.4 Methane formation from acetate (left) and carbon dioxide (right) [11]

The whole anaerobic digestion process is complete when both hydrogen and acetic acid are converted to methane during the methanogenesis. The anaerobic process to produce organic compounds to methane and carbon dioxide is displayed in Figure 2.5.

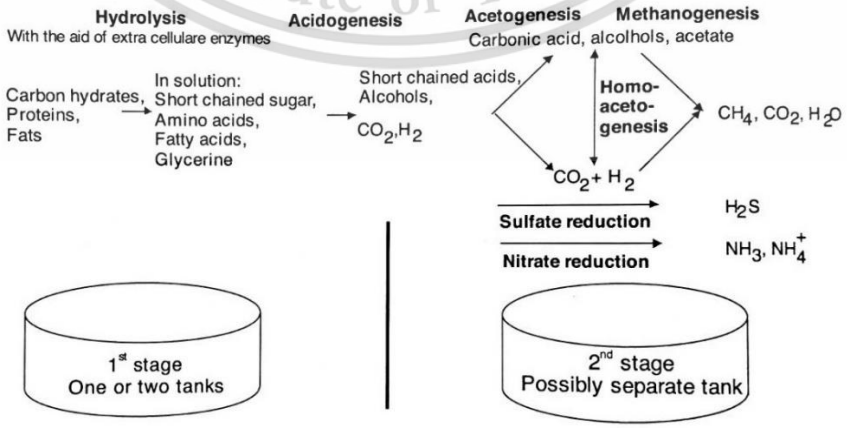

Figure 2.5 Biochemistry of the methane production [11]

2.3 Biogas purification [11, 13-14]

Biogas mainly contains 50%-80% of methane and 20%-40% of carbon dioxide as well as some minor gas components, for example, hydrogen sulfide (0.05%-1%). The components of biogas are illustrated in Table 2.3. Among the components, methane is the only one that can generate energy through combustion. CO_2 does not change during the combustion, but its existence dilutes methane concentration. Therefore, the completed combustion can occur at high temperature. Hydrogen sulfide is oxidized into sulfur dioxide and water, which forms sulfuric acid. Sulfuric acid is a very strong acid and corrosive. This acid can rapidly dissolve metal parts of the combustion engines, especially at high temperatures.

The removal of CO_2 and H_2S could upgrade the biogas to natural gas (>99% methane). As natural gas, purified biogas can then be sent to the natural gas lines for households or used as fuel for the automobiles that utilize natural gas.

Table 2.3 Typical components and impurities in biogas [11]

Component	Content	Effect
CO_2	25-50% by vol.	- Lower the calorific value - Increase the methane number and the anti-knock properties of engines - Cause corrosion (low concentrated carbon acid)
H_2S	0-0.5% by vol.	- Corrosive effect on equipment and piping systems (stress corrosion); many manufacturers of engines set an upper limit of 0.05% - The emission of SO_2 can be obtained with imperfect combustion of H_2S
NH_3	0-0.05% by vol.	- NO_x emissions after burners damage fuel cells - Increase the anti-knock properties of engines
Water vapor	1-5% by vol.	- Causes corrosion of equipment and piping systems - Condensate damage instruments and plants
Dust	> 5 μm.	- Block nozzles and fuel cell
N_2	0-5% by vol.	- Lower the calorific value
Siloxanes	0-50 mg/m^3	- Act likes an abrasive resulting in damaged engines

2.3.1 H_2S Scrubbing from biogas [11, 13]

The concentration of hydrogen sulfide in biogas depends on the waste materials treatment in anaerobic digesters. Biogas is generated from the anaerobic digestion of concentrated animal wastes that usually contain a high level of hydrogen sulfide, as shown in Table 2.4.

Table 2.4 Hydrogen sulfide concentration in biogas from different organic wastes [13]

Waste material	H_2S in Biogas (ppm)
Swine manure	600-4000
Cattle manure	600-7000
Landfill wastes	0-2000

Currently, there are several methods to remove H_2S from biogas, including precipitation, physical adsorption, chemical absorption and biological oxidation.

Precipitation: when H_2S was produced during the anaerobic digestion that is dissociated in water. Many metal ions (Fe^{2+}, Fe^{3+}, Cu^{2+}, Zn^{2+}, Mn^{2+}, Ni^{2+}) can react with sulfide ion to form precipitation. Among these metals, the most economical choice is iron in the form of iron chloride, iron phosphate and iron oxide.

Physical adsorption: H_2S can be adsorbed on porous media, such as activated carbon and zeolites. The adsorption process is a clean process without any by-products. It is very expensive process because H_2S adsorption on activated carbon or zeolites is irreversible so it takes a large amount of adsorbent.

Chemical absorption: similar to precipitation, H_2S reacts with chemicals such as $Fe(OH)_2$, $FeCl_3$ to form solids and water, so H_2S can be removed from the biogas. In practice, $Fe(OH)_2$ or $FeCl_3$ sponges were installed in biogas pipeline. When the wet biogas passes through the sponges, H_2S was removed from the biogas. The chemical absorbents need to be replaced when their H_2S-absorbing capacity is exhausted.

Biological oxidation: in practical terms, the biological oxidation is usually achieved by passing the biogas through moisturized biofilters or fixed film bio-scrubbers with attached H_2S-oxidizing aerobic bacteria. Prior to the biogas entering the biofilters or film bio-scrubbers, a small amount of air (usually 2-4% of the biogas volume) is added to the biogas to provide oxygen for the oxidation. The biological oxidation has been proven to be a very economical process for removing H_2S from biogas.

2.3.2 CO_2 Scrubbing from biogas [11]

Typically, methane-enriched biogas contains a methane concentration more than 95%. To reach this concentration, CO_2 has to be removed.

Physical adsorption: in industrial practice, pressurized water is usually used in scrubbing towers to remove CO_2 from biogas. When the biogas passed through a CO_2 scrubbing tower filled with pressured water, most of CO_2 can be dissolved in water as shown by the following equation:

$$CO_2\ (g.) + H_2O\ (l.) \longrightarrow H_2CO_3\ (aq.) \qquad (2.2)$$

The relationship between CO_2 in gas and H_2CO_3 in water is determined by Henry's law. At high pressure, the phase equilibrium between CO_2 in gas and H_2CO_3 in water is favorable toward the dissolution of CO_2 into the water. The CO_2 removal efficiency in the scrubbing towers filled with pressured water can be as high as 99%.

Chemical absorption: even higher loads and selectivity are achieved with chemical absorbents. Chemical absorption into alkaline solvent occurs under medium or low partial pressure. Absorbents are mainly amine, for instance, monoethanolamine (MEA), diglycolamine, diethanolamine (DEA), triethanolamine and dimethylethanolamine (DMEA) or a hot potassium carbonate solution. The absorptive power of amine is impaired by impurities in the biogas, such as solid particles, SO_2, NO_x and oxygen. The precleaning of the biogas from such impurities is applied before chemical absorption for cleaning exhaust gas streams, which contains organic materials. Additionally, for satisfaction in an industrial-scale the installations of chemical base on glycol, e.g., polyethylene glycol dialkyl ether are required.

Cryogenic biogas purification: cryogenic or low-temperature biogas purification is a procedure, which has not yet been sufficiently tested. It is expected to deliver methane of a quality suitable for vehicles. After compression to approximately 200 bar and liquefaction of biogas, the impurities like H_2S are adsorbed onto molecular sieves as depicted in Figure. 2.6.

The liquefied gas mixture is then separated by means of low-temperature distillation, often called "very low-temperature rectification" at approximately 30 bar, because the cooling causes an appropriate reduction of the pressure. The technology of the separation is based on the different boiling points of the biogas components: at a pressure of 50 bar CH_4 is liquefied at -80 °C and CO_2 at 15 °C. CO_2 and CH_4 are drawn off in liquid form. The liquefied CH_4 is stored at -161 °C, when atmospheric pressure is applied, and the CO_2 in pressure vessels at 20 bar at ambient temperature. The advantage of the liquefication of biogas is high purity of CH_4. However, the large power consumption procedure is needed, leading to a very high cost.

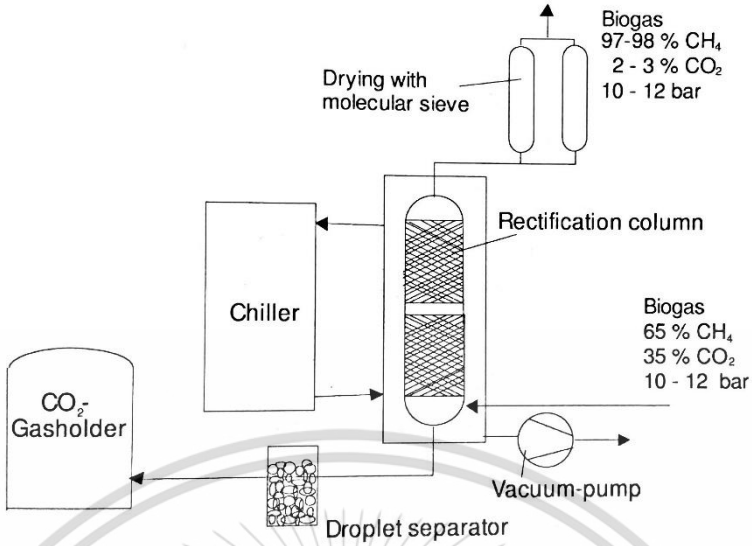

Figure 2.6 Gas liquefication plant with deep-temperature rectification [11]

2.4 Membrane technology

Membrane is a thin layer that is made from various materials, such as metal, ceramic and polymer. In addition, it is a semi-permeable active or passive barrier, which under a certain driving force, permits preferential passage of one or more selected species or components (molecules, particles or polymers) in a gaseous and/or a liquid mixture solution as displayed in Figure 2.7 [15].

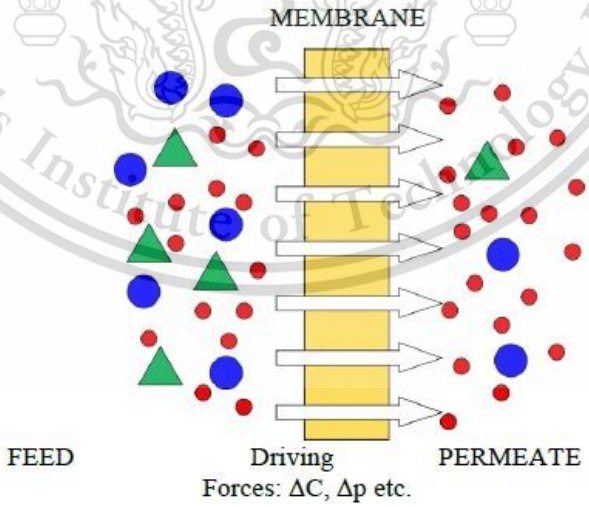

Figure 2.7 Schematic diagram of gas separation process by a membrane [15]

2.4.1 Materials for gas separation membrane [15]

In order to determine the separation efficiency of a membrane, the selection of membrane material is the most important factor for gas separation. This is because the membrane material can be interacted with gas molecules.

The choice of materials is based on the application and cost-effectiveness. The most important requirements of effective separation materials are:

1. Engineering potentiality
2. Good chemical resistance
3. High separation efficiency with reasonable high flux
4. Good mechanical stability
5. High thermal stability
6. Low cost

2.4.2 Membrane in gas separation [16-17]

This technique can be called "Diaphragm technology", which is still very new technique. However, this process is very important role for separation in an industry because it operates without heating, resulting in low-energy consumption.

Gas separation is the ability to separate substance using a membrane that is divided into 2 mechanisms for porous and dense membrane.

1. Gas diffusion mechanism

Gas diffusion mechanism is occurred in porous membranes that have inter-connected pores in membrane. Chemical potential gradient acts as a driving force to push gas pass through the membranes. The chemical potential may exist in the form of concentration, partial pressure, electric filed and temperature, which is classified into 3 types as shown in Figure 2.8.

1) *Knudsen diffusion*: this separation occurs when the diameter of porous in the membrane is smaller than mean free path (distance which gas molecules can be moved without collision). So, the molecules of gas diffuse into the porous rather than collide. Especially, smaller and lighter molecules can permeate through the membrane.

2) *Molecular sieving*: this separation of gas follows by different sizes of molecules as compared with the pore size of the membrane. Thus, only molecules, which are smaller than a porous, leading to the gas permeability through the membrane.

3) *Surface diffusion*: this separation occurs when the molecules of gas are adsorbed on the porous surface. Then gas molecules are diffused through these porouses due to concentration gradient. Moreover, the adsorbed gas on the porous surface can be permeated throughout the membrane.

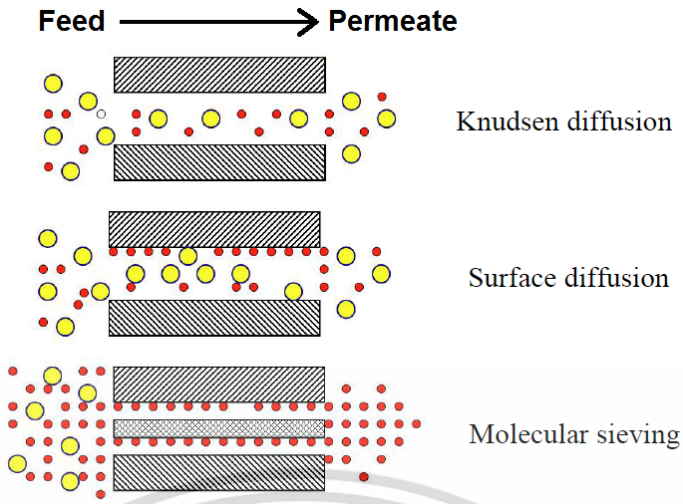

Figure 2.8 Mechanism of gas transport through the porous membranes [18]

2. Gas permeation mechanism [17, 19]

For dense membranes, gas permeation through the membrane is explained by the solution-diffusion mechanism. The different concentrations between upstream and downstream of the membrane is called concentration gradient. This is an important key to determine in the permeability of each gas that transfers through the dense membrane. Moreover, the duration of permeation depends on the thickness when the thickness is low, resulting in fast permeability.

The solution-diffusion mechanism is described in 3 steps:

1) Gas molecules are adsorbed on the upstream side of the membrane.

2) Diffusion of the absorbed species through the membrane driven by the concentration gradient (partial pressure difference).

3) Gas molecules desorption on the downstream side of the membrane. The mechanism is illustrated in Figure 2.9.

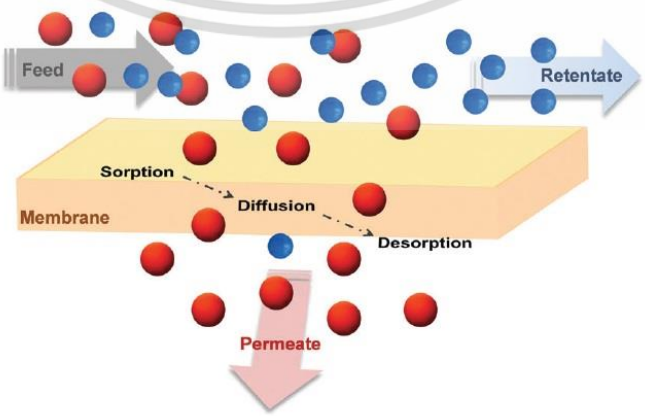

Figure 2.9 Gas transport mechanism through dense membranes [19]

In addition, permeability relates to both thermodynamic factors, such as condensability of the gas species and its interaction with the membrane. Besides, the kinetic factors are mainly controlled by the size of gas molecules, membrane material's segmental mobility and packing, fractional free volume.

Selectivity is another important parameter of the membrane that is the ability to separate two gases. Membranes have different permeabilities for each gas. The selectivity of gas permeation is relative to how fast of each gas permeability in the dense membrane. The ideal permeability and selectivity, is commonly called permselectivity.

2.4.3 Polymeric membranes [17]

Polymeric membrane can be classified into 3 categories based on polymer materials.

1) Thermoplastic: this polymer has molecular structure of the chains as linear or branch that are solid at room temperature. They can be softened and melted when the high temperature is applied and may be re-melt several times. They are simple chain, which may vary in molecular weight, degree of branching with short or long chains, stereo structure or composition.

2) Thermosetting: the polymer has a cross-linked structure, which does not re-melt and decompose before melting. The three-dimensional network of strong covalent bonds (crosslinking) leads to the thermosetting materials that are stronger than thermoplastic, and can be suited to high temperature applications.

3) Rubbery polymer: rubber is another choice of material to employ in membrane application. Rubbery polymers have the same amorphous structure as glassy polymers but this order is not frozen in as these polymers are above the glass transition temperature (T_g).

Factors affected on gas permeability of dense membranes are: [20]

1. Interchain distance or free volume: when the free volume is increased in the membrane, resulting in an enhancement of gas permeability.

2. Glass transition temperature (T_g): the polymer, which has T_g below the room temperature. The polymer chain in amorphous phase can be moved, leading to a better gas permeability.

3. Degree of crystallinity: crystallinity is an important role to obstruct gas diffusivity in the membrane. Therefore, the membranes with high crystallinity could give poor gas permeation.

The oxygen (O_2) and carbon dioxide (CO_2) permeability coefficients in various plastic films are listed Table 2.5.

Table 2.5 Permeability coefficients of O_2 and CO_2 in various plastic films [20]

Types of plastic	O_2 permeability coefficients ($cm^3 \cdot mm/m^2 \cdot atm \cdot day$)	CO_2 permeability coefficients ($cm^3 \cdot mm/m^2 \cdot atm \cdot day$)
PET	2.0 – 3.9	4.7 – 7.9
PVC	2.0 – 7.9	7.9 – 19.7
LDPE	247.0	959.0
PP	68.5	208.0
PS	101.0	527.0
EVA, VA 12%	180.0	1,100.0
EVOH, Ethylene 32/44 mole%	1.02/0.03	0.01/0.08

The membrane materials for CO_2 and CH_4 separations according to manufacturers' data are shown in Table 2.6.

Table 2.6 Manufacturers of diaphragm [11]

Membrane material	Producer
Polyethersulfone	Bayer, BASF, Monsanto
Cellulose acetate	Grace
Polyetherimide	General Electric
Hydrin C	Zeon
Pebax	Atochem
Polyacrylate	Rohm
Polydimethylsiloxane	Wacker, GKSS
Polyhydantoin	Bayer

2.5 Polymer blends

Blending process is an improvement of polymers properties and is the most popular because of simplicity, excellent properties and cost efficiency. This is made by combining different polymers with specific properties in order to obtain the new materials with optimized choice, such as chemical, structural, mechanical and morphological properties. Blend properties are strongly influenced by interphase (region between polymer matrix and surface of dispersed phase) and the size or shape of the dispersed phase that is developed by the processing condition [21].

Generally, it was found that most of the polymer blends were not homogeneous or immiscible blend. The cause of the immiscible blend is free energy of mixing (ΔG) with positive value, leading to phase separation in polymer blends. Therefore, the thermodynamic condition is the first important to recognize in blending process.

In thermodynamic of polymer blends, the primary requirement for two polymers to be miscible according to the necessity of having negative Gibbs free energy of mixing (ΔG), which is controlled by enthalpy and entropy. Gibbs free energy value can be described in the equation 2.3 [21].

$$\Delta G_m = \Delta H_m - T\Delta S_m \qquad (2.3)$$

Where ΔG_m = Gibbs free energy
ΔH_m = Free enthalpy
ΔS_m = Entropy
T = Temperature (K)

2.5.1 Classification of polymer blends [22]

When considered from free energy of mixing, polymer blends are classified into 2 types based on Gibbs free energy (ΔG_m).

1) Miscible blend: the polymer blend is homogeneous down to the molecular level associated with the negative value of the free energy of mixing; $\Delta H_m - T\Delta S_m < 0$. As a result, the homogeneity in a polymer blend is obtained. This suggests that the two polymers have the similarity of solubility parameter. Typically, amorphous polymers can be mixed to be miscible blend easier than semi-crystalline polymers. This is because amorphous polymer has higher disorder chains, resulting in high entropy (ΔS_m) and thus miscible mixing can be occurred.

Normally, miscible blends have properties between those of the individual polymers. These properties depend on the ratio of the two polymers and these various ratios are often used to obtain a specific property. However, most of the polymer blends prefer to be immiscible because of the positive free energy of mixing.

2) Immiscible blend: The polymers cannot be truly mixed together. They exhibit phase separation that related with positive value of the free energy of mixing; $\Delta H_m - T\Delta S_m > 0$. Most of the polymer blends especially, the semi-crystalline polymers are immiscible with poor physical properties as compared with the parent polymers. This is owing to the lack of favorable interaction between the phases of polymers that is related to largely different solubility parameters.

Immiscible polymer blends exhibit different types of morphologies, which depend on composition, viscosity ratio and elasticity ratio between the component, interfacial tension, process conditions and etc. The phase morphology in an immiscible blend is shown in Figure 2.10.

Figure 2.10 Phase morphology in an immiscible blend [24]

2.5.2 Characterization on compatibility of polymer blends [23]

1) The morphology of polymer blend is investigated using scanning electron microscope (SEM). When both polymers have a similar architecture, the homogeneous phase is obtained. Likewise, immiscible blends perform phase separation, which consists of matrix and dispersed phase.

2) Thermal properties of polymer blend, glass transition temperature (T_g) is examined using differential scanning calorimeter (DSC). It was found that the T_g can be appeared for 1 or 2 points in miscible and immiscible blends, respectively.

3) Mechanical properties are measured using universal testing machine (UTM), which is reported as tensile strength, %elongation at break, impact strength and Young's modulus. The polymer blends exhibited phase separation (immiscible blend), resulting in poor mechanical properties.

2.5.3 Blending process [17]

Preparation of polymer blends can be done in several methods. However, solution blending and melt blending are the most commonly used method.

1) Solution blending: this process is prepared by dissolving the different polymers into the suitable solvent. The polymer blend is dried at room temperature or in an oven in order to evaporate solvent. The drawback of this process is the high

solvent consumption and the long cycle time for solvent evaporation. Additionally, some solvents are also harmful to the human and the environment.

2) Melt blending: this process is carried out using machines, such as an internal mixer, extruder, injection molding machine and etc. One of the advantages of this process is a better compatibility of both polymers because of the shear stress from mixing condition of machine. In addition, melt blending process can be produced in large amount of polymer blend and without hazard from solvent.

2.6 Polymer

2.6.1 Ethylene vinyl acetate copolymer (EVA) [25]

Ethylene vinyl acetate copolymer (EVA) is the thermoplastic that classified as a polyolefin. EVA was originally prepared by the polymerization under high pressure between ethylene monomer and vinyl acetate monomer (VAM). The most commonly used initiators are azo-bis-isobutyronitrile, organic peroxide and persulphate. The EVA copolymer consists of the ethylene segment around 60-90% and the other moiety is vinyl acetate functional group that hinders the growth of crystallinity, resulting in disorder chain and better flexible in copolymer. Additionally, it was found that the properties of EVA copolymer can be changed with different percentages of vinyl acetate segment. The structure of EVA copolymer is displayed in Figure 2.11.

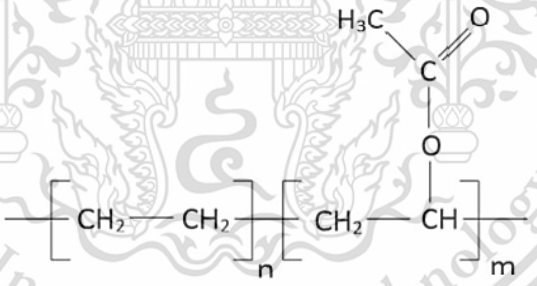

Figure 2.11 Repeating unit of EVA copolymer [7]

The common properties of EVA copolymer

- Clarity or opaque thermoplastic polymer pellet (depend on amount of vinyl acetate in copolymer)
- Specific gravity: 0.926 – 0.950
- Dissolve in aromatic solutions and chlorinated hydrocarbon at high temperature
- Brittle point: < -70 ℃
- Softening point: 60 - 80 ℃
- Glass transition temperature (T_g): -20 to 20 ℃

- Hardness (shore D): 90 - 95
- Tensile strength: 2.9 - 19.6 MPa
- Elongation at break: 500 - 700%
- Easy to process
- High flexibility without plasticizers
- Light and UV resistance
- Resistance to leaching conditions and long service life

Applications of EVA copolymer

Commonly, EVA is used to produce shoes and mattress. However, EVA with low M_w is mostly used as an adhesive, plasticizers and wax additives for coating paper. In addition, EVA has mainly flexible properties, which can be applied as food packaging and medical plastic applications e.g. tubing, devices and medical bags.

2.6.2 Ethylene vinyl alcohol copolymer (EVOH) [26-27]

Ethylene vinyl alcohol copolymer (EVOH) is the semi-crystalline copolymer, which composed of ethylene and vinyl alcohol segment. The composition between both segments has an important role to determine the properties, such as gas permeability and mechanical strength. EVOH is prepared by copolymerization of monomer units based on PVOH and PE. In addition, EVOH can prepared from hydrolysis reaction from EVA, which the %hydrolysis is depended on reaction time and concentration of mixture solution. The repeating unit of EVOH copolymer is depicted in Figure 2.12.

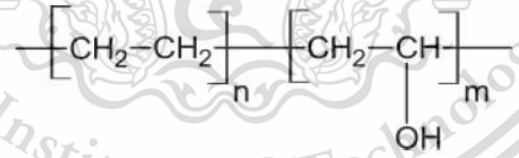

Figure 2.12 Repeating unit of EVOH copolymer [27]

The common properties of EVOH copolymer

- Glass transition temperature (T_g): 55 - 69 °C
- Melting point (T_m): 164 - 181 °C
- Tensile strength: 8,520 - 11,220 MPa
- Elongation at break: 230 - 280%
- Excellent gas barrier properties in the low humidity conditions
- Chemical, oil and solvent resistance
- Excellent transparency and high gloss

- Heat resistance
- Relatively sensitive to moisture
- Can be co-extrusion with various polymers

Applications of EVOH copolymer

Commonly, EVOH is used in food packaging to extend the shelf life of food products and protect their nutrients against bacteria. This is because it can prevent the oxygen and other gasses from the atmosphere to come in contact with food products. Additionally, the food packaging is usually made from PP/EVOH/PP that is prepared by an extrusion lamination process.

2.6.3 Polyethylene glycol (PEG) [28-31]

PEG is also known as polyethylene oxide (PEO) or polyoxyethylene (POE), which is depending on the molecular weight (M_w). PEG is available in a variety of M_w from 200 to 10,000 g/mol. It has a colorless viscous liquid at the M_w below 600 g/mol and a waxy, white solid at M_w above 800 g/mol. In addition, at the room temperature, PEG exhibits as the water-soluble and hygroscopic polymer. Typically, PEG is produced by the chemical reaction of ethylene oxide with water, ethylene glycol, or ethylene glycol oligomers and catalyzed by acidic or basic catalysts. The structure and its repeating unit of PEG are shown in Figure 2.13.

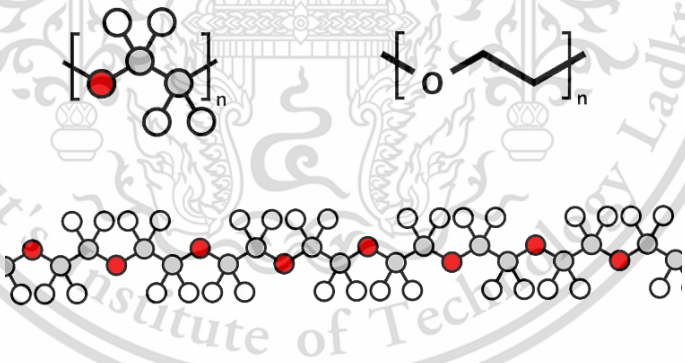

Figure 2.13 Structure and its repeating unit of PEG [31]

It was found that PEG is stable to acid, base, high temperature, O_2, H_2O_2 high oxidation systems and $NaBH_4$ reduction systems. Moreover, PEG may be recovered from aqueous solution by extraction with a suitable solvent or by direct distillation of water or solvent.

Application of PEG

PEG has different physical appearances, which are caused by various M_w from polymerization process. This is led to wide range of applications, for example, an excipient in many pharmaceutical products, ingredient in skin creams and personal

lubricants (frequently combined with glycerin). In addition, it is used as a polar stationary phase for gas chromatography technique (GC) and as an additive (anti-foaming agent) in food. Additionally, PEG derivatives with narrow range ethoxylates are used as surfactants.

2.7 Silica (SiO_2) [32-35]

Silica, also known as silicon dioxide, is a compound formed by the integration between oxide and silicon with the chemical formula SiO_2. Silica has a lattice structure that is a 3-dimensional network solid in which each silicon atom is covalently bonded in a tetrahedral manner to 4 oxygen atoms as shown in Figure 2.14.

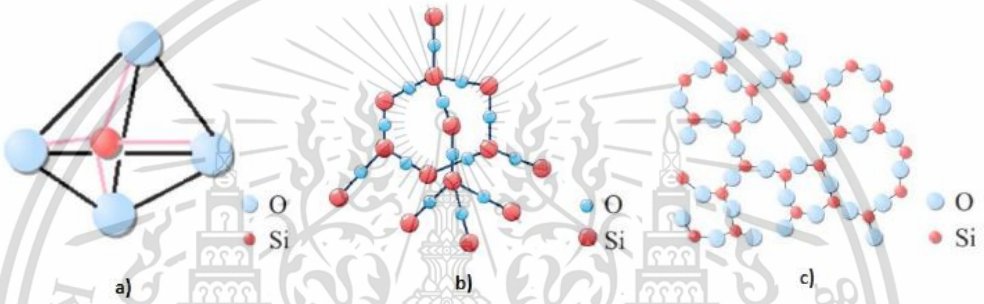

Figure 2.14 Chemical structure of silica: a) tetrahedral basic unit, b) quartz-like silica crystal and c) amorphous network [32]

2.7.1 Structure of silica

In general, silica is rarely in the form of primary particles but gathered to the primary structure, called an aggregate, which cannot be destroyed during the mixing process due to the strong chemical attraction (covalent bonding). Besides, the silica aggregates are also preferred to form the secondary structure, which is called agglomerates. This is because the coagulation of silica to the secondary structure is constructed by the hydrogen bonding (H-bond), which is a very strong attractive (dipole-dipole) interaction [33]. The primary and secondary structures of silica are depicted in Figure 2.15.

2.7.2 Types of silica

Silica can occur in natural and synthesis processes but most commonly found in nature as quartz. In addition, the physical structure of silica is classified for crystalline, amorphous and synthetic amorphous. The category of silica can be divided into 2 types; fumed silica and precipitated silica.

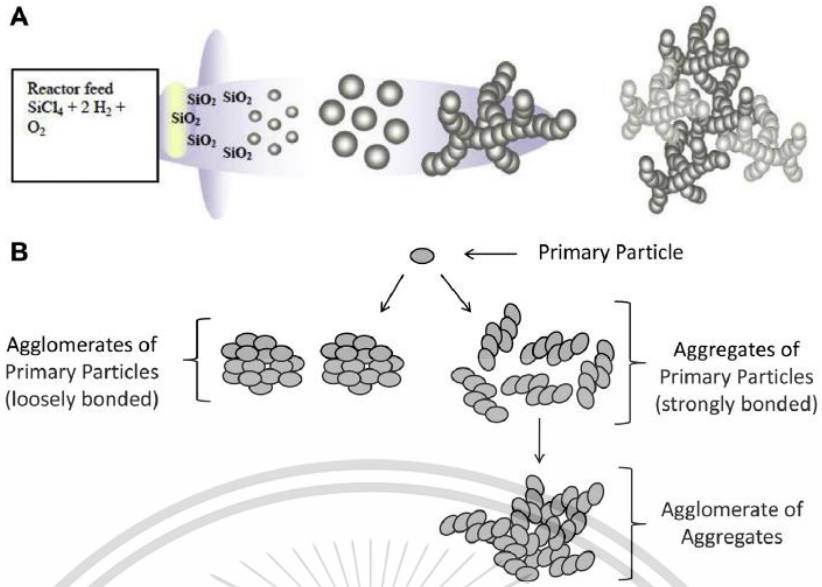

Figure 2.15 Primary and secondary structures of silica [34]

1) Fumed silica: fumed silica, also known as pyrogenic silica is acquired from a pyrolitic process, as the product of the hydrolysis of silicon tetrachloride vapor or quartz sand vaporized in a condition of oxygen-rich hydrogen flame, according to the equation 2.4.

$$2H_2 + O_2 \longrightarrow 2H_2O$$
$$SiCl_4 + 2H_2O \longrightarrow SiO_2 + 4HCl \qquad (2.4)$$

The residual adsorbed HCl on the surface of fumed silica is then reduced to less than 200 ppm through the calcination process. However, fumed silica has a trace of metallic contaminants, e.g. aluminum, calcium, zinc and etc. During the combustion process, elementary spheres of molten silica are formed, so-called primary particles in the diameter of 7-30 nm. The primary particle can collide with another one to provide three-dimensional chainlike objects, so-called aggregate in the diameter of few tenths of micron range. Fumed silica is a non-porous and amorphous material that has a low bulk density (0.03 g/cm^3) and a high surface area (100-400 m^2/g) [35].

2) Precipitated silica: the precipitated silica, also known as amorphous silica, has a surface area in the range of 25-700 m^2/g. It can be produced by wet process from solutions of alkali silicate under the condition of high temperature and pressure. The vitreous silicate is precipitated by adding the sulfuric acid (or the solution of metal salts for high performance grades), according to the equation 2.5.

$$Na_2Si_3O_7 + H_2SO_4 \longrightarrow 3SiO_2 + Na_2SO_4 + H_2O \quad (2.5)$$

The sodium sulfate is a byproduct, which is removed by filtration and washing. The product consists of 85-90% silica and 10-15% water [35].

2.7.3 Surface chemistry of silica

Generally, it is accepted that the surface of silica has a complete tetrahedral configuration. The siloxane groups (Si-O-Si) are nonpolar and provide a hydrophobic characteristic on the silica surface. However, there are various types of hydroxyl groups on the surface that possess strongly hydrophilic characteristics, as shown in Figure 2.16.

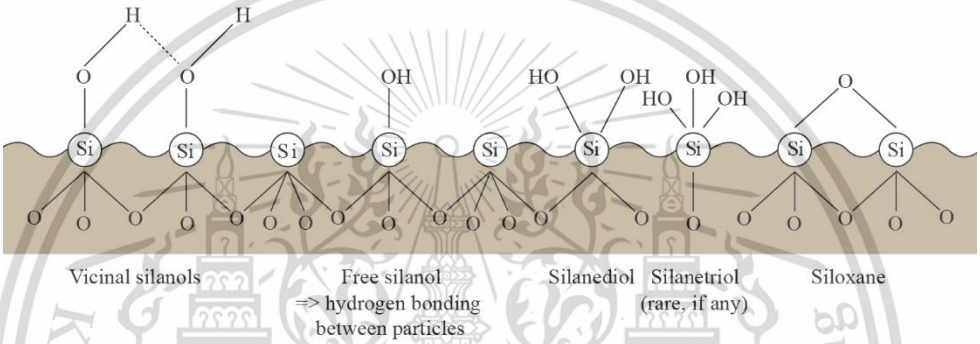

Figure 2.16 Various types of hydroxyl groups on the surface of silica [35]

Hydrogen-bonded vicinal, single and geminal silanols, including terminal groups can generate hydrogen bonding and eventually siloxane groups through water elimination. Free silanol groups, also called isolated silanol, are more reactive than vicinal groups, leading to being the prime reactive sites for organic molecules, namely organo-silanes. The important consequence of such as oxygen-rich surface chemistry results in strong inter-particles interactions through hydrogen bonding. Therefore, a poor dispersibility in nonpolar polymers is observed and consequently special compounding procedures are required [33].

2.8 Silane coupling agent [36-37]

Silane coupling agents are silicon-based chemical compounds whose molecules comprise functional groups that bond with both organic and inorganic materials. The silane coupling agents role as a sort of intermediate, which consists of two types of reactivity (inorganic and organic) in the same molecule. The structure of silane coupling agent is depicted in Figure 2.17.

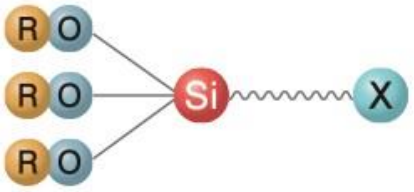

Figure 2.17 Structure of silane coupling agent [36]

Typically, general structure is $(RO)_3$-Si-X. Where R is a hydrocarbon group, for instance, methyl, ethyl, octadecyl and etc. The hydrocarbon group can form the chemical bond with inorganic materials including inorganic fillers, glass and metal. Prior using, the silane coupling agent is hydrolyzed to produce silanol, which forms metal-oxygen or siloxane bond with the inorganic material on one side. On the other side, X is an organic functional group, such as vinyl group, amino group, methacryloxy group, epoxy group, mercapto group and others. The organic functional group can react with the organic materials, e.g., polymers to produce a chemical bond. As a result, the organic and inorganic materials are tightly bounded to each other. The mechanism of coupling is displayed in Figure 2.18.

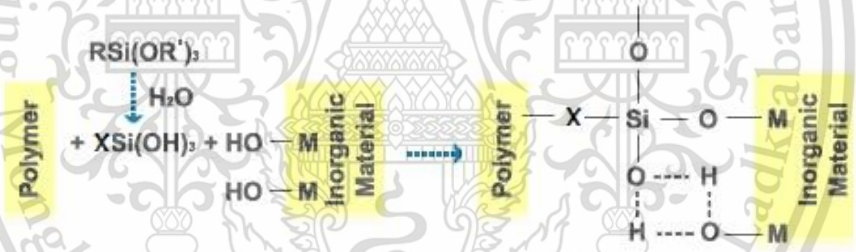

Figure 2.18 Silane coupling mechanism [38]

2.8.1 Aminosilane [37, 39]

Aminosilane is an amino-functional silane, for instance, aminophenyltrimethoxysilane ($C_9H_{15}NO_3Si$), 3-aminopropyltriethoxsilane ($C_9H_{23}NO_3Si$) (Figure 2.19), N-(2-amino ethyl)-3-aminopropyltriethoxysilane ($C_{11}H_{28}N_2O_3Si$) and etc. These are utilized over a broad range of applications to gain an improvement of bonding between fillers or reinforcements and resins. In addition, aminosilane is widely used as coupling agents for fiberglass insulation and composites.

Aminosilane is especially recommended for thermoplastic and thermosetting resins, for example, epoxy, polyethylene, phenolics, melamine, nylons, PVC, acrylics, polyolefins, polyurethanes and nitrile rubber. Aminosilane can enhance mechanical, and physical properties; for example, flexural strength, compression strength and shear

strength. Additionally, aminosilane can improve the dispersion and wettability of filler in the high molecular materials.

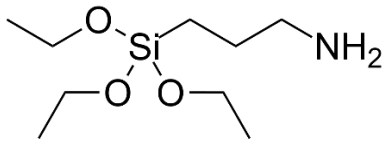

Figure 2.19 Structure of the 3-aminopropyltriethoxysilane (APTES) [39]

2.8 Literature reviews

Tang M. et al. [40], prepared the partially hydrolyzed EVA films at various percentages of hydrolysis for studying the properties of controlled drug release. The EVA at vinyl acetate content 42% was chosen for hydrolysis reaction in NaOH solution (0.5mol/l) and the reaction times at 1, 3 and 5 h were performed. Then the hydrolysis degree was investigated via an indirect method (back titration). The three different hydrolysis reaction times resulted in three different hydrolysis degrees at 12.2%, 32.6% and 46.9%, respectively. Partially hydrolyzed EVA (E1, E3 and E5) were obtained. It was noticeable that the hydrolysis degree was evidently increased when the reaction time was extended, as confirmed by the ATR-FTIR (Figure 2.20). It was indicated that the intensity of E5 peak at 1735 cm^{-1} was obviously decreased comparing with the EVA one. In addition, the peak related to hydroxyl group at about 3302 cm^{-1} was occurred. The results suggested that some of acetate groups were successfully changed to hydroxyl groups. Additionally, as the hydrolysis degree increased, the elastic modulus and maximum tensile strength was decreased. This is because of the inter molecular hydrogen bonds between hydroxyl groups.

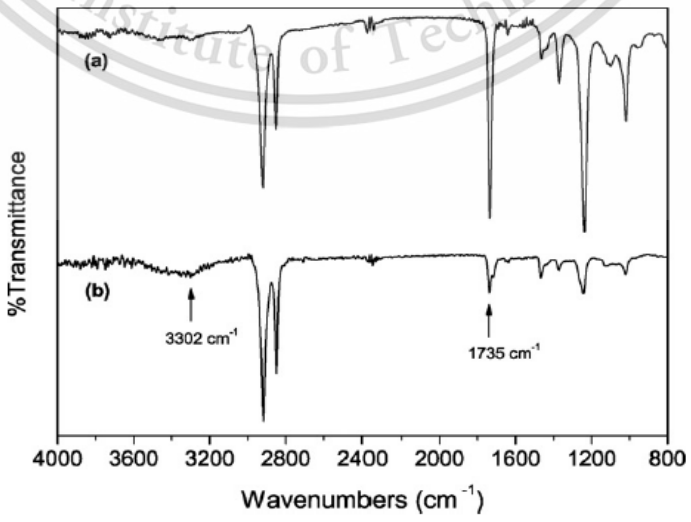

Figure 2.20 ATR-FTIR spectra of a) EVA and b) E5

Hong SM. et al. [41], modified graphite oxide for enhancing the CO_2 adsorption performance. 3-aminopropyltriethoxysilane (APTES) was chosen for surface modification of the graphite because of basicity (amine group), which is favorable for adsorption of acidic CO_2. The 3-aminopropyl-triethoxysilane-modified-graphite oxide (Gr-APTS) was prepared by oxidizing graphite powder with $NaClO_3$ in fuming HNO_3 in order to introduce several oxygen-containing functional groups on the surface. The result of morphology indicated that Gr-APTS had similar morphology as GO without noticeable change after the amine modification. However, the result of EDX and FTIR revealed that APTS was successfully attached to surface of GO by the reaction between oxygen functional groups and amine molecules. In addition, XRD analysis confirmed that interlayer distance (d-spacing) of Gr-APTS was increased to 11.4 Å, as compared with that of graphite (3.4 Å) because a long chain APTS inserted between graphite layers. The CO_2 adsorption uptake of Gr-APTS was significantly enhanced as compared to that of graphite (Figure 2.21) owing to the increase of basicity from amine molecules that were attached on the surface of the graphite. The feasible mechanism of the CO_2 adsorption is illustrated in Figure 2.22.

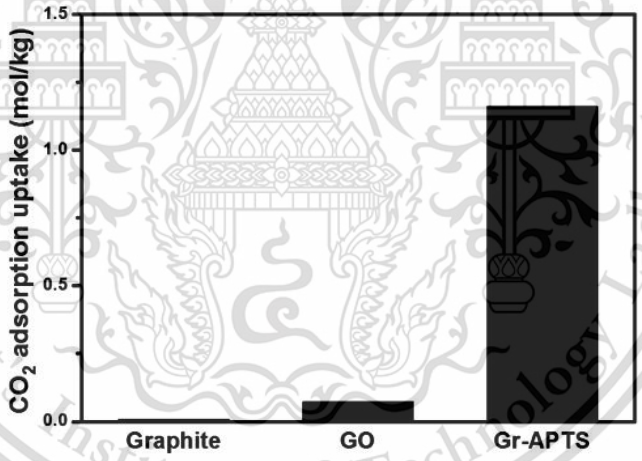

Figure 2.21 CO_2 adsorption uptake of graphite, GO and Gr-APTS at 30 °C under atmospheric pressure

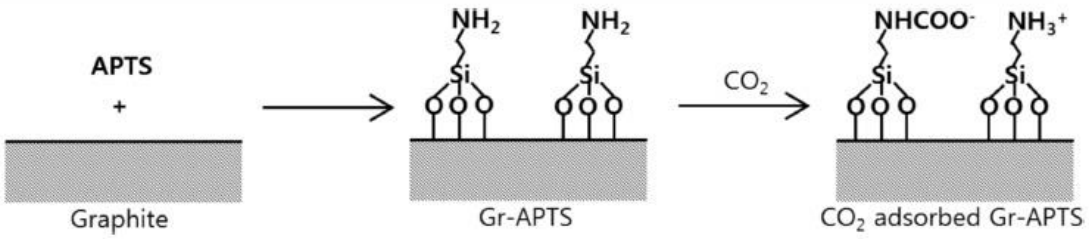

Figure 2.22 Schematic of possible mechanism of CO_2 adsorption on Gr-APTS

Castro-Munoz R. et al. [42], prepared Matrimid® 5218/PEG-200/ZIF-8 mixed-matrix membranes (MMMs) for improving CO_2/CH_4 separation. The factors affecting properties of the film were investigated, for instance, amount of polyethylene glycol (PEG) 1-5wt% and amount of zeolitic imidazolate frameworks (ZIF-8) 10-30wt%. It was found that the blend membranes containing PEG at 4wt% gave the best CO_2 permeability, from 7.16 in pristine Matrimid® up to 27.54 barrer because the polar ether segment (ethylene oxide units) of PEG can interact positively with CO_2 molecules by dipole-quadrupole interaction, resulting in the transport through the membrane. In addition, the incorporation of ZIF-8 nanoparticles in the binary matrix membrane also considerably enhanced the CO_2 permeability and an increased amount of ZIF-8 facilitated a better CO_2 permeation. This is because nanoparticles can disrupt chain packing in polymer chains, leading to an increased free volume in polymer. The results revealed that the best formula for CO_2 permeability was ternary MMMs that had PEG at 4wt% and 30wt% of ZIF-8 (Figure 2.23). On the other hand, most of the binary and ternary MMMs exhibited a slight decrease of separation factor due to the addition of PEG, leading to enhancing local segment motions of polymer. Hence, the CH_4 permeability was significantly increased.

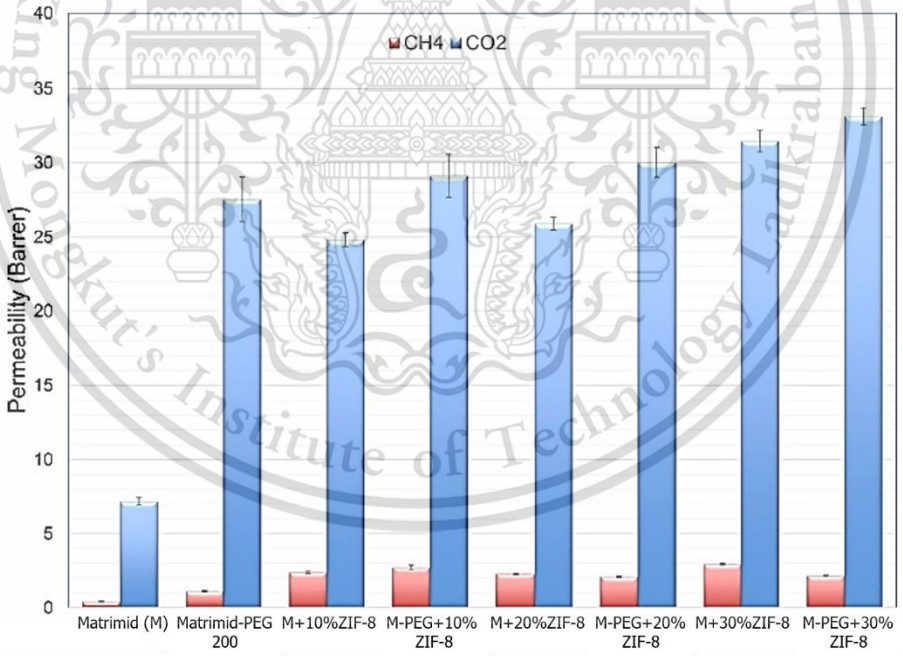

Figure 2.23 Permeabilities for pure Matrimid®, Matrimid®-PEG, Matrimid®-ZIF-8 binary and ternary MMMs at steady-state (8 bar)

Zhu H. et al. [43], improved CO_2/N_2 separation in polyether block amide (PEBA) mixed-matrix membranes with TiO_2 grafted with polyethyleneimine (PEI) using dopamine (DA) as a bridging (Figure 2.24). TiO_2 is a mesoporous material that exhibits

very high adsorption capacity and size-selective adsorption for certain gases, e.g. CO_2. Therefore, the density of active sites with high accessibility facilitates the gas diffusion. Meanwhile, the PEI chain contains plenty of amine groups that are beneficial to improve the gas separation performance through the reversible reaction between amine group and CO_2. The effect of TiO_2 loading (1-4wt%), Mw of PEI (600, 1800 and 10000 g/mol) and the ratio of PEI and dopamine (1:2, 1:1, 2:1) were investigated. The results from FTIR and XPS confirmed that successful grafting of PEI and DA on the TiO_2 surface was obtained. Moreover, CO_2 adsorption isotherm suggested that the DA/PEI modified TiO_2 had a higher affinity toward CO_2 (Figure 2.25), which would enhance the CO_2 sorption in the mixed-matrix membranes. It was found that the incorporation of amine-functionalized TiO_2 facilitated an enhancement in CO_2/N_2 separation. Especially, the long chain PEI (10000 g/mol) may interfere the CO_2 diffusivity. The membrane of PEBA with PEI 800 g/mol grated TiO_2 at 3%wt, especially at PEI/DA ratio 1:1, gives the best efficiency for gas separation.

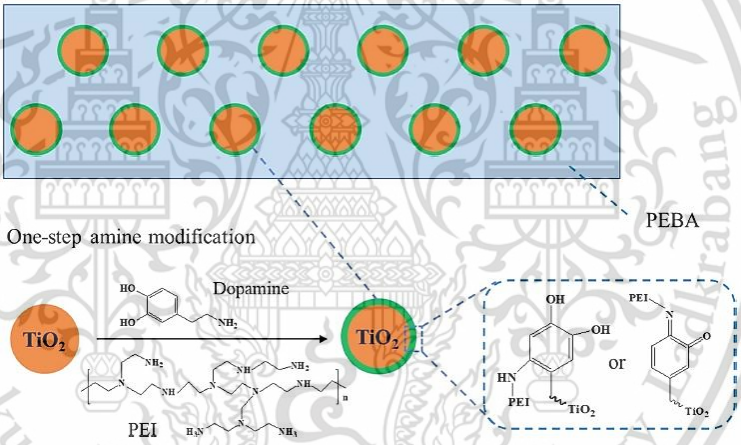

Figure 2.24 Schematic structure of the DP/PEI grafted TiO_2/PEBA MMM

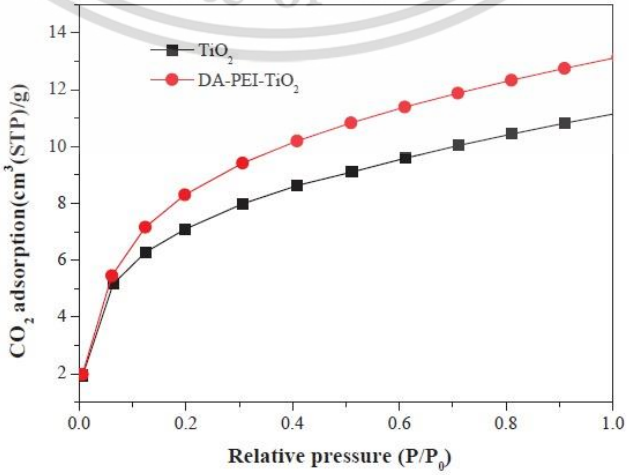

Figure 2.25 CO_2 adsorption isotherm at 298 K of unmodified and modified TiO_2

Sonpoo T. et al. [26], reported the mechanical properties and water vapor permeability (WVP) of LDPE films by blending with EVA, EVOH and zeolite A (20%wt) for a longer shelf-life packaging of fresh product. Effect of the mass ratio of LDPE/EVA/EVOH (80/20/0, 80/15/5, 80/10/10, 80/5/15, 80/0/20) were investigated. All compounds were prepared using an internal mixer and films were formed by compression molding process. The result from DSC revealed that the crystallinity was increased when EVOH was added in LDPE/ EVA/ EVOH films. In addition, Young's modulus was increased in LDPE/ EVA/ EVOH films that has higher EVOH and zeolite A loading. This is owing to semi-crystalline structure of EVOH, which induces by an internal hydrogen bonding. Moreover, zeolite A is a solid particle that plays key-role in an increment of modulus. On the other hand, the LDPE/ EVA/ EVOH films had similar tensile strength at yield and tensile strength at break as compared with LDPE films. The WVP of all LDPE/ EVA/ EVOH films were in the same range because of polarity of EVOH. In conclusion, WVP depended on morphology and polarity of the film. However, when the zeolite A was incorporated in LDPE/EVA/EVOH, the WVP markedly enhanced due to high polarity and selectivity of the zeolites.

Amooghin A.E. et al. [44], modified the membrane of acrylonitrile butadiene styrene (ABS) with polyethylene glycol (PEG) for separation CO_2 from CO_2/N_2 streams. Effect of M_w of PEG (400, 1000, 1500, 4000, 10000 and 20000 g/mol) on gas permeability was examined. It was noticed that an increasing M_w of PEG resulted a slightly increased CO_2 permeability. This is because PEGs with high M_w (20000 g/mol) has a higher polar moiety density in main chain that leads to an increase in flexibility and enhances the interaction between polar ether group of PEG and CO_2 molecules. On the other hand, PEGs with low M_w has small amount of polar moiety (polar ether groups) density in main chain and so acts as plasticizer to separate chains from each other. However, PEG with high M_w had potentially to form crystalline region. Thus, it might be concluded that PEG has an inverse effect between the negative effect of crystallinity and the positive effect of polar moiety density and main chain flexibility. Additionally, it was found that when having high content (>10-30%wt) of PEG with M_w 20000 g/mol, the CO_2 permeation was decreased because of an obstacle role in CO_2 diffusion through the membrane.

Isanejad M. and Mohammadi T. [45], studied the effects of amine modification on the surface of fumed silica in nanocomposite membranes for CO_2/CH_4 separation. 3-Aminopropyltriethoxysilane (APTES) was used as a coupling agent between the fumed silica (SiO_2) and poly(ether-block-amide) (PEBAX) in order to improve compatibility of organic and inorganic materials as well as increasing the interactions with CO_2 molecules. The results from FTIR and CHN analysis confirmed that successful APTES-grafting on SiO_2 surface was occurred. However, only some of amine sites are "active" to react with CO_2 molecules because of the possibility for the aminopropyl chains to attach undesirably on the surface (Figure 2.26). In addition, the result from field emission scanning electron microscope (FESEM) revealed that both neat SiO_2 and amine functionalized silica (AFS) with 5-15%wt loadings had well-dispersed without bulky agglomeration in PEBAX. The result from XRD suggested that the total of crystallinity of membranes was reduced when the AFS was dispersed in membrane. This is because the hydrogen bonding between polymer segments was disrupted from a presence of nanoparticles. Moreover, it was found that CO_2 adsorption on AFS was higher than that of SiO_2 surface. This is because the nucleophilic interaction between CO_2 molecules with NH_2 functional groups was stronger than that of OH groups. When AFS loading was increased from 0-10%wt, CO_2 permeability was also enhanced owing to increasing in polymer fraction free volume (FFV), d-spacing and chain mobility. In contrary, AFS loading was increased above 10%wt, it acted as the blocker, which obstructs the gas diffusion paths and increases tortuosity of the permeation paths. Therefore, the CO_2 permeability was declined when increasing filler loading at 10-20%wt (Figure 2.27). Besides, the CO_2/CH_4 selectivity of the membranes was improved with 0-15%wt of nanoparticle loading but a decrease trend was observed at 20%wt owing to formation of voids in the polymer matrix.

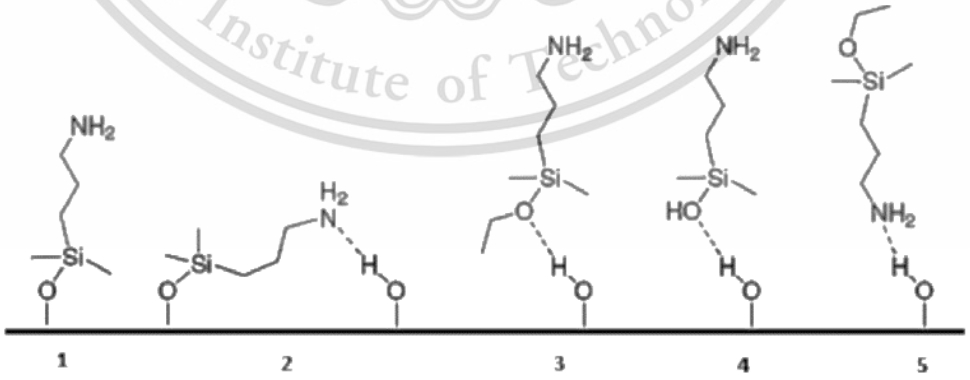

Figure 2.26 Various interactions of aminosilane molecules on the SiO_2 surface

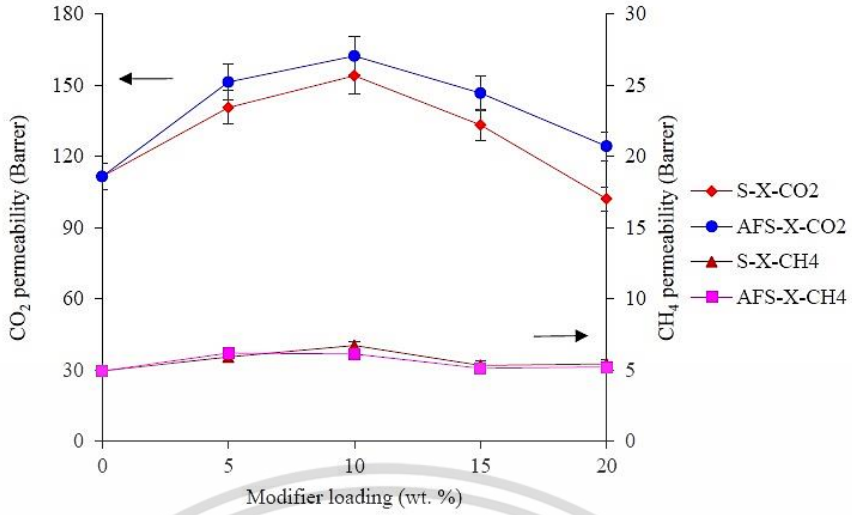

Figure 2.27 CO_2 and CH_4 permeabilities of unmodified SiO_2 (S) and AFS membranes

Rahman MD. M. et al. [46], modified matrix of different PEBAX® (PEBAX® MH 1657 and PEBAX® 2533) with PEG functionalized POSS (PEG-POSS) for CO_2 separation. Polyoctahedral oligomeric silsesquioxanes (POSS) is an organic-inorganic hybrid nano-composite material that is rigid cage-like structure. POSS has an empirical formula $(RSiO_{1.5})_n$, n=6-12 and R is various types of functional groups. The mixtures of PEG-POSS and PEBAX® were prepared by solution casting in Teflon molds. The result from DSC revealed that glass transition temperature (T_g) of neat PEBAX® 2533 was lower than that of PEBAX® MH 1657 owing to the different amounts of polyether content in polyether phase. Furthermore, the thermal transition of polyamide segment in both PEBAX was not affected by the incorporation of PEG-POSS nanoparticles. However, a decrease in thermal transition of PE segment of PEBAX® MH 1657 was observed. The results from AFM indicated that surface roughness of PEBAX® MH 1657 was higher, as compared with that of PEBAX® 2533. The SEM micrograph exhibited that surface of PEBAX® MH 1657 nanocomposite membrane had a needle like structure (Figure 2.28(a)). In contrast, surface of PEBAX® 2533 nano-composite membrane showed distinct darker regions with a needle like structure, and smoother regions appeared bright (Figure 2.28(b)). Moreover, gas permeability of both nanocomposite membranes tended to increase when amount of PEG-POSS was added from 0-30%wt but a decreasing tend was gained after at 30%wt. The selectivity of both nanocomposite membranes did not change significantly when the nanoparticle was incorporated. However, CO_2/N_2 selectivity gave the highest value, as compared with CO_2/O_2, CO_2/CH_4 and CO_2/H_2.

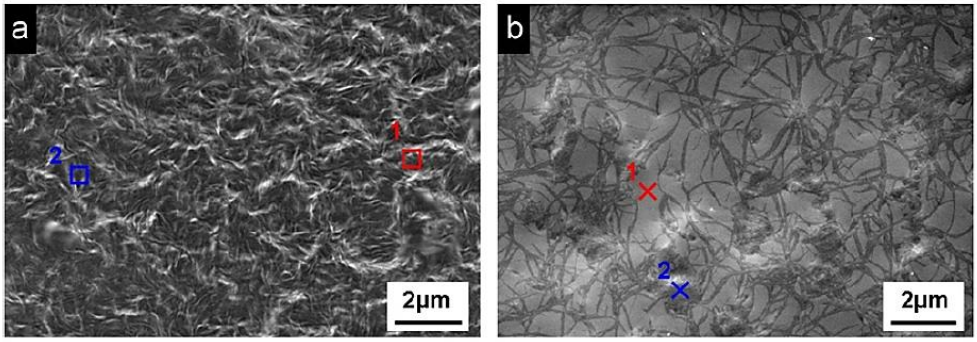

Figure 2.28 SEM micrographs of a) PEBAX® MH 1657 nanocomposite membrane and b) PEBAX® 2533 nanocomposite membrane

Xing R. and Ho W.WS. [47], prepared crosslinked polyvinyl alcohol/ polyethylene glycol (PVA/PEG) blend membranes for CO_2/CH_4 separation. Glutaraldehyde was chosen to use as crosslinking agent. Effects of crosslinking time (40-115 min), PEG loading content (≥50%wt) and molecular weight of PEG (200, 300, 550, 775 and 1000 g/mol) were investigated. Then the appropriate formula was selected for examining the effect of zeolite 5A loading. The result showed a continuous decrease in CO_2 permeability when crosslinking time was increased. This is owing to reduction of chain mobility and decreasing in fraction of free volume. However, CO_2/CH_4 selectivity was increased with increasing the crosslinking time 40 to 84 min. In contrast, after 84 min, the CO_2/CH_4 selectivity was decreased owing to loss of hydroxyl groups from crosslink reaction. Effect of PEG (200 g/mol) loading showed that the CO_2 permeability of membrane was declined when PEG loading was above 50%wt due to an enhancing crosslink and the entanglement of PEG with PVA. In addition, an increase in CO_2/CH_4 selectivity was observed with up to 64%wt PEG loading. However, at higher than 64%wt PEG loading, the CO_2/CH_4 was then dropped. This is because of intensified interaction between CO_2 and polar ether but the excess amount of PEG resulted in non-selective gas permeation. The molecular weight of PEG had slight effect on the CO_2/CH_4 selectivity. Conversely, CO_2 permeability gradually decreased with an increase of PEG molecular weight. Additionally, it was found that when amount of zeolite 5A was increased, an enhancement of CO_2 permeability was achieved. Due to the fact that, permeated CO_2 not only pass through polymer matrix, but also could pass through the porous network formed by interconnected zeolite 5A particles. However, CO_2/CH_4 selectivity was decreased as the zeolite loading increased because of the poor adhesion between zeolite particles and the PVA/PEG blend.

From the researches as mentioned above, the elastic modulus and maximum tensile strength of partially hydrolyzed EVA membranes (p-EVA) were greater than that of EVA membrane. This might be caused by the intermolecular hydrogen bonds between hydroxyl groups in p-EVA. In addition, PEG with various molecular weights provided high CO_2 permeability owing to the quadrupole-dipole interaction between ether functional group with CO_2 molecules and also acted as the plasticizer in the polymer matrix, resulting in additional fraction free volume and allowing more chain flexibility. The addition of amine-functionalized silica (AFS) particles into the polymer also gave a higher CO_2 permeability because of the nucleophilic reaction between CO_2 molecules and NH_2 functional groups. Therefore, in this research, the EVA was partially hydrolyzed for increasing the mechanical properties. PEG with M_w of 400 and 1450 g/mol was blended with p-EVA for increasing the CO_2 permeation. Subsequently, SiO_2 surface was functionalized with 3-aminopropyltriethoxysilane (APTES) prior to add into the membrane for enhancement the CO_2/CH_4 selectivity as well as the CO_2 solubility.

Chapter 3
Research methodology

3.1 Chemicals and materials

1. Ethylene vinyl acetate copolymer (EVA): Escorene® LD 783.ND, ExxonMobil Chemical Co., Ltd.

Table 3.1 Specification of ExxonMobil Escorene® LD 783.ND [48]

Properties	Value
Vinyl acetate content, %	33
Melt flow index (190 °C, 2.16 kg), g/10 min	43
Density, g/cm^3	0.955
Melting point, °C	57.8
Hardness (shore A)	55
Tensile strength at break, psi	440
Elongation at break, %	≥800
Flexural modulus (1% secant), psi	1820

2. 3-Aminopropyltriethoxysilane (APTES) 99%, Thermo Fisher Scientific Inc.

Table 3.2 Specification of APTES [49]

Properties	Value
Physical state	Liquid
Appearance	Colorless
Odor	Rotten-egg like
Boiling point, °C	217
Specific gravity	0.942
Solubility	React with water

3. Polyethylene glycol, 400 (PEG 400): CARBOWAX™ SENTRY™ 400, The Dow Chemical Co., Ltd.

Table 3.3 Specification of CARBOWAX™ SENTRY™ 400 [50]

Properties	Value
Molecular weight (g/mol)	380 - 420
Hydroxyl number, mg/g	264-300
Physical state	Liquid
Appearance	Colorless
Boiling point, °C	>200
Density, g/cm^3 at 20 °C	1.1255

4. Polyethylene glycol, 1450 (PEG 1450): CARBOWAX™ SENTRY™ 1450 NF Flake (Inhibited), The Dow Chemical Co., Ltd.

Table 3.4 Specification of CARBOWAX™ SENTRY™ 1450 NF Flake (Inhibited) [51]

Properties	Value
Molecular weight (g/mol)	1,305 - 1,595
Hydroxyl Number, mg/g	70-86
Physical state	Waxy solid (Flake)
Average Number of Repeating Oxyethylene Unit	32
Melting point, °C	43-46
Boiling point, °C	>200

5. Silica (SiO_2): Hi-Sil™ 255CG-D, PPG Industries, Inc.

Table 3.5 Specification of Hi-Sil™ 255CG-D [52]

Properties	Value
Particle size, nm	5-20
Surface area (BET-5), m^2/g	175
pH-value	6.3
Na_2SO_4, wt.%	2.0 Max
Skeletal density, g/cm^3	2.1

6. Potassium hydroxide (KOH): CARLO ERBA Reagents Co., Ltd.
7. Xylene (Analytical grade): CARLO ERBA Reagents Co., Ltd.
8. Toluene (Analytical grade): CARLO ERBA Reagents Co., Ltd.
9. Dichloromethane (Analytical grade): CARLO ERBA Reagents Co., Ltd.
10. Ethanol (Commercial grade)
11. Methanol (Commercial grade)
12. Distilled water
13. Paraffin oil
14. Helium gas, (Purity 99.9%): Praxair (Thailand) Co., Ltd.
15. Carbon dioxide gas, (Purity 99.9%): Thai industrial Gases Co., Ltd.
16. Methane gas, (Purity 99.9%): Guangdong Huate Gas Co., Ltd (China)

3.2 Apparatus

1. Hot plate and thermocouple
2. pH-indicator strips: Merck Co., Ltd.
3. Filter paper: GE Healthcare Inc.
4. Micrometer: OZAKI MFG Co., Ltd.
5. Permeation cell
6. Permeation rig
7. Water aspirator with suction flask and Buchner funnel
8. Oven (UN 500): Memmert (Germany) Co., Ltd.
9. Ultrasonic bath (208H ULTRAsonik): NEY Co., Ltd.
10. Compression molding machine: LabTech Engineering Co., Ltd.
11. Universal testing machine (LR 5K): LLOYD Instrument Co., Ltd.
12. Thermal conductivity detector: Valco Instruments Co., Ltd.
13. Differential scanning calorimeter (DSC 204 F1 Phoenix): Netzsch Co., Ltd.
14. X-ray Photoelectron Spectroscopy (AXIS ULTRA): Kratos Analytical Inc.
15. Scanning electron microscope (JSM-5410LV): JEOL Co., Ltd.
16. Fourier-transform infrared spectrometer (IRTracer-100): Shimadzu Co., Ltd.
17. Elemental analyzer (CHNS) (Flashsmart): Thermo Fisher Scientific Co., Ltd.

3.3 Synthesis of partially hydrolyzed EVA (p-EVA)

In a 500 ml round bottom flask with condenser, 25 g of the EVA was added in 250 ml of xylene before placing in an oil bath and stirred using a magnetic bar at 100 °C until the solution was homogeneous. Then the temperature of mixture solution was decreased to 80 °C in order to add 32 ml alcoholic KOH solution (0.5 mol/l). The reaction was continuously stirred for 3 h at 100 °C. Thereafter, the pH of residual KOH was controlled at 7 and rechecked by pH paper. The reaction solution was then poured

into 2L of methanol to obtain precipitation. The precipitated polymers were cut into pieces and washed repeatedly with methanol and distilled water to remove organic solvent and inorganic salts, respectively. Finally, it was dried overnight in an air oven at 50 °C.

3.3.1 Investigation of %hydrolysis of EVA from hydrolysis reaction

Carbonyl index (C.I.) is an indirect method for evaluation %hydrolysis inspection of EVA after hydrolysis, which were determined using FTIR in Attenuated Total Reflectance (ATR) mode in the wavenumber range of 650-4000 cm^{-1}. Then, the ratio between absorbance peak of C=O stretching at 1714 cm^{-1} and absorbance peak of C-H rocking at 720 cm^{-1} was calculated as equation 3.1 [26].

$$C.I. = \frac{\text{Area under absorbance peak at 1714 } cm^{-1}}{\text{Area under absorbance peak at 720 } cm^{-1}} \quad (3.1)$$

3.4 Surface modification of SiO_2

3.4.1 Preparation of amine functionalized SiO_2

SiO_2 was functionalized with amine before loaded into the polymer matrix. First, the ethoxy groups of APTES was hydrolyzed for grafting aminopropyl chains of APTES on the surface of SiO_2. The hydrolysis procedure was carried out using acidic water (pH=2) and 16 %v/v methanolic APTES solution in which H_2O/APTES was equal to 2:3 by mole. In a 50 ml round bottom flask containing 11.6 ml of APTES-methanol solution, 0.2 ml of acidic water was added dropwise under vigorously stirring. After 6 h, the hydrolyzed APTES was ready to be used in the functionalization reaction [45].

In a 250 ml three-neck round bottom flask, 5 g of non-porous SiO_2 was dispersed uniformly in 120 ml of anhydrous toluene via an ultrasonic homogenizer for 20 min. After that, the hydrolyzed APTES was added into the solution, and the mixture was stirred overnight at 110 °C under N_2 atmosphere. After completion of the reaction time, the product was filtered and washed with ethanol and then dried in an oven at 65 °C overnight, light-yellow of the amine functionalized SiO_2 (AFS) was obtained. The mechanism of amine functionalization is shown in Figure 3.1

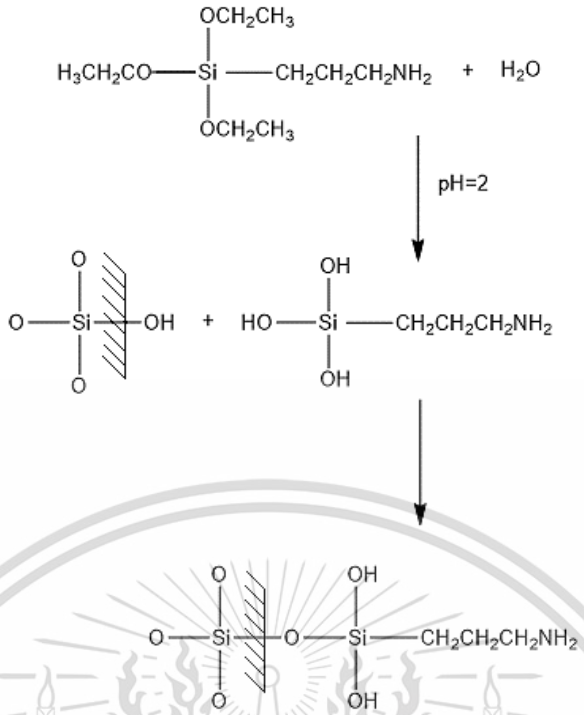

Figure 3.1 Mechanism of amine functionalization reaction of SiO_2

3.4.2 Characterization of amine functionalized SiO_2

3.4.2.1 The binding energy of chemical bonds

Binding energy of unmodified SiO_2 and amine-functionalized SiO_2 were conducted using the X-ray photoelectron spectroscopy (XPS). The monochromatic AlKα was used as a source (anode HT = 15 kV). The XPS peaks were referenced to the binding energy of C1s, O1s, Si2p and N1s peaks at about 284.8, 532.9, 103.5 and 400 eV, respectively. The sample was attached onto a stub with a carbon tape. It was placed in a chamber and the internal pressure was decreased down to 1×10^{-8} torr at room temperature. The qualitative spectra of the samples were collected. The correction of the background due to a carbon substrate was also performed.

3.4.2.2 CHNS elemental analysis [53]

The amine-functionalized SiO_2 (AFS) was conducted to examine the number of amine sites in a certain amount of sample using a CHNS elemental analyzer. The sample was combusted in a pure O_2 environment and then the gasses were carried through the system by He, converted and measured as CO_2, H_2O, N_2, and SO_2. These gasses were separated under steady-state conditions and detected by thermal conductivity. The percentages of C, H and N elements in the samples were reported.

3.4.2.3 Calculation an efficiency of functionalization by back titration

In 50 ml of round bottom flask, 10 mg of AFS nanoparticles were dispersed in 20 ml of HCl solution (1.0 mM) and stirred for 40 min. Then AFS were separated by centrifugation at 9000 rpm for 10 min. The colorless solution was collected to be titrated with the standardized NaOH solution (1.0 mM) in the presence of phenolphthalein indicator. From the difference of HCl concentrations after treating with AFS particles, the molar concentration of active amine sites on the AFS particles was estimated. This value was converted to the number of amine sites per unit area (nm^2) of the surface of SiO_2 [54].

3.5 Partially hydrolyzed EVA modification

3.5.1 Addition of PEG by solution blending

3 g of partially hydrolyzed EVA (p-EVA) was dissolved in a 250 ml round bottom flask with condenser containing 150 ml of mix solvents (toluene/dichloro-methane, 85:65 v/v). The mixture solution was placed in an oil bath and stirred using a magnetic bar at 55 °C until homogeneous solution was obtained. Then PEG was added and stirred for 3 h. Subsequently, the solution was poured on a glass plate, which is covered by punched aluminum foil for controlled evaporation at room temperature overnight. The resulting polymeric membrane was removed from the glass plate and further dried at 40°C in an air oven for 12 h to remove the residual solvents.

3.5.2 Addition of modified SiO_2 into p-EVA/PEG blend membrane

In a 250 ml round bottom flask containing 85 ml of toluene, modified SiO_2 was dispersed uniformly by sonication for 30 min. Afterward, 65 ml of dichloromethane and PEG were added and stirred using a magnetic bar at 55 °C until a homogeneous solution was observed. 3 g of p-EVA was then added into the solution and continued stirring for 3 h. Thereafter, the solution was poured on a glass plate, which is covered by punched aluminum foil for controlled evaporation at room temperature overnight. The resulting polymeric membrane was removed from the glass plate and further dried at 40°C in an air oven for 12 h to remove the residual solvents.

3.6 Formulation of modified EVA membranes

The compositions of modified EVA membranes with PEG and AFS are listed in Tables 3.6 and 3.7.

Table 3.6 Formula of modified EVA membranes with PEG loadings

Formula	PEG (%wt)		Weight content (g)		
			p-EVA	PEG	
	400	1450		400	1450
EVA	-	-	-	-	-
p-EVA	-	-	3	-	-
p-EVA/5PEG400*	5	-	3	0.16	-
p-EVA/10PEG400	10	-	3	0.33	-
p-EVA/15PEG400	15	-	3	0.53	-
p-EVA/5PEG1450	-	5	3	-	0.16
p-EVA/10PEG1450	-	10	3	-	0.33
p-EVA/15PEG1450	-	15	3	-	0.53

Example definition:

** p-EVA/5PEG400 = partially hydrolyzed EVA was blended with 5%wt of PEG 400 g/mol*

Table 3.7 Formula of modified EVA membranes with PEG and AFS

Formula	PEG (%wt)		AFS (%wt)	Weight content (g)			
				p-EVA	PEG		AFS
	400	1450			400	1450	
p-EVA/15PEG400-0.3AFS*	15	-	0.3	3	0.53	-	0.006
p-EVA/15PEG400-0.6AFS	15	-	0.6	3	0.53	-	0.012
p-EVA/15PEG400-0.9AFS	15	-	0.9	3	0.53	-	0.018
p-EVA/15PEG1450-0.3AFS	-	15	0.3	3	-	0.53	0.006
p-EVA/15PEG1450-0.6AFS	-	15	0.6	3	-	0.53	0.012
p-EVA/15PEG1450-0.9AFS	-	15	0.9	3	-	0.53	0.018

Example definition:

**p-EVA/15PEG400-0.3AFS = partially hydrolyzed EVA was blended with 15%wt of PEG 400 g/mol and added 0.3%wt of AFS*

3.7 Membrane preparation

p-EVA/PEG and p-EVA/PEG-AFS membranes were prepared using a compression molding machine. Firstly, the compound was rapidly compressed twice to remove the air bubbles. Then, the compound was compressed to obtain a thin film. Finally, the thin film was cooled with cold water. The films were prepared into 2 sizes:

1. The membranes for permeation test: membrane thickness is about 60-80 μm with a diameter 6×6 cm^2 by weighing compound about 0.35 g.

2. The membranes for mechanical test: membrane thickness is about 60-80 μm with a diameter 10 cm by weighing compound about 0.7 g.

The compression molding condition is shown as follows:

Mold size	20×20×1 cm^3
Pressure of pressing	1000 psi
Temperature of hot press	180 °C
Time of preheating mold	10 min
Time of preheating polymer	10 min
Time of hot press	10 min
Temperature of cold press	18 °C
Time of cold press	10 min

3.8 Characterizations

3.8.1 Determination of functional group

FTIR spectrum of the membrane sample was detected using an IRTracer-100 with Attenuated Total Reflectance (ATR) mode. The average of 32 scans was taken in the wavenumber range of 600-4000 cm^{-1} to investigate the functional groups and determine the changes of chemical composition of synthesized membranes.

3.8.2 Investigation of thermal analysis

Differential scanning calorimetry (DSC) was employed for evaluation of glass transition temperature (T_g), melting temperature (T_m), crystallization temperature (T_c) and %crystallinity. A sample was examined by a DSC 204 F1 Phoenix. Approximately 5-10 mg of sample was placed in aluminum pan. The sample was heat up from -100 to 100 °C with a heating rate of 10 °C/min under N_2 atmosphere, then cooled down to room temperature with a cooling rate of 10 °C/min. [55] The degree of crystallization (X_c) of EVA was calculated following equation 3.2.

$$\%\text{Crystallization} = \frac{\Delta H_f \times 100}{\Delta H_f^0} \times \frac{100}{\%\text{ of polymer in the sample}} \quad (3.2)$$

Where ΔH_f is the enthalpy of melting

ΔH_f^0 is the enthalpy of 100% crystalline polyethylene (PE) (293J/g) [56]

3.8.3 Investigation of morphology

The surface and cross-sectional morphologies of the membranes were examined using scanning electron microscope (JSM-5410LV) at accelerating voltage of 10 KV. Before analysis, the membranes were cut to size 1×3 cm^2 and immersed in liquid nitrogen about 45 min and then cryogenically fractured. Thereafter, PEG contents in the membrane were extracted by immersion in distilled water and sonicated (44-48 KHz) for 30 min. Eventually, the samples were sputtered with metallic gold to obtain an adequate contrast of the micrograph [39].

3.8.4 Mechanical property test

Tensile properties of the membrane sample with dimension of 10×80 mm^2 were determined using a universal testing machine (LR 5K) at room temperature according to ASTM D882 (Figure 3.2). The tensile properties including tensile strength at break, %elongation at break and Young's modulus were evaluated. In order to obtain plausible data, 5 samples of each formula were measured and the average value was reported. The tensile testing conditions are as follows [17]:

Load cell	100 N
Test speed	100 mm/min
Gauge length	25 mm

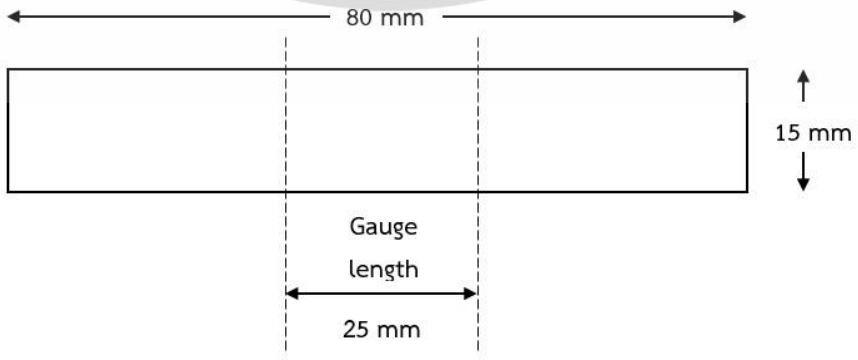

Figure 3.2 Schematic of test specimens

Tensile strength at break, %elongation at break and Young's modulus can be calculated from the following equations:

$$\text{Tensile strength} = \frac{\text{Maximum force at break}}{\text{Original cross-section area of sample } (mm^2)} \quad (3.3)$$

$$\%\text{Elongation at break} = \frac{(\text{Final-Original gauge length})}{\text{Original gauge length}} \times 100 \quad (3.4)$$

$$\text{Young's modulus (taking a slope between 3-5\% elongation)} = \frac{\text{Stress}}{\text{Strain}} \quad (3.5)$$

3.8.5 Permeation test [17,54]

The CO_2 and CH_4 gas permeabilities of the membrane was observed using the principle of concentration gradient in atmospheric pressure. The membrane size of 6×6 cm^2 was placed in the permeation cell, which has the gas permeation area of 5×5 cm^2. Permeation cell includes two pieces of polypropylene (PP) plates sandwiched with two O-ring seal plates to avoid gas leakage and covered with two metal plates. The permeation cell was tightened with four screws. The permeation cell is depicted in Figure 3.3.

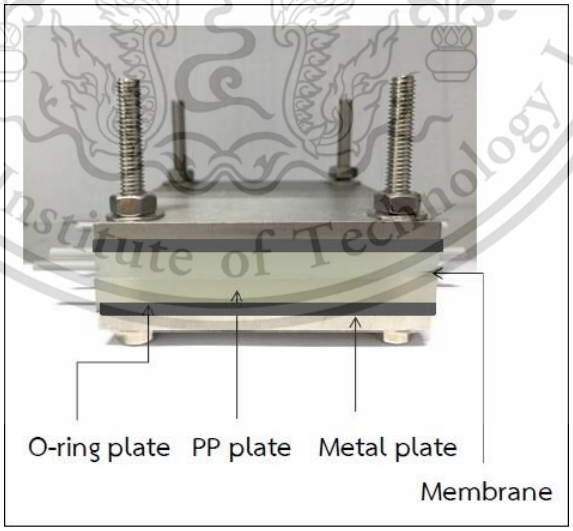

Figure 3.3 Permeation cell of the permeation test

Feed gas (CO_2 or CH_4) was flowed into the lower plate (Feed side) while carrier gas (He) was flowed into the upper plate (Permeate side) of the permeation cell. The

flow rates of the feed gas and the carrier gas were 30 ml/min. These gases separately controlled using mass flow controllers. The mechanism of permeation cell can describe: as the feed gas flow across the film surface and some gas could diffuse through the membrane to the permeating side. The permeated gas was conveyed by the carrier gas into the permeate outlet and analyzed using the thermal conductivity detector (TCD). In contrast, some gas could not diffuse through the membrane and then it was passed to the retentate outlet and vented as shown in Figure 3.4 and schematic of permeation rig is illustrated in Figure 3.5.

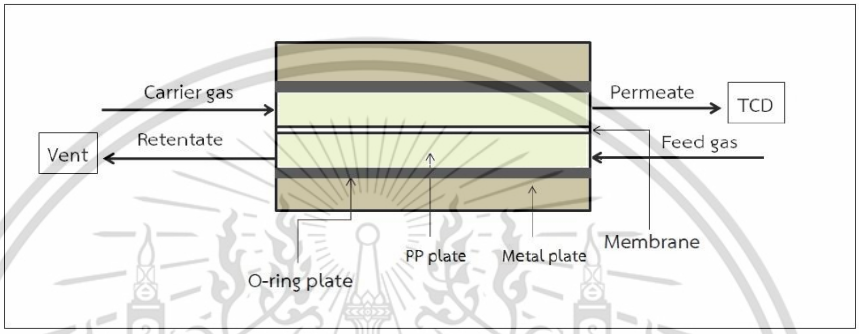

Figure 3.4 Schematic of the permeation test

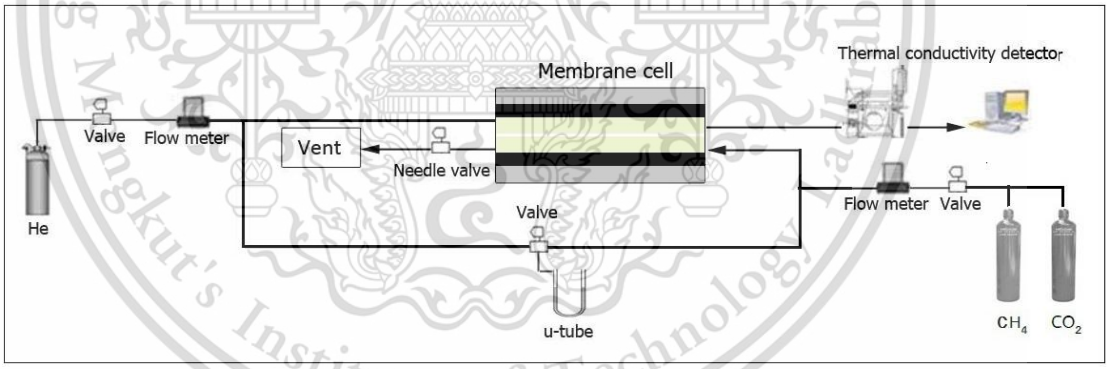

Figure 3.5 Schematic of the permeation rig

Gas permeability of the membrane can be evaluated from sample area under a TCD signal (Peak area), which is calibrated with standard gas. The CO_2 permeation rate can be calculated in the equation 3.6.

$$CO_2 \text{ permeation rate } (g/m^2 \cdot day) = \frac{J}{S_C} \quad (3.6)$$

When J = Transmission rate of CO_2 (g/day)

S_c = Area of permeation cell (m^2)

Transmission rate (J) of CO_2 can be calculated in the equation 3.7.

$$J = \frac{\left[\left(\frac{A_{CO_2}}{A_S}\right) \times P \times M_w \times F_f\right]}{R \times T} \times 1440 \quad (3.7)$$

When A_{CO_2} = Peak area of the permeated CO_2 (V·s)

A_s = Peak area of the standard CO_2 (V·s)

P = Pressure (atm)

M_w = Molecular weight of CO_2

F_f = Flow rate of the feed gas (L/min)

R = Ideal gas constant (L·atm/K·mol)

T = Temperature (K)

1440 = minutes in 1 day

The CH_4 permeation rate (Q) can be calculated in the equation 3.8.

$$CH_4 \text{ permeation rate } (g/m^2 \cdot day) = \frac{Q}{S_c} \quad (3.8)$$

When Q = Transmission rate of CH_4 (g/day)

S_c = Area of permeation cell (m^2)

Transmission rate of CH_4 can be calculated in the equation 3.9.

$$Q = \frac{\left[\left(\frac{A_{CH_4}}{A_S}\right) \times P \times M_w \times F_f\right]}{R \times T} \times 1440 \quad (3.9)$$

When A_{CH_4} = Peak area of the permeated CH_4 (V·s)

A_s = Peak area of the standard CH_4 (V·s)

P = Pressure (atm)

M_w = Molecular weight of CH_4

F_f = Flow rate of the feed gas (L/min)

R = Ideal gas constant (L·atm/K·mol)

T = Temperature (K)

1440 = minutes in 1 day

In addition, the CO_2/CH_4 selectivity (α_{CO_2/CH_4}) of the membranes can be estimated in the equation 3.10.

$$\alpha_{CO_2/CH_4} = \frac{CO_2 \text{ permeation rate}}{CH_4 \text{ permeation rate}} \quad (3.10)$$

Chapter 4
Results and discussion

This research developed the high CO_2/CH_4 selective membrane for the application of biogas purification by CO_2 removal. EVA copolymer with 33% of VA and PEG with molecular weights of 400 and 1450 g/mol are chosen as additive materials for the membranes. EVA is partially hydrolyzed as named p-EVA before blending with PEG at 5, 10 and 15%wt. In addition, the SiO_2 surface is modified by functionalization with 3-aminopropyltriethoxysilane (APTES) before adding SiO_2 into the blends of p-EVA/PEG for increasing the CO_2/CH_4 selectivity. The membranes are characterized for FTIR analysis, morphology, thermal and mechanical properties, including gas permeability. Research results are divided in terms of the factors affecting of the membranes into 3 parts; 1) hydrolysis of EVA, 2) PEG molecular weight and loadings and 3) surface-modified SiO_2 content.

4.1 Effect of EVA hydrolysis

EVA was partially hydrolyzed via hydrolysis reaction using KOH as a catalyst in order to enhance the polarity and mechanical properties of the films. Effect of partially hydrolysis of EVA on the properties of film was investigated.

4.1.1 FT-IR analysis & %hydrolysis calculation

The partially hydrolyzed EVA (p-EVA) was obtained from hydrolysis reaction, as shown in Figure 4.1. The spectrum of p-EVA is noticeable that the peak intensities at 1740 cm^{-1} (carbonyl groups) and 1210 cm^{-1} (ester groups) are sorely decreased. Meanwhile, the peak at 3300 cm^{-1} (hydroxyl group) is clearly seen. This is because after the hydrolysis reaction, acetate groups are converted to be the hydroxyl groups [40]. However, the peak of carbonyl group can be still observed because of the incomplete hydrolysis of acetate groups, as depicted in Figure 4.2. Therefore, the results confirmed that the partially hydrolyzed EVA is successfully prepared.

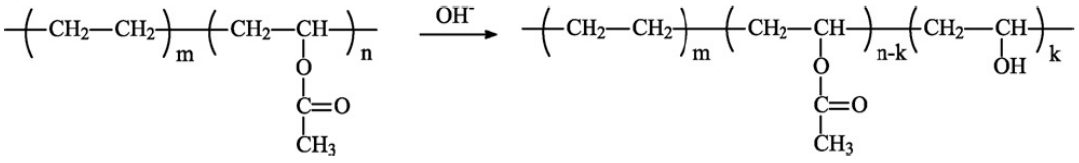

Figure 4.1 Hydrolysis reaction of EVA [40]

The percentage of EVA hydrolysis was determined via indirect method using carbonyl index (C.I). After complete reaction time (3 h), EVA is hydrolyzed for 44%. The calculation of carbonyl index is exhibited in Appendix A.

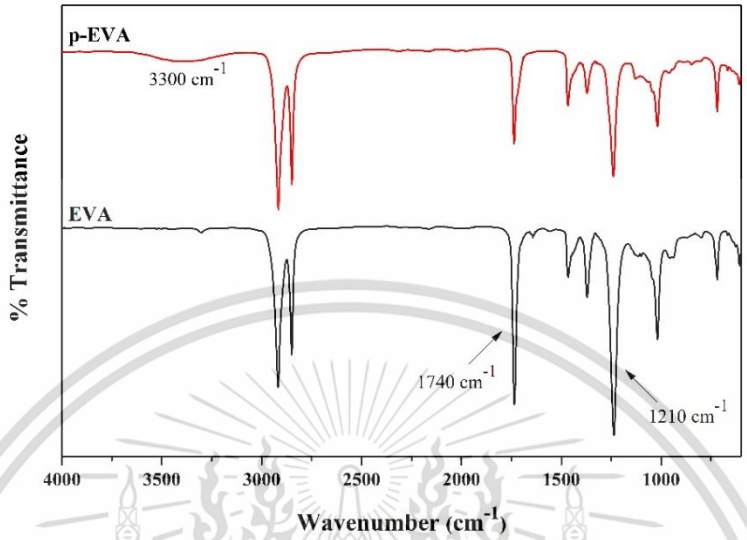

Figure 4.2 ATR-FTIR spectra of EVA and p-EVA

4.1.2 Mechanical properties of the membranes

Tensile strength, %elongation at break and Young's modulus of EVA and p-EVA membranes are exhibited in Figures 4.3-4.5, respectively. It is found that tensile strength and Young's modulus of p-EVA membrane are increased meanwhile, %elongation at break is decreased, as compared with the EVA membrane. This is because of the effect from hydrogen bonding (-OH groups) that is initiated after hydrolysis reaction, which is confirmed by FT-IR analysis. The hydrogen bonds between polymer chains lead to the chains attached to each other, so the crystallinity of the membrane is increased. From the reasons mentioned, the membrane has high strength and good hardness. Therefore, it can be concluded that the mechanical properties of the membrane are effectively improved.

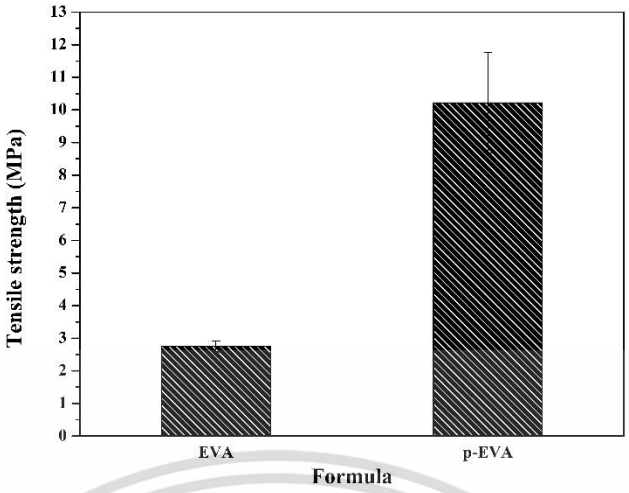

Figure 4.3 Tensile strength of EVA and p-EVA

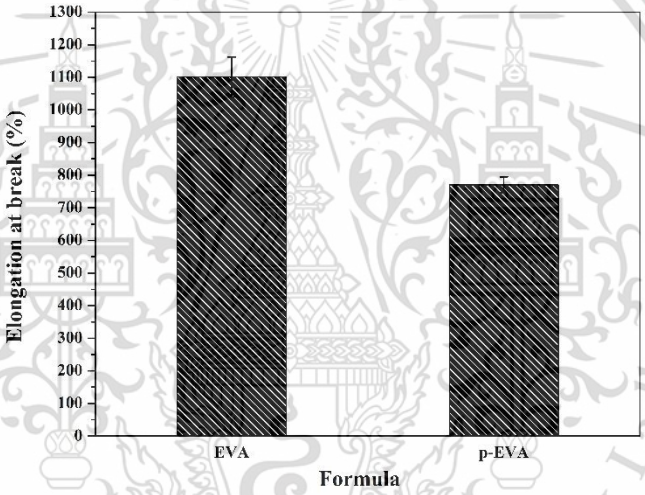

Figure 4.4 %Elongation at break of EVA and p-EVA

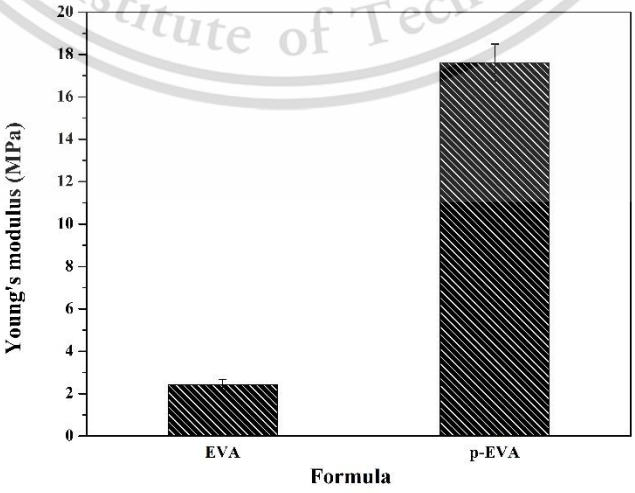

Figure 4.5 Young's modulus of EVA and p-EVA

4.1.4 Gas permeation of the membranes

The CO_2 and CH_4 gas permeabilities of EVA and p-EVA membranes are demonstrated in Figure 4.6. The signals from thermal conductivity detector (TCD) of these gasses were obtained to calculate the CO_2 and CH_4 permeation rates as shown in Appendix B.

From Figure 4.6, it is seen that the EVA membrane has greater gas permeabilities than p-EVA membrane. EVA is the semi-crystalline polymer that consists of 2 segments: ethylene and vinyl acetate. The ethylene segment could arrange chains to be the crystalline phase, resulting in low gas permeability. Conversely, the gas can be easily passed through vinyl acetate segment. Since the segment of vinyl acetate has the steric effect from acetate groups (-$COOCH_3$), which obstruct the chain packing, so this area becomes a part of amorphous region. Moreover, it can be noted that EVA membrane has CO_2 permeation rate (317.04 g·m^2/day) higher than CH_4 (38.36 g·m^2/day). This is owing to the polarity effect of carbonyl groups in acetate segment having a strong interaction with CO_2 molecules.

On the other hand, even though the p-EVA membrane has a higher polarity from -OH groups, as compared with EVA, but crystalline region due to the hydrogen bond is occurred, so the diffusion pathway of gas is obstructed. Consequently, p-EVA membrane has low gas permeabilities for both CO_2 and CH_4.

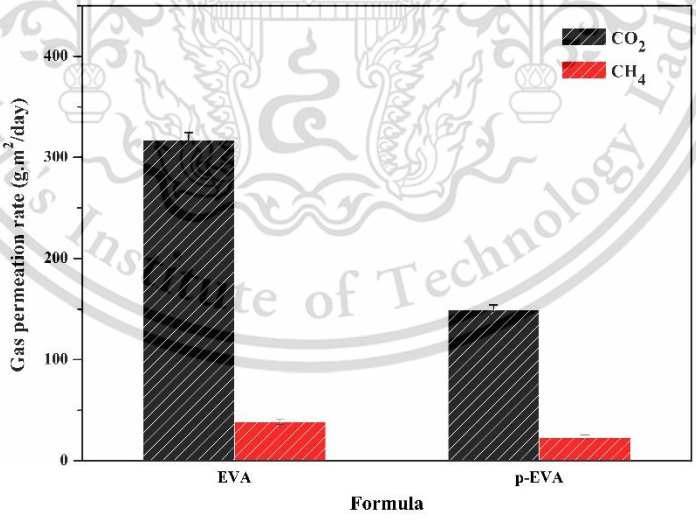

Figure 4.6 The comparison of gas permeation rate between EVA and p-EVA

4.2 Effect of PEG molecular weight and loadings

Because of the decrement of CO_2 and CH_4 permeabilities of the membrane after hydrolysis reaction, the PEG with the molecular weight of 400 or 1450 g/mol was added into p-EVA at 5, 10 and 15%wt (EVA:PEG weight ratios of 95:5, 90:10 and 85:15). The effect of polyethylene glycol on p-EVA/PEG blended membrane was examined.

4.2.1 FTIR analysis

Figures 4.7 and 4.8 present the ATR-FTIR spectra of p-EVA, PEG and p-EVA/PEG blended membranes with PEG with M_w of 400 and 1450 g/mol, respectively. It is found that characteristic peaks of p-EVA membrane are 1740 cm^{-1} (carbonyl group), 1210 cm^{-1} (ester group) and 3465 cm^{-1} (hydroxyl group). The PEG has characteristic peaks at 1120 cm^{-1} (ether group) and 3465 cm^{-1} (hydroxyl group). Accordingly, it is noticeable that p-EVA/PEG blended membrane at various %PEG loadings appeared the peak at 1120 cm^{-1} and the peak intensity of hydroxyl group is risen slightly, which is assigned to the ether and hydroxyl groups from the increase of PEG into the blended membranes. Therefore, this confirmed an existence of ethylene oxide (EO) unit of PEG in the blend membranes. [7]

However, the position peak of ether group in p-EVA/PEG blend membranes are shifted to the left (1143 cm^{-1}, higher wavenumber), as a result of interaction between ether group of PEG molecules and hydroxyl group of p-EVA.

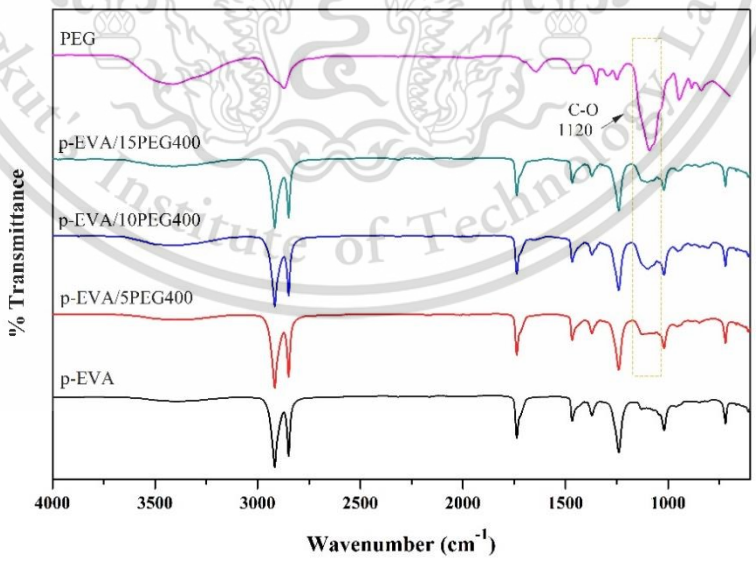

Figure 4.7 ATR-FTIR spectra of p-EVA, PEG and p-EVA blended with PEG at M_w of 400 g/mol at 5, 10 and 15%wt

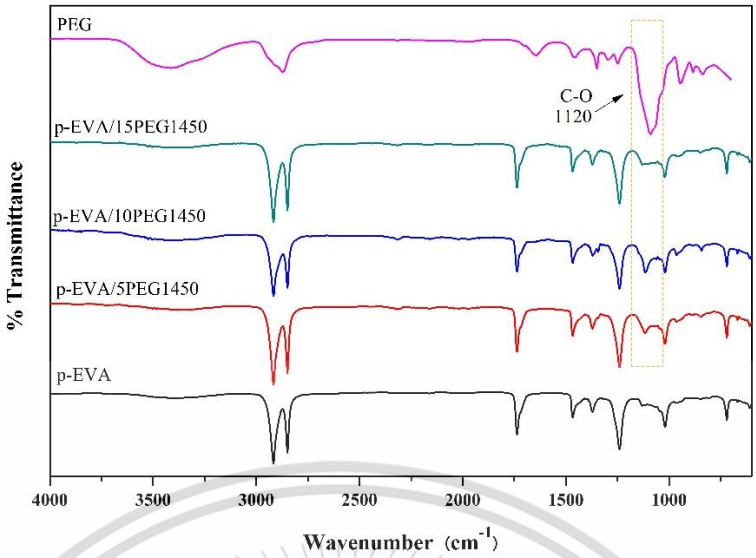

Figure 4.8 ATR-FTIR spectra of p-EVA, PEG and p-EVA blended with PEG at M_w of 1450 g/mol at 5, 10 and 15%wt

4.2.2 Thermal properties of the membranes

The thermal behavior of EVA, PEG, p-EVA and p-EVA/PEG blend membranes with different molecular weights of PEG and various %PEG loadings was investigated using DSC, which is represented in Table 4.1 and the DSC thermograms are displayed in Appendix C. It is found that the glass transition temperature (T_g) of EVA is -33.2 °C, which is revealed the rubbery state of membrane at room temperature. After hydrolysis reaction, the p-EVA membrane has a higher T_g (-17.5 °C) than the EVA one because of intermolecular hydrogen bond. For the p-EVA/PEG blend membranes, two T_g were detected referring the phase separation nature of the blends [57]. The lower T_g is of the PEG phase and the higher one is indicated to the p-EVA phase. Additionally, the contribution of PEG also affects on the decrement in T_g of p-EVA, especially in the formula of p-EVA/PEG400. The smaller M_w of PEG is favorable to penetrate through the polymer chains. Hence, it acts as a plasticizer and generates more free volume for the ease of chain mobility.

The melting temperature (T_m), crystallization temperature (T_c) and %crystallinity (X_c) of p-EVA are higher than those of the EVA. This indicates that the lamellar thickness is increased corresponding to the increase in crystallinity of p-EVA along with higher temperature of crystallization. Nevertheless, T_m, T_c and X_c of p-EVA/PEG are in the same range (63-66°C, 55-61°C and 5-7%, respectively). This is because PEG is added in small amount and p-EVA/PEG blends are also immiscible. Accordingly, the addition of PEG could not interfere the crystallization of p-EVA in the blend membranes.

Table 4.1 T_g, T_m, T_c and %crystallinity of the EVA, PEG, p-EVA and p-EVA/PEG blend membranes with various %PEG loadings

Formula	T_g (°C)		T_m (°C)		T_c (°C)	X_c of EVA (%)
	PEG	EVA	PEG	EVA		
EVA	-	-33.2	-	62.2	32.5	2.5
p-EVA	-	-17.5	-	64.8	54.0	5.8
P-EVA/5PEG400	-52.0	-28.0	-14.1	65.0	57.1	6.4
P-EVA/10PEG400	-53.5	-27.5	-13.7	63.8	56.8	6.6
P-EVA/15PEG400	-54.9	-30.1	-14.8	64.0	57.2	5.6
PEG400	-85.1	-	-14.0	-	-48.3	-
P-EVA/5PEG1450	-50.0	-23.9	30.5	66.0	55.0	6.4
p-EVA/10PEG1450	-53.7	-21.3	33.2	65.8	57.0	6.8
p-EVA/15PEG1450	-55.0	-21.5	32.5	65.5	60.7	6.0
PEG1450	-78.1	-	45.2	-	20.2	-

4.2.3 Morphology of the membranes

Figure 4.9 displays SEM micrographs from the cross-section of EVA, p-EVA and p-EVA/PEG blend membranes after extraction at magnifications 3000X and 8000X. SEM micrographs of the p-EVA/PEG400 and p-EVA/PEG1450 blend membranes before extraction are shown in Appendix D. It is observed that the EVA and p-EVA presented the smooth appearance with no micropores or any cavities (Figures 4.9a and 4.9b, respectively).

Moreover, it is found that by adding PEG into the p-EVA, the cavities are appeared and uniformly dispersed in the membrane matrix. Additionally, it is notable that the p-EVA/PEG blend with PEG of M_w 1450 g/mol has cavities larger than the one with PEG of M_w 400 g/mol at same amount of PEG adding. This is because the higher molecular weight of PEG-1450 has a higher polarity from the structure. Therefore, they are likely to agglomerate as a cluster rather than to disperse in the matrix. Besides, the size of cavities become larger and seem to be longitudinal shape when higher amount of PEG was loaded owing to low compatibility between p-EVA and PEG [24].

EVA (3000X) **(a)** EVA (8000X)

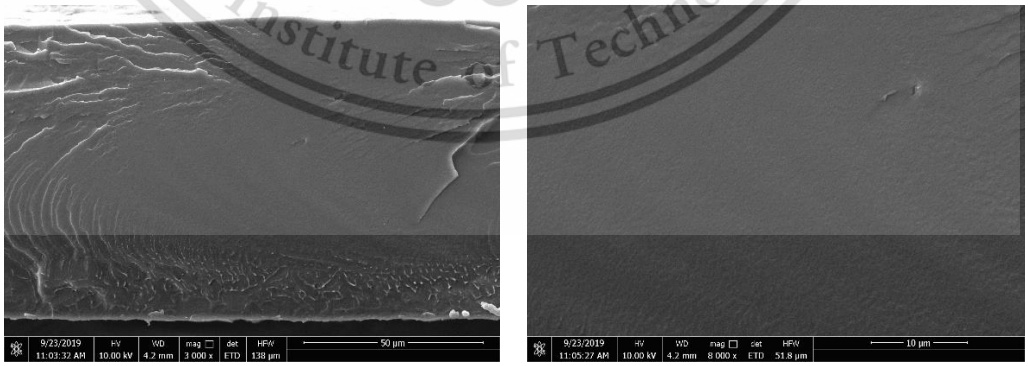

p-EVA (3000X) **(b)** p-EVA (8000X)

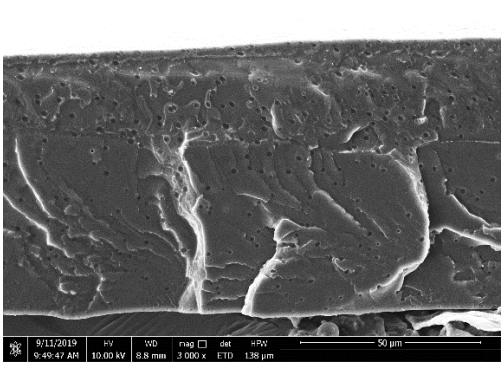

p-EVA/5PEG400 (3000X) **(c)** p-EVA/5PEG400 (8000X)

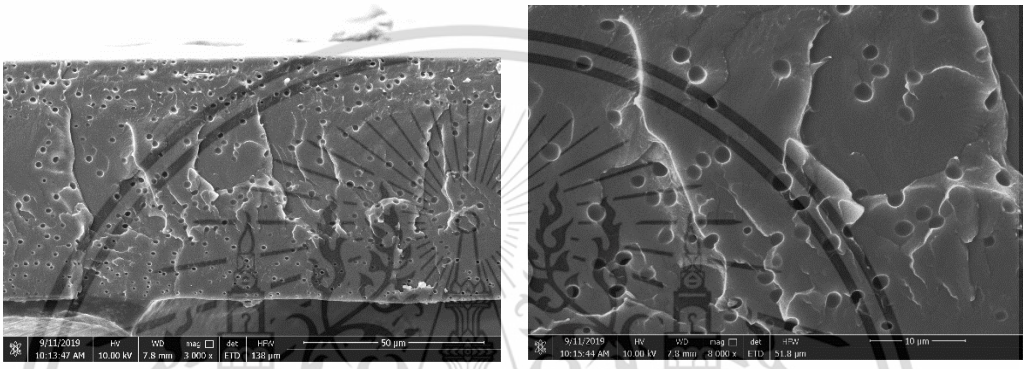

p-EVA/10PEG400 (3000X) **(d)** p-EVA/10PEG400 (8000X)

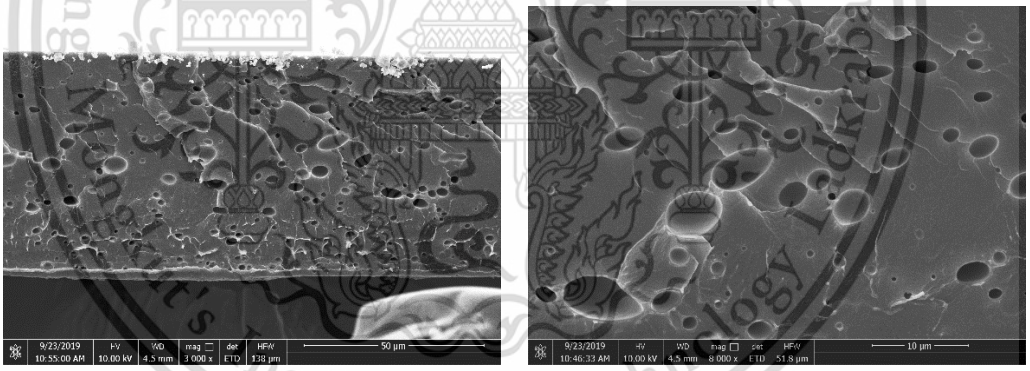

p-EVA/15PEG400 (3000X) **(e)** p-EVA/15PEG400 (8000X)

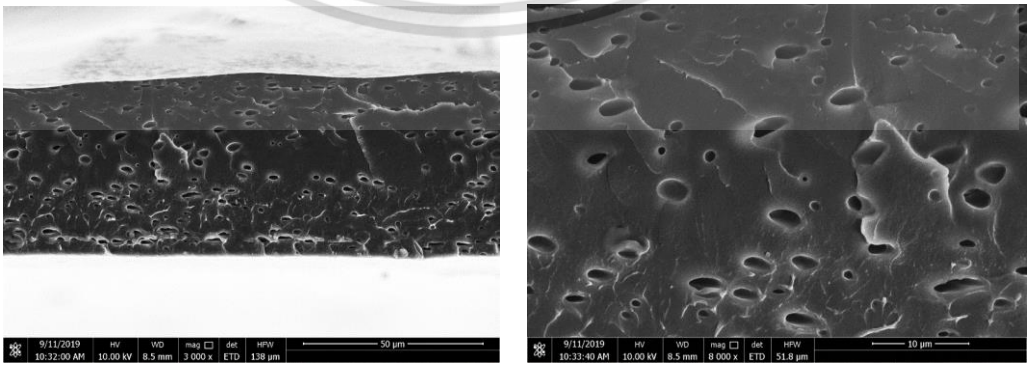

p-EVA/5PEG1450 (3000X) **(f)** p-EVA/5PEG1450 (8000X)

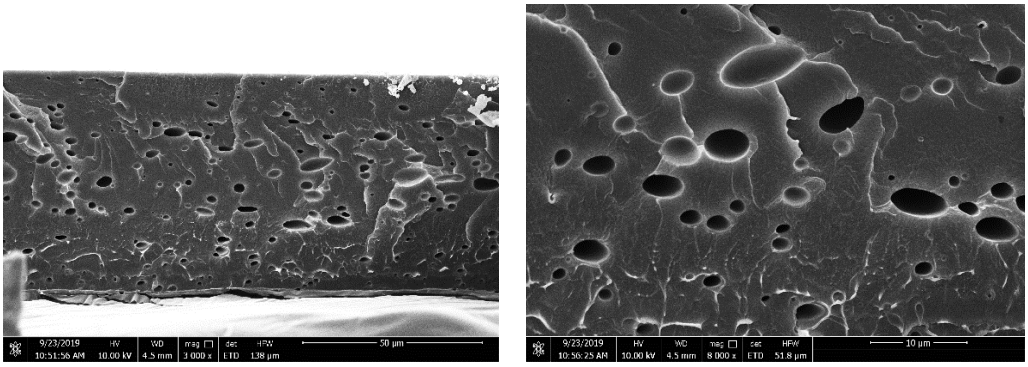

p-EVA/10PEG1450 (3000X) **(g)** p-EVA/10PEG1450 (8000X)

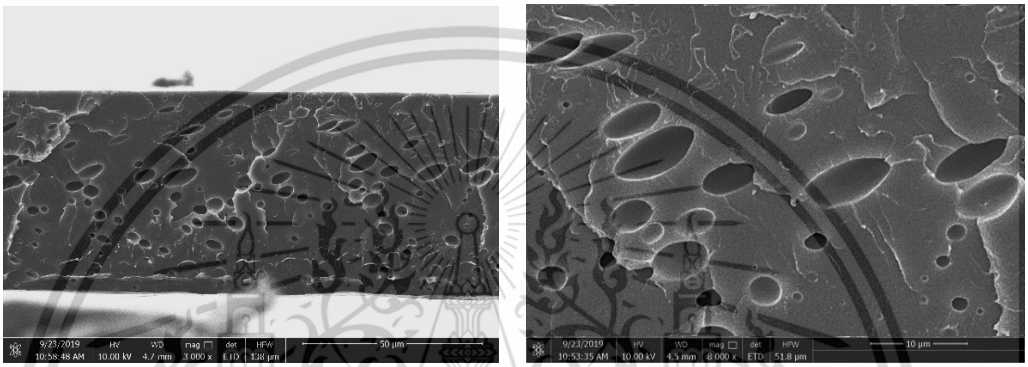

p-EVA/15PEG1450 (3000X) **(h)** p-EVA/15PEG1450 (8000X)

Figure 4.9 SEM micrographs from cross-section of EVA, p-EVA and p-EVA/PEG blend membranes (3000X and 8000X magnifications)

Figure 4.10 displays the surface morphology of EVA, p-EVA, p-EVA/15PEG400 and p-EVA/15PEG1450 blend membranes. It shows that the EVA and p-EVA membranes (Figures 4.10a and 4.10b, respectively) have the smooth surface and no micropores. Nevertheless, some micropores are observed on the surface of p-EVA/15PEG400 but not that of p-EVA/15PEG1450. This is because the PEG-400 g/mol has lower M_w than PEG-1450 g/mol. Hence, during the membrane preparation process, it could penetrate through the polymer chains to the membrane surface and evaporate when the membrane was cooled down, the micropores on the surface appeared.

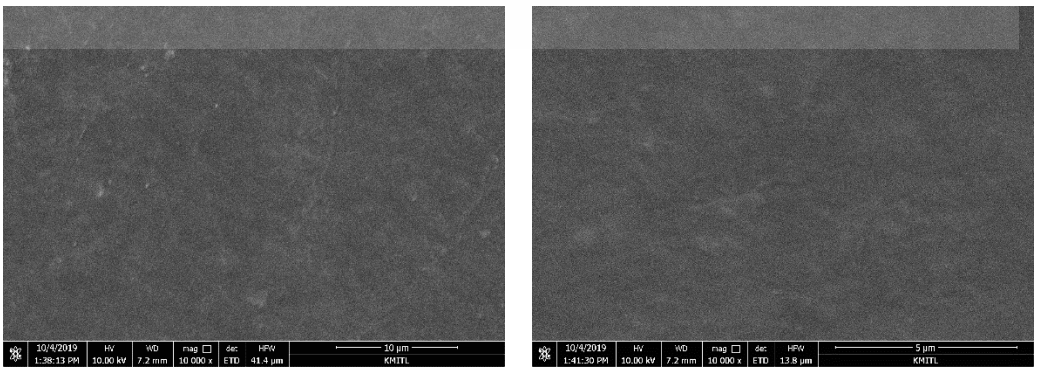

(a) EVA (b) p-EVA

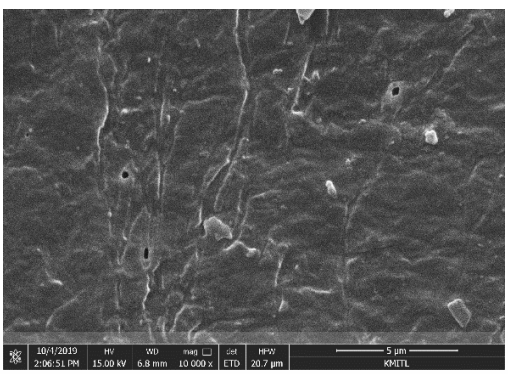

(c) p-EVA/15PEG400

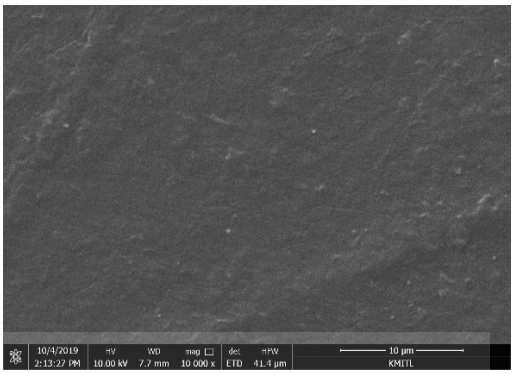

(d) p-EVA/15PEG1450

Figure 4.10 SEM micrographs from top surface of EVA, p-EVA, p-EVA/15PEG400 and p-EVA/15PEG1450 blend membranes (10000X magnification)

4.2.4 Mechanical properties of the membranes

Tensile strength, %elongation at break and Young's modulus of p-EVA/PEG blend membranes with PEG having M_w at 400 and 1450 g/mol and with various PEG loadings as depicted in Figures 4.11-4.13, respectively and Appendix E. The results show that tensile strength of blend membranes is decreased with increasing PEG loading, especially at 15%wt for both M_w of PEG. This is because PEG acts as the plasticizer in the membrane, leading to an increase in free volume and so the decrement in the strength of membranes [58]. Additionally, with 5-10%wt PEG loadings, Young's modulus of the membrane is significantly unchanged because PEG was added in small amount and it cannot interfere the crystallization of membrane (confirmed via DSC results). However, the use of 15%wt of PEG M_w 1450 g/mol gives the decreasing trend of membrane rigidity. The structure of PEG-1450 is bigger than that of PEG-400 because the PEG-1450 contains a higher number of ether group in its polymer chain. Thus, the polymer matrix seems to be softened as PEG-1450 is added. Furthermore, %elongation at break of the p-EVA/PEG400 and p-EVA/PEG1450 blend membranes is insignificantly changed with increasing PEG loading. This is because of a less amount of PEG addition into the membrane.

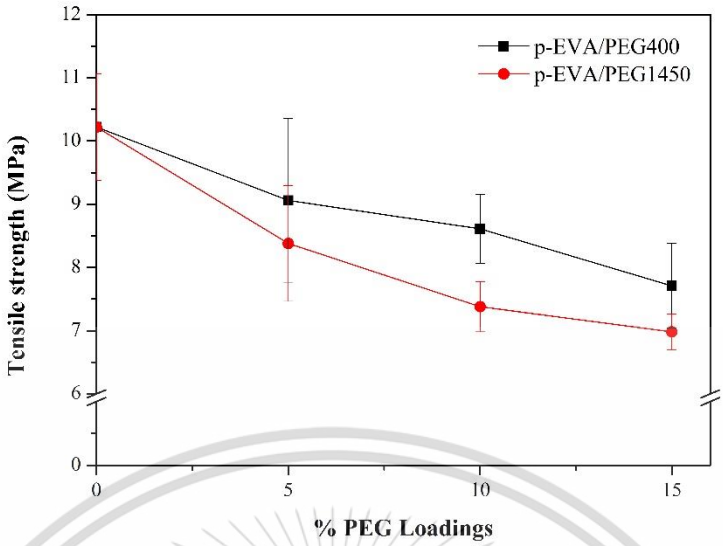

Figure 4.11 Tensile strength of p-EVA/PEG blend membranes with various %PEG loadings

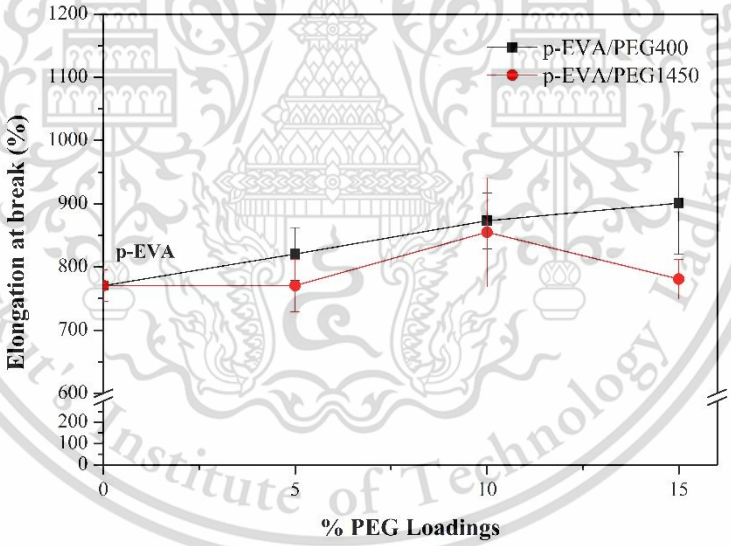

Figure 4.12 %Elongation at break of p-EVA/PEG blend membranes with various %PEG loadings

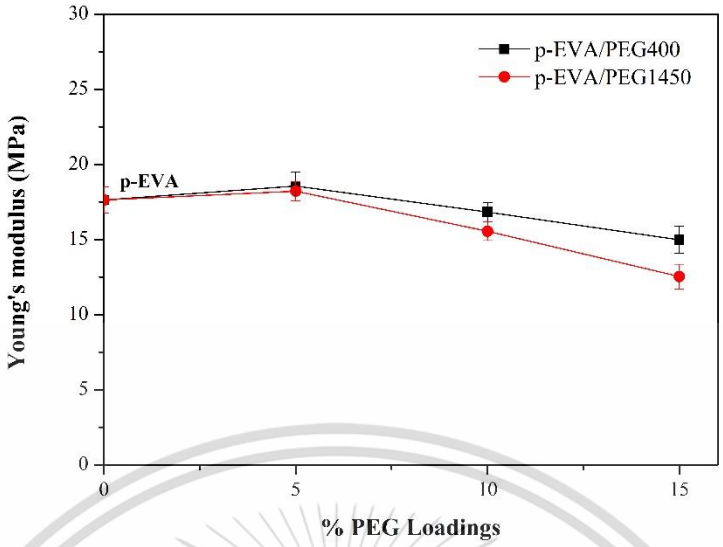

Figure 4.13 Young's modulus of p-EVA/PEG blend membranes with various %PEG loadings

4.2.5 Gas permeation of the membranes

The study of CO_2 and CH_4 permeabilities of p-EVA/PEG blend membranes is divided into 3 parts; 1) effect of PEG loadings 2) effect of PEG M_w and 3) the CO_2/CH_4 selectivity.

4.2.5.1 Effect of PEG loadings

From the results mentioned in section 4.1.4, CO_2 permeability of p-EVA (148.96 g/m^2·day) is lower than EVA (317.04 g/m^2·day) due to crystallinity in the membrane. Because the crystalline phase induces the difficult diffusion pathway from lowering chain mobility. Therefore, it is considered as an impermeable domain in the polymeric membrane. The CO_2 and CH_4 permeabilities of p-EVA/PEG 400 and p-EVA/PEG1450 blend membranes to present the effect of PEG loadings are displayed in Figures 4.14 and 4.15, respectively. They show that the CO_2 and CH_4 permeabilities of membranes are the highest at 15%wt PEG loading.

Accordingly, PEG was added into the p-EVA in order to increase free volume and polarity of membrane. By increasing the PEG loadings, it is found that the CO_2 and CH_4 permeabilities are increased owing to facilitation of gas diffusivity. In other words, PEG acts as the plasticizer, diffusing its molecules between the chain segment of p-EVA and then produces additional intermolecular space [59]. Moreover, it could be noticeable that CO_2 permeability is considerably increased, as compared with CH_4. This is because the presence of ether oxygen in PEG structure could promote strong interaction with CO_2 molecules due to the quadrupole-dipole interactions, leading to

the improvement of CO_2 molecules solubility on the membrane surface. Therefore, the accumulation of CO_2 concentration at upper-surface of the membrane is obtained, following by the increment of CO_2 molecular diffusion passed through the membrane. In other words, it resulted in greater concentration gradient effect.

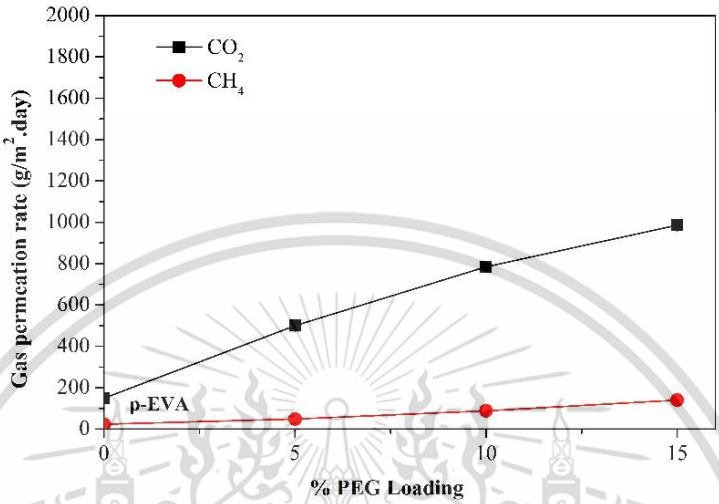

Figure 4.14 Effect of PEG loadings on CO_2 and CH_4 permeation rate of p-EVA/PEG400 blend membranes

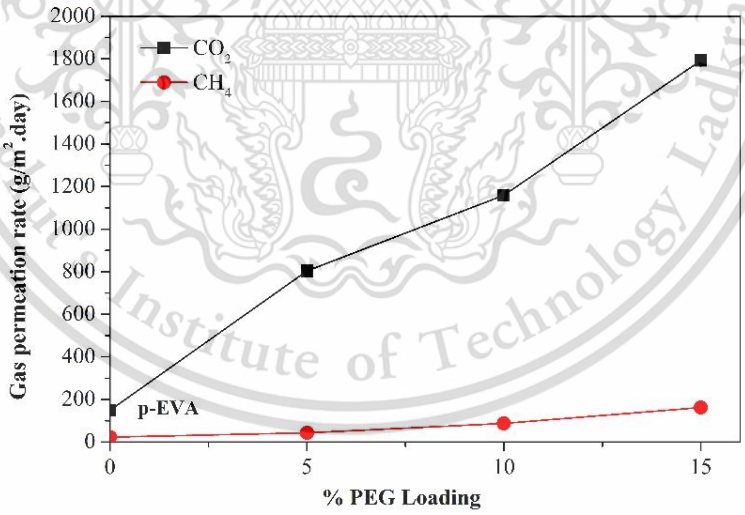

Figure 4.15 Effect of PEG loadings on CO_2 and CH_4 permeation rate of p-EVA/PEG1450 blend membranes

4.2.5.2 Effect of molecular weight of PEG

Figure 4.16 shows that p-EVA/PEG1450 has a higher CO_2 permeability than p-EVA/PEG400. This is because PEG-1450 g/mol (having higher M_w) provided larger cavities in the membrane than PEG-400 g/mol, as discussed in SEM analysis (section 4.2.3). Since PEG-1450 is likely to agglomerate as a cluster rather than to disperse in the matrix owing to low compatibility between p-EVA and PEG-1450 (higher polarity). Thus, both of gases CO_2 and CH_4 easily passed through the p-EVA/PEG1450 membranes. In addition, the presence of ether oxygen in the membrane can be performed strong interaction with CO_2 molecules and also possessed in CO_2 solubility, leading to a higher CO_2 permeability as compared with CH_4 permeability.

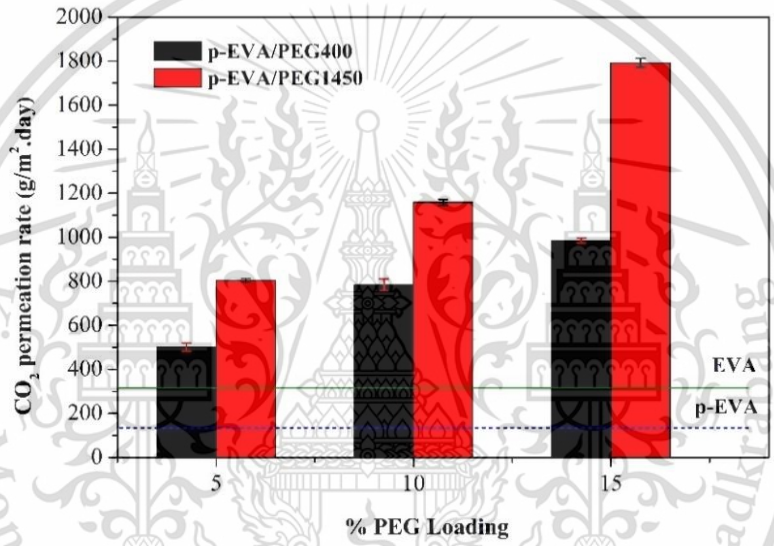

Figure 4.16 Effect of M_w of PEG on CO_2 permeation rate of p-EVA/PEG membrane with various PEG loadings

4.2.5.3 CO_2/CH_4 selectivity

The CO_2/CH_4 selectivity of p-EVA/PEG400 and p-EVA/PEG1450 membranes with various PEG loadings is shown in Figure 4.17. The CO_2/CH_4 selectivity is the highest at 5%wt PEG loading in both membranes and then it drops by further increasing amount of PEG (10-15%wt). This could be explained by the formation of cavities in the blend membranes, as discussed in the section 4.2.3. The blend membrane with a higher amount of PEG loadings has larger cavities and brings about the less effective thickness of the membrane, generating the increment in the diffusivity of both gases (low-selective membrane). However, it is concluded that the p-EVA/5PEG1450 membrane provided the highest CO_2/CH_4 selectivity at 18.6.

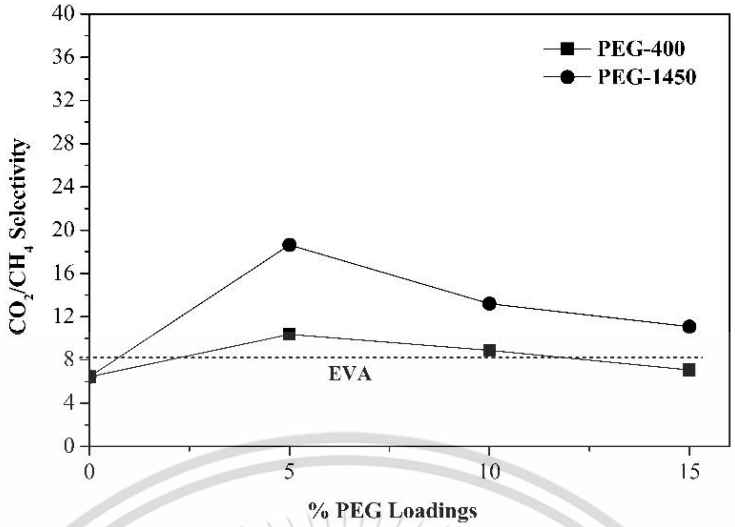

Figure 4.17 CO_2/CH_4 selectivity of p-EVA/PEG400 and p-EVA/PEG1450 membranes with various PEG loadings

4.3 Effect of surface-modified SiO_2 content

From the CO_2/CH_4 selectivity result mentioned above, it is concluded that CO_2/CH_4 selectivity is decreased after 5% of PEG loadings. Therefore, amine-functionalized silica (AFS) (with 0.3, 0.6 and 0.9%wt based on p-EVA content) was incorporated into the p-EVA/PEG blend membranes for increasing the CO_2/CH_4 selectivity together with excellent CO_2 permeability. The effect of AFS on the p-EVA/PEG blend membranes was investigated.

4.3.1 Characterization of modified SiO_2

The nonporous-silica (SiO_2) was functionalized with APTES by grafting the aminopropyl chains of APTES to the surface of SiO_2. The efficiency of functionalization was examined.

4.3.1.1 FTIR analysis

The AFS, SiO_2 and APTES were characterized and is displayed in Figure 4.18. The spectrum of SiO_2 is denoted the peak intensities at 1068 cm^{-1} and 480 cm^{-1} which are attributed to the Si-O-Si asymmetric stretching and bending vibrations, respectively. Moreover, Si-O-(H-H_2O) bending vibration is observed at near 960 cm^{-1} and peak intensity at 798 cm^{-1} indicates the in-plane bending vibration of geminal groups. The peak intensity around 3400 cm^{-1} is owing to the -OH groups of SiO_2 [60-61]. In addition, the specific peaks of APTES that represent the amine functional groups are N-H bending vibrations for primary amine (1°amine) at 768 cm^{-1} and 1392 cm^{-1}.

The spectrum of AFS shows the peak intensities at 1392 cm^{-1} and 2800-2950 cm^{-1}, indicating the amino groups, which are fixed onto the SiO_2 surface successfully. Besides, it is noticeable that the intensity of Si-O-Si characteristic peak of AFS at 1068 cm^{-1} is increased, as compared to that of SiO_2. This is due to the replacing the Si-OH with Si-O-Si from functionalization of the aminosilane on the surface [62-63].

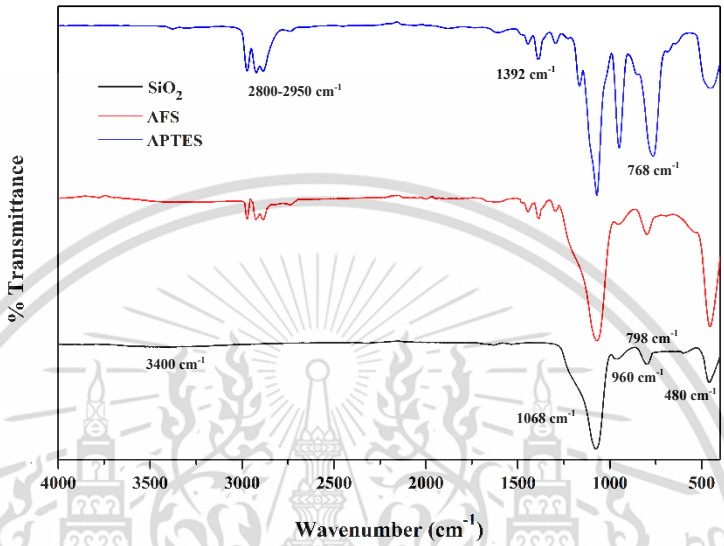

Figure 4.18 FTIR spectra of SiO_2, AFS and APTES

4.3.1.2 Contents of APTES on SiO_2 surface

Because the FTIR spectra could not confirm the quantification of amine groups, the presence of amine groups and number of elementals (C, H and N) was determined using back titration and CHN elemental analysis, respectively. The CHN analysis results are presented in Table 4.2.

Since each nitrogen atom represents one amine functional group attached to a propyl chain, the percentage of nitrogen in the AFS suggests the total number of amine sites which are grafted on SiO_2 surfaces. The percentage of nitrogen in the pristine SiO_2 is zero regarding to the manufacturer's information. Using the total surface area of the AFS, the total number of amine sites could be calculated as 2.85 n/nm^2 of surface.

Table 4.2 CHN elemental analysis results

Element	Weight (mg)	Weight (%)	Reten, Time (min)	Area
Nitrogen	0.049	1.17	0.808	108729
Carbon	0.213	5.04	1.233	1029254
Hydrogen	0.057	1.34	3.042	883395.5
Total	4.224	7.55		

However, only some the amine sites are active to react with CO_2 molecules. There is the possibility for the amino propyl chains attaching undesirably to the SiO_2 surface during the functionalization process [45], as schematically illustrated in Figure 4.19 (2 and 5). Therefore, an amine efficiency could be evaluated by comparing the total number of amine sites (2.85 n/nm^2) and the number of active amine sites resulting from back titration analysis (1.82 n/nm^2), which is 64.0%.

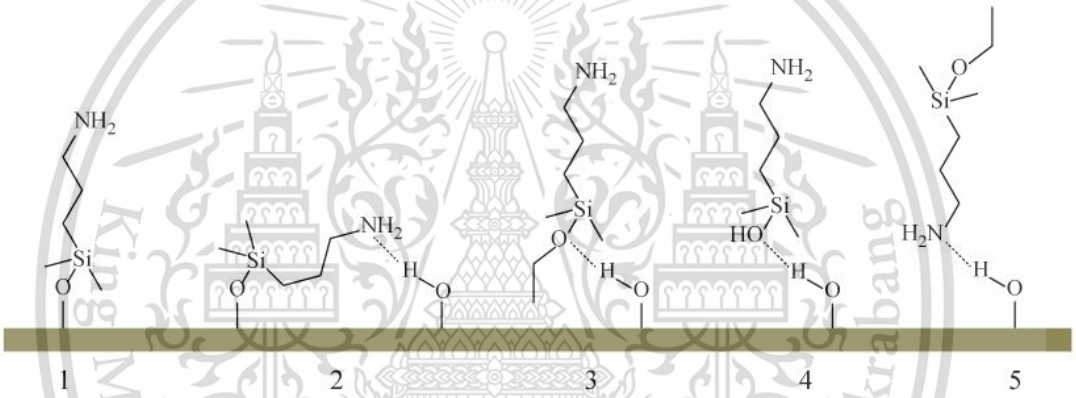

Figure 4.19 Possibilities of interactions between APTES molecules and SiO_2 surface

4.3.1.3 Electronic structure of the surface species

The surface chemical species exposed on unmodified SiO_2 and amine-functionalized SiO_2 (AFS) were determined using XPS. The C1s, O1s, Si2p and N1s spectra are demonstrated in Figures 4.20-4.23 and surface chemical composition is tabulated in Appendix F.

As seen from Figure 4.20, C1s spectrum of AFS presents a band with high intensity as compared to that of the parent SiO_2. Deconvoluted C1s spectrum of the AFS resolves into the contributions centered at 284.8, 284.5, and 286.4 eV arising from sp^3 carbon (C-C and C-H), C-Si bond, and C-N or C-O, respectively. It should be noted that the peak with low intensity at 288.5 eV seems to be C-C=O emerging from impurity [64-65].

O1s spectra of the samples are illustrated in Figure 4.21, showing that the binding energy at 533.2 is related to the surface silanol. After AFS grafting, the binding energy is shifted to 531.9 eV indicating that the siloxane bridge occurs from the

silanization [65-66]. Nonetheless, O1s spectra of AFS present a relatively lower intensity compared to those of unmodified SiO_2 owing to the shielding of secondary electron from other surface components. In a similar manner, Si2p spectra main peak is also shifted from 103.9 (Si-OH) to 102.6 eV (Si-O-Si). However, the peak of Si-OH is still remained. This is indicated that the functionalization is not a hundred percent successfully.

Finally, amino group on the SiO_2 surface was confirmed by N1s XPS spectra, as depicted in Figure 4.23. The deconvoluted N1s spectrum of AFS sample reveals the intense peaks at 400.4 and 402.1 eV, in agreement with single N-H and NH_2 contribution, respectively. Besides, the peak at 402.1 eV is corresponded to the hydrogen-bonded -NH_2 (NH_3) with the hydroxyl groups on SiO_2 surface [65-67]. As expected, the N1s signal of unmodified SiO_2 is not observed as it is an amine-free sample.

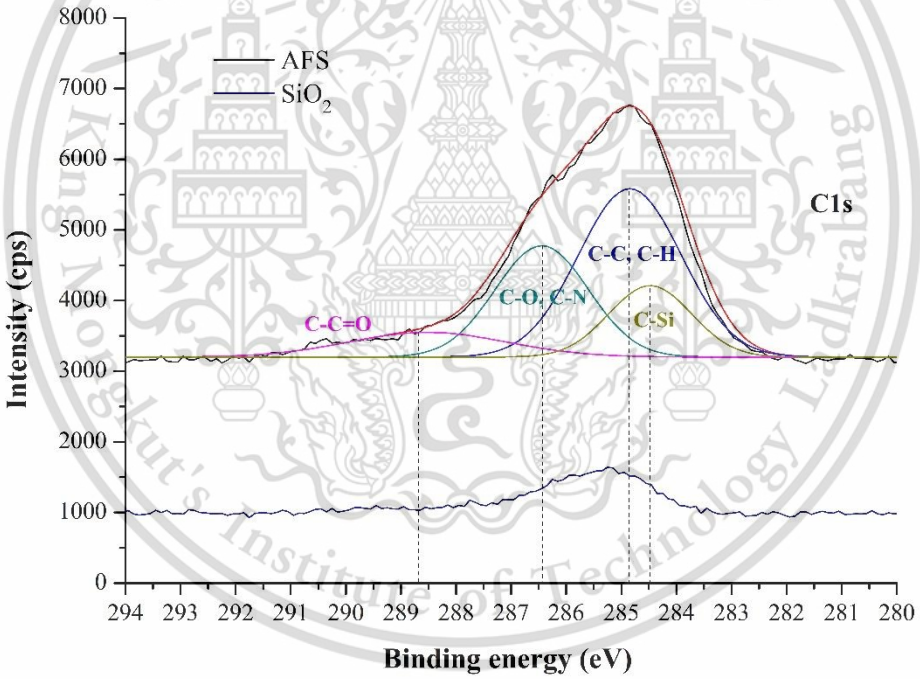

Figure 4.20 C1s level XPS spectra of SiO_2 and AFS

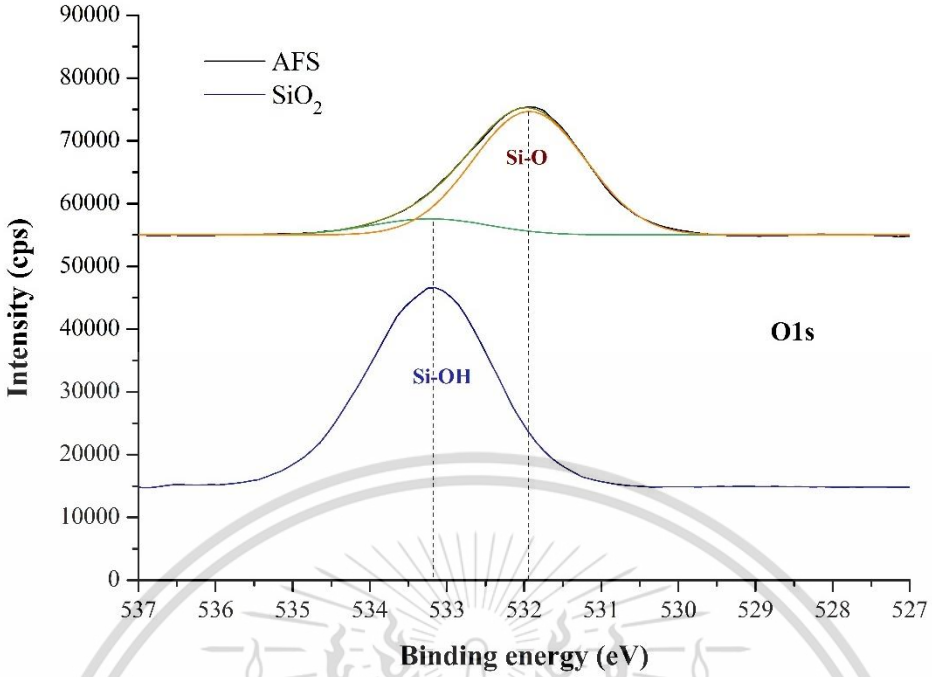

Figure 4.21 O1s level XPS spectra of SiO_2 and AFS

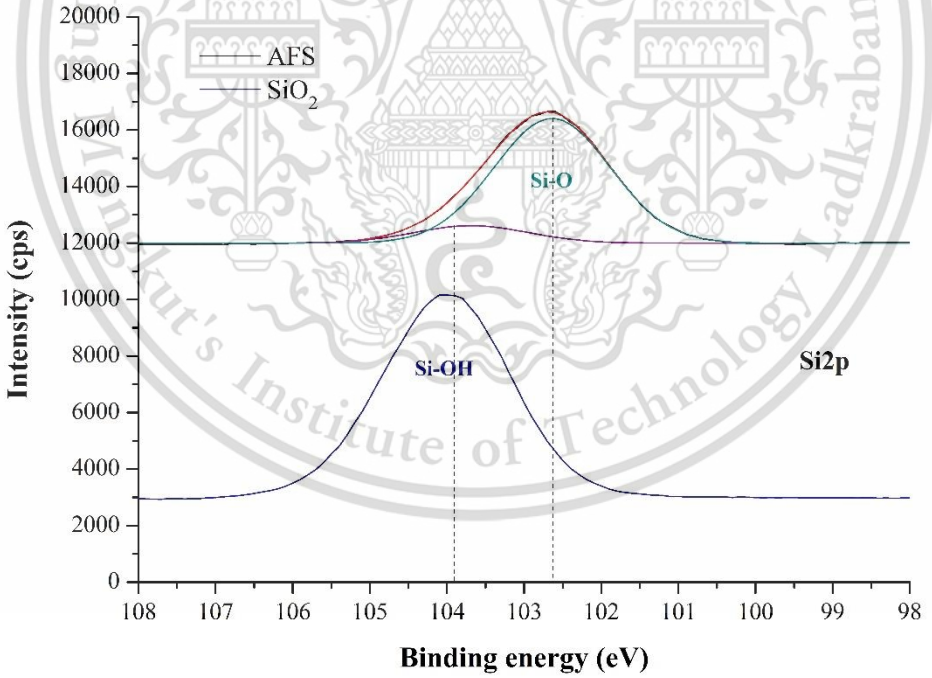

Figure 4.22 Si2p level XPS spectra of SiO_2 and AFS

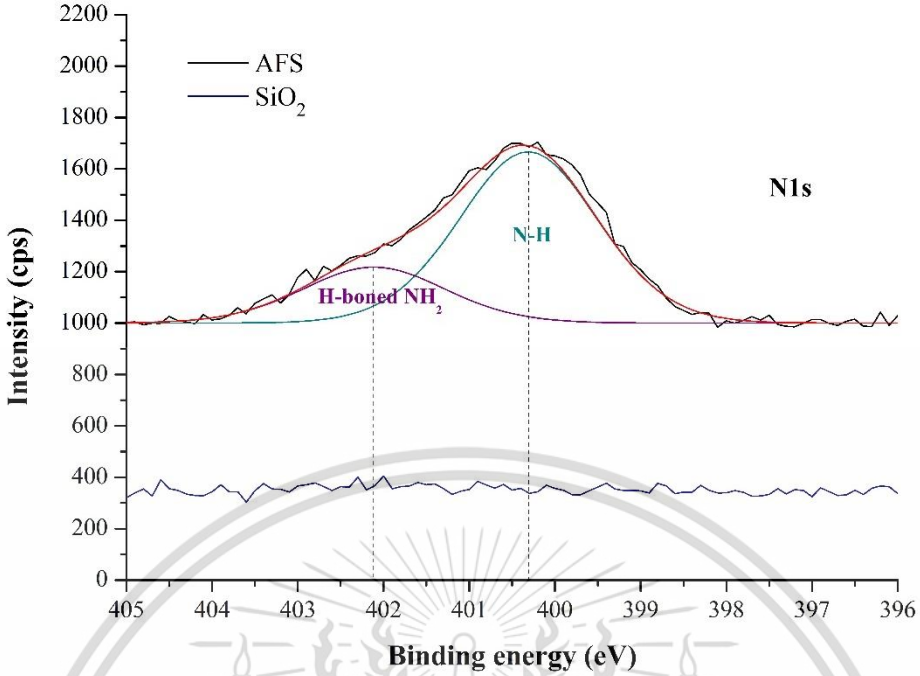

Figure 4.23 N1s level XPS spectra of SiO_2 and AFS

4.3.2 Characterization and test of the membranes

AFS was added into the p-EVA/15PEG400 and p-EVA/15PEG1450 blend membranes with 0.3, 0.6 and 0.9%wt to improve the CO_2/CH_4 selectivity. The morphology of membranes and gas permeabilities were evaluated.

4.3.2.1 Morphology of the membranes

The dispersion of AFS in the p-EVA/PEG blend membranes was determined using SEM analysis. It is found that AFS particles tend to agglomerate upon the loading, from 0.3, 0.6 and 0.9%, resulting in poor AFS dispersion. Typically, AFS particle has a higher polarity related to p-EVA, it is thus likely incompatible to each other and favorable to form separated phase. The formation of AFS agglomeration in the all p-EVA/15PEG1450-XAFS (X are 0.3, 0.6 and 0.9%wt) membranes is displayed in Figures 4.24 to 4.26.

Conversely, Figures 4.27 and 4.28 show that the p-EVA/15PEG400-0.3AFS and p-EVA/15PEG400-0.6AFS, respectively, have good dispersion of AFS in the blend membranes and imply the good compatibility between AFS with PEG-400 phase. This is because the polarity of PEG-400 is lower than PEG-1450. However, the agglomeration of AFS particles, representing poor dispersion of AFS in matrix phase, is observed when adding 0.9%wt AFS (p-EVA/15PEG400-0.9AFS membrane) as illustrated in Figure 4.29.

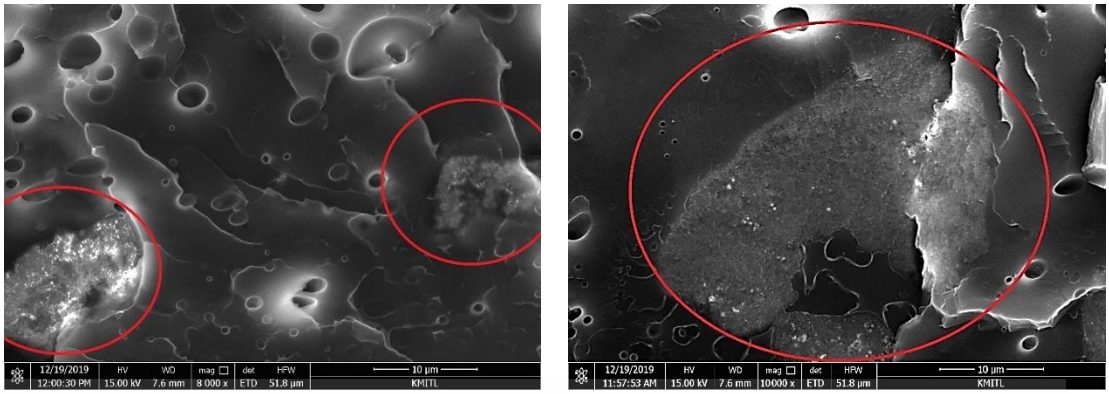

(a) (b)

Figure 4.24 SEM micrographs of p-EVA/15PEG1450-0.3AFS at magnifications of a) 8000X and b) 10000X

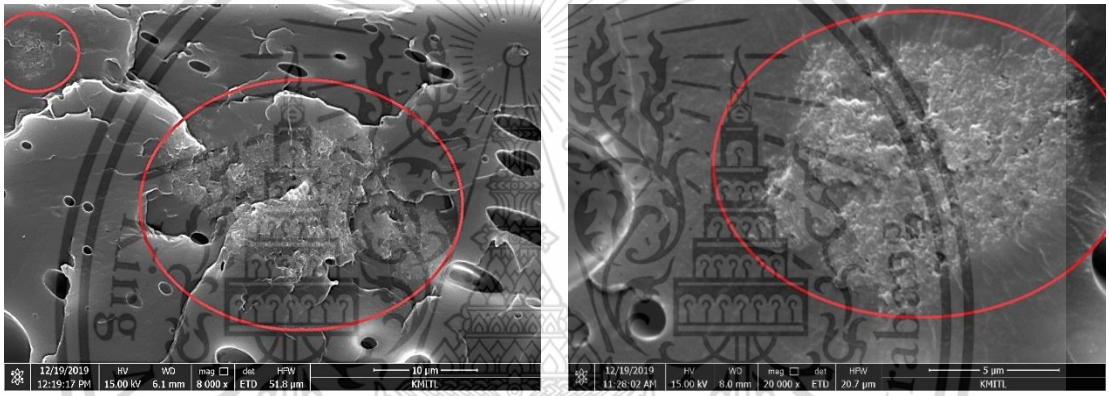

(a) (b)

Figure 4.25 SEM micrographs of p-EVA/15PEG1450-0.6AFS at magnifications of a) 8000X and b) 20000X

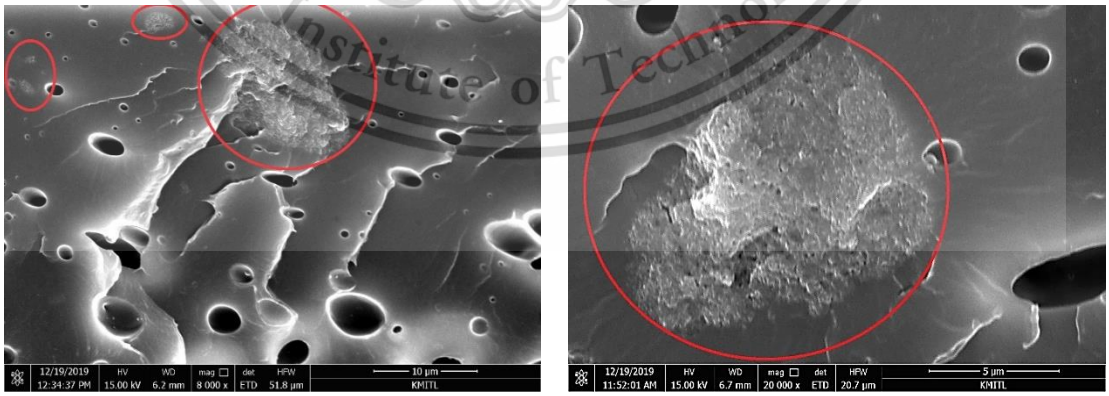

(a) (b)

Figure 4.26 SEM micrographs of p-EVA/15PEG1450-0.9AFS at magnifications of a) 8000X and b) 20000X

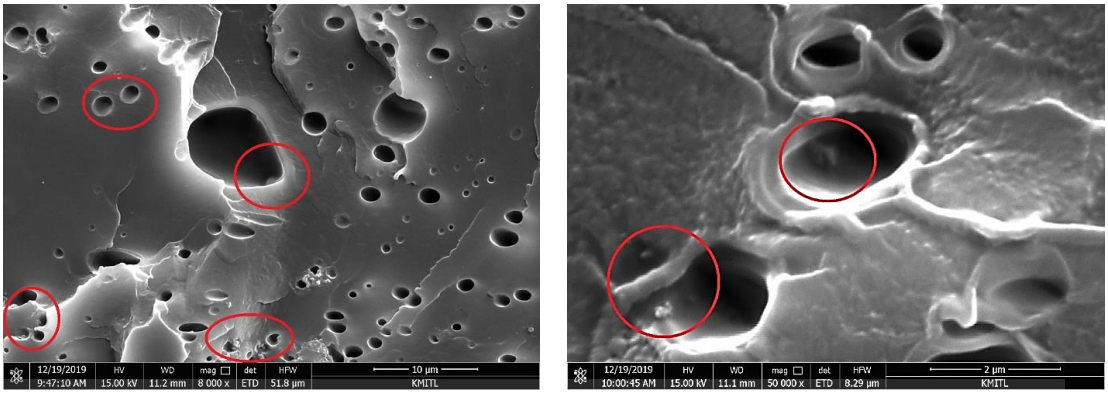

(a) (b)

Figure 4.27 SEM micrographs of p-EVA/15PEG400-0.3AFS at magnifications of a) 8000X and b) 50000X

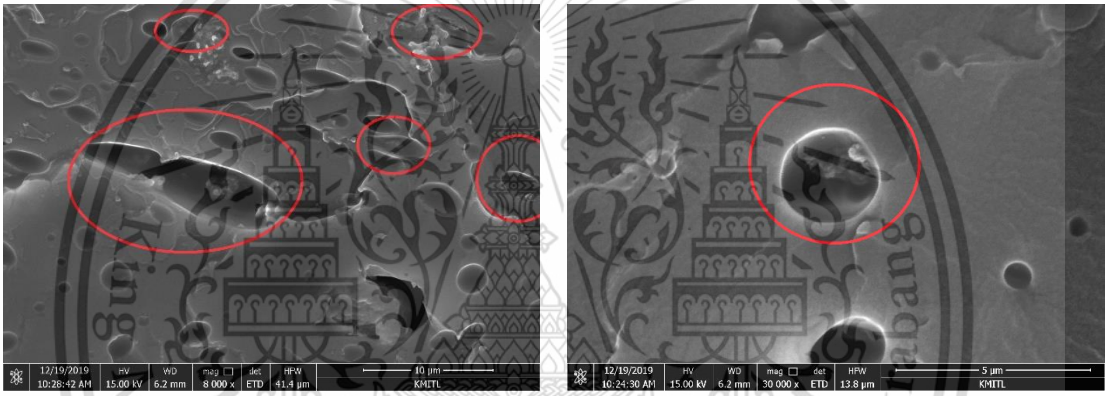

(a) (b)

Figure 4.28 SEM micrographs of p-EVA/15PEG400-0.6AFS at magnifications of a) 8000X and b) 30000X

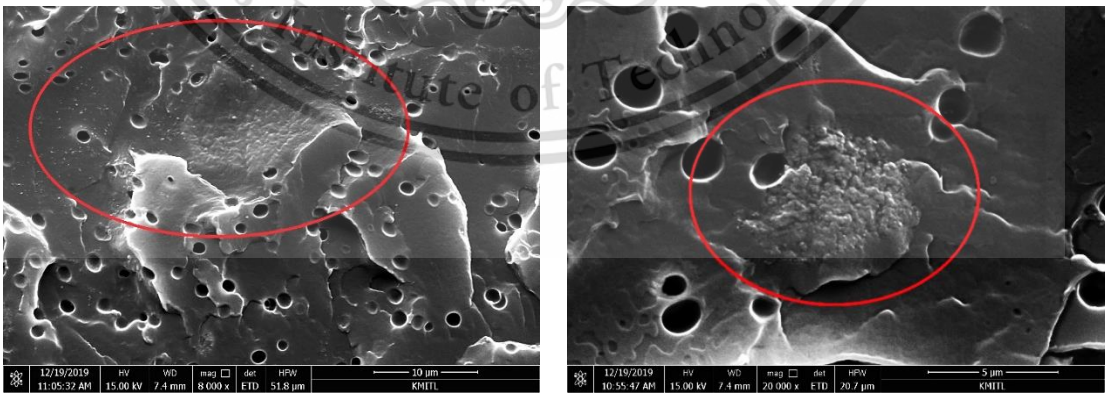

(a) (b)

Figure 4.29 SEM micrographs of p-EVA/15PEG400-0.9AFS at magnifications of a) 8000X and b) 20000X

4.3.2.2 Gas permeation of membranes

The CO_2 and CH_4 gas permeabilities of p-EVA/15PEG400 and p-EVA/15PEG 1450 membranes with various %AFS loadings are demonstrated in Figures 4.30 and 4.31, respectively. In the formula of PEG-400 (p-EVA/15PEG400), it is observed that by increasing the AFS loading up to 0.6%wt, the CO_2 permeability is increased owing to the presence of amine sites on the surface of AFS. They could interact with CO_2 molecules and the CO_2 solubility is increased effectively, leading to the higher CO_2 permeation [68]. The reactive amine functional groups with electron donating nitrogen act as the Lewis base for attaching CO_2 molecules. The reaction between active amine sites and CO_2 molecules can be described in the equation 4.1.

$$CO_2 + RNH_2 \longleftrightarrow RNH_2^+ \ COO^-$$
$$RNH_2 + COO^- + RNH_2 \longleftrightarrow RNH_3^+ + RNHCOO^- \qquad (4.1)$$

From the equation 4.1, the CO_2 firstly reacts with a propylamine group and produces carbamic acid. After that the product reacts with another free amine group and results in a carbamate molecule and RH_3^+ [69-70]. As the reactions are reversible and carbonate compounds are unstable, the CO_2 molecules may completely desorb and regenerate the initial surface of particle [45]. However, the CH_4 does not show this behavior because this non-polar gas has no considerable interaction with NH_2 groups.

Additionally, when adding 0.9%wt AFS, the CO_2 permeability is considerably decreased due to the higher amounts of non-permeable particles that block the gas diffusion pathway and increase the tortuosity of the permeation pathway [71]. In other words, the effect of pathway blocking is dominant compared to the effect of amine functional groups, at higher AFS loadings.

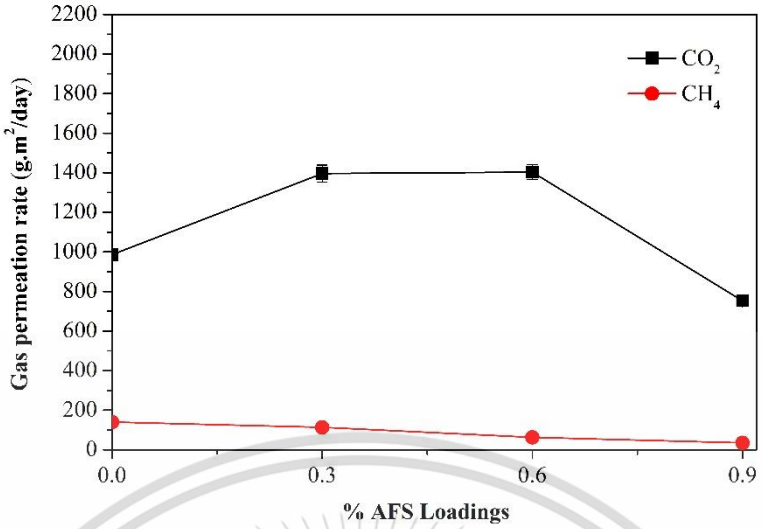

Figure 4.30 Gases permeability of p-EVA/15PEG400 membrane with various %AFS loadings

Besides, in the formula of PEG-1450 (p-EVA/PEG1450), it is found that CO_2 permeability is dramatically decreased with increasing AFS loading. This is because the AFS particles have poor dispersion, as agglomeration in the matrix phase (p-EVA) that was evidenced by SEM micrographs. PEG-1450 possesses a higher polarity related to AFS, resulting in poor compatibility between PEG-1450 and AFS. Hence, the AFS particles play role in the non-permeable particle and block the gas diffusion pathway, leading to the increase in tortuosity of the permeation pathway [71].

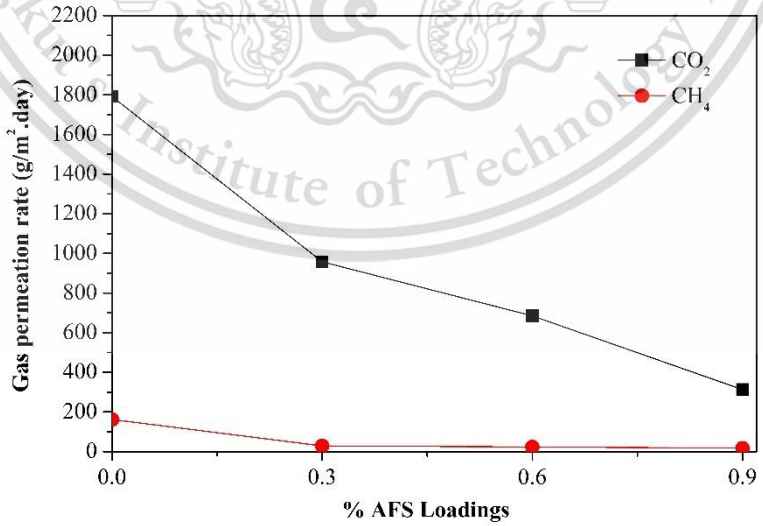

Figure 4.31 Gases permeability of p-EVA/15PEG1450 membrane with various %AFS loadings

The CO_2/CH_4 selectivity of p-EVA/15PEG400 and p-EVA/15PEG1450 membranes with various AFS loadings is illustrated in Figure 4.32. The CO_2/CH_4 selectivity of p-EVA/15PEG400 and p-EVA/15PEG1450 membranes is the highest at 0.6%wt and 0.3%wt AFS loadings, respectively. Then the decreasing trends are observed because of the undesirably agglomerated AFS particles, leading to the difficult gas diffusion.

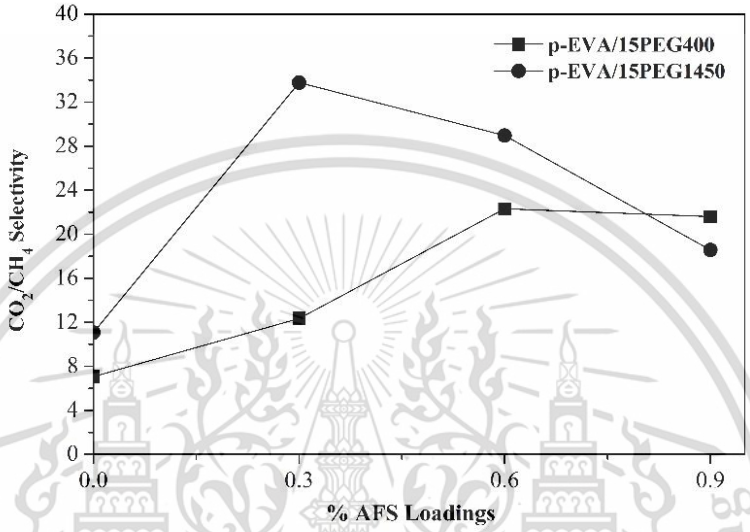

Figure 4.32 CO_2/CH_4 selectivity of p-EVA/15PEG400 and p-EVA/15PEG1450 membranes with various %AFS loadings

It is seen that p-EVA/15PEG1450 has the highest CO_2 permeability up to 1791.7 g/m^2·day. However, it has a low CO_2/CH_4 selectivity (11.1). After adding AFS into the p-EVA/15PEG blended membranes, it is found that p-EVA/15PEG1450-0.3AFS possesses the highest CO_2/CH_4 selectivity up to 33.8 from the effect of NH_2 functional groups. In contrast, it has a relatively low CO_2 permeability (957.2 g/m^2·day) because the gas diffusion pathway is blocked from agglomeration of AFS particles. Therefore, the p-EVA/15PEG400-0.6AFS is a suitable membrane for CO_2 permeability and CO_2/CH_4 selectivity with optimum values at 1402.3 g/m^2·day and 22.3, respectively.

Consequently, it is shown that the p-EVA/15PEG400-0.6AFS blend membrane from present work revealing the enhancement of CO_2/CH_4 selectivity, as compared to other membranes, which are listed in Table 4.3.

Table 4.3 The comparison of the CO_2/CH_4 selectivity performance of p-EVA/15PEG 400-0.6AFS with other mixed matrix membranes (MMMs)

Entry	Sample	Condition	Selectivity	Reference
1	Matrimid®-PEG (96:4) + 30 wt% ZIF-8	CO_2/CH_4 binary mixture gas (50:50), 8 bar, 25 °C	15.4	[42]
2	PEBAX MH1657 + 30 wt% PEG-POSS	CO_2/CH_4 single gas permeation, 70 °C	8.1	[46]
3	PES + TiO_2 + UV 3 min + cross linking	CO_2/CH_4 single gas permeation	15.6	[72]
4	PU-ZnO 0.5 wt% MMM	CO_2/CH_4 single gas permeation, 10 bar, 30 °C	19.8	[73]
5	NH_2-MIL-53(Al)/ Cellulose Acetate HFMMM	CO_2/CH_4 binary mixture gas (15:85%v/v), 15 bar, 30 °C	14.4	[74]
6	Pebax (7 wt%)/PEG (7.5 wt%)/TiNT-TEPA (3 wt%)	CO_2/CH_4 single gas permeation, >10 bar, 35 °C	16.2	[75]
7	Pebax- Al_2O_3 (4 wt%)	CO_2/CH_4 single gas permeation, 3 bar, 25 °C	21.2	[76]
8	p-EVA/15PEG400-0.6AFS	CO_2/CH_4 single gas permeation, 25 °C	22.3	This work

Chapter 5
Conclusions and suggestions

5.1 Conclusions

The EVA with 33% vinyl acetate (VA) was chosen to prepare the membrane for application of the CO_2 separation in biogas industry, on account of its high carbonyl functional groups. In contrast, it has poor mechanical properties. Hence, EVA with 33%VA was partially hydrolyzed, as named p-EVA, to improve the mechanical properties. The tensile strength of p-EVA is greater than that of EVA, as a result of hydrogen bonding between the polymer chains during hydrolysis reaction. However, the negative effect from this reaction resulted in low CO_2 permeability. In order to enhance the CO_2 permeation, PEG was selected for blending with p-EVA due to the high polarity from the ether functional groups and the plasticizer effect.

PEG with the molecular weights of 400 and 1450 g/mol at 5, 10 and 15%wt loadings was blended with p-EVA to increase the polarity and free volume of the membranes. The blend membranes with PEG 15%wt (p-EVA/15PEG400 and p-EVA/15 PEG1450) exhibited relatively high CO_2 permeability owing to higher intermolecular space (free volume) and polarity from the functional group (ether oxygen). However, they have poor CO_2/CH_4 selectivities. This is because the blend membrane with a higher amount of PEG loadings has larger cavities and brings about the less effective thickness of the membrane, generating the increment in the diffusivity of both gases (non-selective membrane).

For enhancing the CO_2/CH_4 selectivity, SiO_2 was modified surface with APTES and incorporated with p-EVA/15PEG400 and p-EVA/15PEG1450 blend membranes. The results presented that total amine sites exposed on SiO_2 surface was 2.85 n/nm^2, whereas the number of active amine sites was 1.82 n/nm^2. The XPS showed the intense Si-O and N-H peaks at 102.6 eV and 400.4 eV, respectively, which indicated the formation layers of APTES due to successful functionalization. When the AFS particles at 0.3, 0.6 and 0.9%wt were added into the blend membranes, the CO_2/CH_4 selectivity was increased in the all formulas. This is because AFS particles can significantly interact with CO_2 molecules and then CO_2 solubility is increased effectively, leading to the preferable CO_2 permeation. Additionally, the CO_2 permeability in the formula of p-EVA/15PEG400-XAFS was increased with increasing amount of AFS from 0.3-0.6%wt. On the other hand, the CO_2 permeability of p-EVA/15PEG1450-XAFS was considerably decreased with increasing the AFS loadings due to the agglomeration (poor dispersion) of AFS particles in the matrix phase, resulting in the gas diffusion pathway blocking.

Consequently, the appropriate formula for CO_2 separation was p-EVA/15PEG400-0.6AFS with CO_2 permeability 1402.34 g/m^2·day and 22.31 of CO_2/CH_4 selectivity.

5.2 Suggestions

1) Processing methods of membrane production as used in an industry such as melt process (melt casting and blown film extrusion) could be employed.

2) Porous-silica such as MCM-41 and SBA-15 could be used as functionalized support in order to prevent the gas diffusion blocking.

3) Other properties of membranes such as weatherability and stability could be further investigated.

References

[1] Tong, S., Xiao, L., Lia, X., Zhu, X., Liu, H., Luo, G., Worasuwannarak, N., Kerdsuwan, S., Fungtammasan, B. and Yao, H. 2018. "A gas-pressurized torrefaction method for biomass wastes." Energy Conversion and Management. 173 : 29-36.

[2] Selvaraj, R., Nasira, A., Vasa, N.J. and Nagendra, S. 2017. "Monitoring of CO_2 and CH_4 composition in a biogas matrix from different biomass structures." Sensors and Actuators B. 249 : 378-385.

[3] Clarke Energy a Kohler company. 2018. **Biogas.** [Online]. Available : https://www.clarke-energy.com/biogas/.

[4] Sanaeepur, H., Amooghin, A.E., Moghadassi, A. and Kargari, A. 2011. "Preparation and characterization of acrylonitrile–butadiene–styrene/poly(vinyl acetate) membrane for CO_2 removal." Separation and Purification Technology. 80 : 499-508.

[5] Mannan, H.A., Mukhtar, H., Shaharun, M.S., Othman, M.R. and Murugesan, T. 2016. "Polysulfone/poly(ether sulfone) blended membranes for CO_2 separation." Applied Polymer Science. 133(5) : 42946-42954.

[6] Mousavi, A.S., Gholizadeh, M., Sedghi, S., Pourafshari-Chenarc, M., Barmalad, M. and Soltania, A. 2010. "Effects of preparation conditions on the morphology and gas permeation properties of polyethylene (PE) and ethylene vinyl acetate (EVA) films." Chemical Engineering Research and Design. 88 : 1593-1598.

[7] Zamiri, M.A., Kargari, A. and Sanaeepur, H. 2015. "Ethylene vinyl acetate/poly(ethylene glycol) blend membranes for CO_2/N_2 separation." Greenhouse Gas Science and Technology. 5 : 668-681.

[8] Basu, P. 2010. **Biomass Gasification and Pyrolysis: Practical Design and Theory.** Oxford : Elsevier Inc.

[9] Clark, J.H. and Deswarte, FE.I. 2008. **Introduction to Chemicals from Biomass.** Cornwall : TJ International.

[10] Bioenergy Consult. 2018. **An Introduction to Biomass Energy.** [Online]. Available : https://www.bioenergyconsult.com/biomass-energy-introduction/.

[11] Deublein, D. and Steinhauser, A. 2008. **Biogas from Waste and Renewable Resources.** Hoboken : John Wiley & Sons, Inc.

[12] Photosynthesis Education. 2018. **What is Photosynthesis.** [Online]. Available : https://photosynthesiseducation.com/photosynthesis-for-kids/.

[13] Chen, J. 2010. **Biomass to Renewable Energy Processes.** New York : CRC Press.

[14] Price, E.C. and Cheremisinoff, P.N. 1981. **Biogas: Production and Utilization.** Michigan : Ann Arbor Science Publishers.

[15] Mushtaq, A., Mukhtar, H.B., Shariff, A.M. and Mannan, H.A. 2013. "Development of Polymeric Blend Membrane for Removal of CO_2 from Natural Gas." Engineering and Technology. 2(13) : 53-60.

[16] Seeharaj, P. 2013. "Membranes for Hydrogen Separation." Journal of Science, Ladkrabang. 22(2) : 138-153.

[17] Sudpoung, C., Yenjaima, W. and Krirkmanee, S. 2015. "Study on PP/SEBS/ZSM-5 blends for improving ethylene permeation of packaging film." B.Sc. Special Project, Department of Chemistry, Faculty of Science, King Mongkut's Institute of Technology Ladkrabang.

[18] Ren, X., Kanezashi, M., Nagasawa, H. and Tsuru, T. 2015. "Plasma-assisted multi-layered coating towards improved gas permeation properties for organosilica membranes." RSC Advances. 5(74) : 59837-59844.

[19] Tome,́ L.C. and Marrucho, I.M. 2016. "Ionic liquid-based materials: a platform to design engineered CO_2 separation membranes." Royal Society of Chemistry. 45 : 2785-2824.

[20] Suthapa, K. 2004. **Membrane Separation Technology.** Bangkok : Chulalongkorn University Press.

[21] Subramanian, M.N. 2017. **Polymer blends and Composites.** Beverly : Scrivener Publishing.

[22] Lohse, D.J. and Datta, S. 1996. **Polymeric Compatibilizers: Uses and Benefits in Polymer Blends.** New York : Hanser Publishers.

[23] Thomas, S., Grohens, Y. and Jyotishkumar, P. 2014. **Characterization of Polymer Blends: Miscibility, Morphology, and Interfaces.** Weinheim : Wiley-VCH Verlag.

[24] Deng, Y., Yu, C., Wongwiwattana, P. and Thomas, N.L. 2018. "Optimizing ductility of poly(lactic acid)/poly(butylene adipate-co-terephthalate) blends through co-continuous phase morphology." Polymers and the Environment. 26(9) : 3802-3816.

[25] Brydon, J.A. 1999. **Plastic Materials.** 7th ed. Oxford : Butterworth Heinemann.

[26] Sonpoo, T., Deesamer, S. 2013. "Improvement of mechanical and water vapor permeability properties of LDPE films with EVA, EVOH and zeolite A." B.Sc. Special Project, Department of Chemistry, Faculty of Science, King Mongkut's Institute of Technology Ladkrabang.

[27] Kenawy, E., Shokr, AB. M., and Serag, M. 2016. "Biocidal Polymers by Chemical Modification of (Ethylene-vinyl Alcohol) Copolymers." Materials and Chemistry. 6(2) : 28-39.

[28] Chen, J., Spear, S.K., Huddleston, J.G. and Rogers R.D. 2005. "Polyethylene glycol and solutions of polyethylene glycol as green reaction media." Green chemistry. 7 : 64-82.

[29] Zalipsky, S. and Harris, J.M. 1997. "Introduction to Chemistry and Biological Applications of Poly (ethylene glycol)." ACS Symposium Series. 680 : 1-13.

[30] Bailey, F.E. 1990. **Alkylene Oxides and Their Polymers.** New York : CRC Press.

[31] Jeff Sailstad. 2018. **Proof of Concept to Solution: A Unique Approach to Anti-PEG Antibodies Assessment.** [Online]. Available : https://www.bioagilytix.com/from-the-stage/proof-of-concept-to-solution-a-unique-approach-to-anti-peg-antibodies-assessment/.

[32] Khoury, D. E. 2017. "Toward the use of electrostatic force microscopy to study interphase in nanodielectric materials" Ph.D. energy and material, Thesis of University of Montpellier.

[33] Flörke, O.W., Graetsch, H.A., Brunk, F., Benda, L., Paschen, S., Bergna, H.E., Roberts, W.O., Welsh, W.A., Libanati, C., Ettlinger, M., Kenner, D., Maier, M., Meon, W., Schmoll, R., Gies, H. and Schiffmann, D. 2008. "Silica." Ullmann's Encyclopedia of Industrial Chemistry. 32 : 422-507.

[34] Boverhof, D.R., Bramante, C.M., Butala, J.H., Clancy, S.F., Lafranconi, M., West, J. and Gordon, S.C. 2015. "Comparative assessment of nanomaterial definitions and safety evaluation considerations." Regulatory Toxicology and Pharmacology. (73) : 137-150.

[35] Leblance, J.L. 2010. **Filled Polymers : Science and industrial applications.** Florida : CRC Press.

[36] Shin-Etsu Chemical Co., Ltd. 2017. **Silane Coupling Agents.** Tokyo : Shin-Etsu.

[37] Gelest Inc. 2014. Silane Coupling Agents: Connecting Across Boundaries. 3rd ed. Pennsylvania : Gelest.

[38] JNC AMERICA. 2012. **Sila-Ace.** [Online]. Available : http://www.jncamericany.com/sila-ace/index.html.

[39] Power Chemical Corporation. 2015. **Products–Regular Commercial Amino Silanes.** [Online]. Available : http://www.powerchemical.net/silanes/amino silanes.html.

[40] Tang, M.F., Hou, J.W., Lei, L., Liu, X., Guo, S.R., Wang, Z.M. and Chen, K.M. 2010. "Preparation, characterization and properties of partially hydrolyzed ethylene vinyl acetate copolymer films for controlled drug release." Pharmaceutics. 400 : 66-73.

[41] Hong, S.M., Kim, S.H. and Lee, K.B. 2013. "Adsorption of Carbon Dioxide on 3-Aminopropyl-Triethoxysilane Modified Graphite Oxide." Energy and Fuels. 27(6) : 3358-3363.

[42] Castro-Muñoz, R., Fíla, V., Martin-Gil, V. and Muller, C. 2018. "Enhanced CO_2 permeability in Matrimid® 5218 mixed matrix membranes for separating binary CO_2/CH_4 mixtures." Separation and Purification Technology. 210 : 553-562.

[43] Zhu, H., Yuan, J., Zhao, J., Liu, G. and Jin, W. 2018. "Enhanced CO_2/N_2 separation performance by using dopamine/polyethyleneimine-grafted TiO_2 nanoparticles filled PEBA mixed-matrix membranes." Separation and Purification Technology. 214 : 78-86.

[44] Amooghin, A.E., Sanaeepur, H., Moghadassi, A., Kargari, A., Ghanbari, D. and Mehrabadi, Z.S. 2010. "Modification of ABS membrane by PEG for capturing carbon dioxide from CO_2/N_2 Streams." Separation Science and Technology. 10 : 1385-1394.

[45] Isanejad, M. and Mohammadi, T. 2018. "Effect of amine modification on morphology and performance of poly(ether-block-amide)/fumed silica nanocomposite membranes for CO2/CH4 separation." Materials Chemistry and Physics. 205 : 303-314.

[46] Rahman, MD. M., Filiz, V., Shishaskiy, S., Abetz, C., Neumann, S., Bolmer, S., Khan, M.M. and Abetz, V. 2013. "PEBAX® with PEG functionalized POSS as nanocomposite membranes for CO_2 separation." Membrane Science. 437 : 286-297.

[47] Xing, R. and Ho, W. WS. 2009. "Synthesis and characterization of crosslinked polyvinyl alcohol/polyethylene glycol blend membranes for CO_2/CH_4 separation." Taiwan Institute of Chemical Engineers. 40 : 654-662.

[48] Matweb. 2018. **Material Safety Data Sheet: ExxonMobil Escorene®LD 783.ND Molding, extrusion and compounding resin.** [Online]. Available : http://www.matweb.com/search/datasheet.aspx?MatGUID=f50de2ccc4de4f848b07de840482fc45.

[49] Thermo Fisher Scientific. 2018. **Material Safety Data Sheet: 3-Aminopropyltriethoxysilane.** [Online]. Available : https://assets.thermofisher.com/TFSAssets/LSG/manuals/MAN0011406_3Aminopropyltriethoxysilane_UG.pdf.

[50] The Dow Chemical Company. 2015. **Material Safety Data Sheet: CARBOWAX™ SENTRY™ Polyethylene Glycol 400.** [Online]. Available : http://doc.ccc-group.com/msds/english/288903.pdf.

[51] The Dow Chemical Company. 2015. **Material Safety Data Sheet: CARBOWAX™ SENTRY™ Polyethylene Glycol 1450 NF Flake (Inhibited).** [Online]. Available : http://msdssearch.dow.com/PublishedLiteratureDOWCOM/dh_09ad/0901b803809ad5de.pdf?filepath=polyglycols/pdf.

[52] The PPG Industries, Inc. 2012. **Hi-Sil 255CG-D Silica - PPG Silica Products.** [Online]. Available : https://www.ppgsilica.com/getmedia/bcf42e74-5944-44a3-ba00-8f5fcdde3a8d/HiSil255CGDBrochure.pdf.

[53] Micro-analysis, Inc. 2011. **Elemental Analysis Methods Reference sheet.** [Online]. Available : http://www.microana.com/pdf/Elemental-Analysis-Methods.pdf.

[54] Jung, H.S., Moon, D.S. and Lee, J.K. 2012. "Quantitative analysis and efficient surface modification of silica nanoparticles." Nanomaterials. (2012) : 1-8.

[55] Makphon, K., Rukchonlatee, S., Sooknoi, T., Yamaguchi, M. and Ritvirulh, C. 2016. "Mechanical and rheological properties of LLDPE/SEBS/Modified Zeolite ZSM-5 blends." Proceedings of the International Polymer Conference of Thailand 2016 (PCT-6), Pathumwan Princess Hotel, Bangkok, Thailand, June 30-July 1, pp. 355-360.

[56] Wunderlich, B., 1990. **Thermal Analysis.** Boston : Academic Press.

[57] Cimmino, S., Martuscelli, E., Silvestre, C., Cecere, A. and Fontelos, M. 1993. "Influence of copolymer composition on phase structure and crystallization of poly(ethylene oxide)/poly(ethylene-co-vinyl acetate) blends." Polymer. 34(6) : 1207-1211.

[58] Pielichowski, K. and Flejtuch, K. 2002. "Differential scanning calorimetry studies on poly(ethylene glycol) with different molecular weights for thermal energy storage materials." Polymers for Advanced Technologies. 13 : 690-696.

[59] Reza, M.B. and Abolfazl, J. 2018. "Synthesis and characterization of high performance modified ZIF-8/Pebax1657 mixed matrix membrane for CO_2 separation." Membrane Science and Technology. 8 : 83-91.

[60] Isaac, R., Rajeev, K.G. and Kamal B. 2015. "Effect on superhydrophobic surfaces on electrical porcelain insulator, improved technique at polluted areas for longer life and reliability." Engineering and Technology. 4(4) : 509-519.

[61] Sven, C.F. and Fred, L. 2011. "Silica nanoparticles for the layer-by-layer assembly of fully electro-active cytochrome c multilayers." Nanobiotechnology. 9(59) : 1-12.

[62] Agostino, A., Errico, M.E., Malinconico, M., Rosa, M.D., Avella, M. and Schiraldi C. 2011. "Development of nanocomposite based on hydroxyethyl methacrylate and functionalized fumed silica: mechanical, chemico-physical and biological characterization." Material Science. 22 : 481-490.

[63] Shadi, H., Mohammadamin, K. and Peyman, K. 2014. "Influence of various types of silica nanoparticles on permeation properties of polyurethane/silica mixed matrix membranes." Membrane Science. 453 : 369-383.

[64] Ognen, P.G., Dana, K., Josef, Z., Neda, N., Roman, D., Eliska, M.C., Miroslav, S., Milan, H. and Frantisek R. 2015. "Self-assembled anchor layers/polysaccharide coatings on titanium surfaces: a study of functionalization and stability." Nanotechnology. 6 : 617-631.

[65] Robert, G.A., Amanda, V.E., Jason, A., Claire, E.L., Dmitriy, A.K., Gregory, F.M. and Gunther, G.A. 2012. "Molecular Structure of 3-Aminopropyltriethoxysilane Layers Formed on Silanol-Terminated Silicon Surfaces." Physical Chemistry. 116 : 6289-6297.

[66] Boksebeld, M., Kilin, V., Geoloen, A., Ceccone, G., Jaffal, A., Schmidt, C., Alekseev, S., Lysenko, V., Wolf, J.P., Bonacina, L., Souteyrand, E., Chevolot, Y. and Monnier, V. 2017. "Folate-modified silicon carbide nanoparticles as multiphoton imaging nanoprobes for cancer-cell-specific labeling." Royal Society of Chemistry Advances. 7 : 27361-27369.

[67] Hassen, H., Dae Keun, C., Chang Min, L., Justin, J., Dong Hyun, K., Aeran, S., Kwun Bum, C., Myungkwan, S., Jun Fei, M., Chang Su, K. and Seung Yoon, R. 2019. "Replacement of n-type layers with a non-toxic APTES interfacial layer to improve the performance of amorphous Si thin-film solar cells." Royal Society of Chemistry Advances. 9 : 7536-7542.

[68] Zhao, D., Ren, J., Li, H. and Deng, M. 2014. "Gas separation properties of poly(amide-6-b-ethylene oxide)/amino modified multi-walled carbon nanotubes mixed matrix membranes." Membrane Science. 467 : 41-47.

[69] Shishatskiy, S., Pauls, J.R., Nunes, S.P. and Peinemann, KV. 2010. "Quaternary ammonium membrane materials for CO_2 separation." Membrane Science. 359 : 44-53.

[70] Wang, L., Lei, M., Wang, A., Liu, Q. and Zhang, T. 2007. "CO_2 adsorption on SBA-15 modified by aminosilane." Catalysis. 28(9) : 805-810.

[71] Ghadimi, A., Mohammadi, T. and Kasiri, N. 2014. "A novel chemical surface modification for fabrication of PEBA/SiO_2 nanocomposites membranes to separate CO_2 from syngas and natural gas streams." Industrial and Engineering Chemistry Research. 53(44) : 17476-17486.

[72] Kusworo, TD., Qudratun. B., Utomo. DP., Ramadhan. IR. and Indriyanti. 2018. "Synthesis and characterization of nano hybrid membrane PES-TiO_2 for biogas purification: Combination effect of ultra violet and cross-linking." MATEC Web of Conferences. 156 : 1-4.

[73] Soltani, B. and Asghari, M. 2017. "Effects of ZnO nanoparticle on the gas separation performance of polyurethane mixed matrix membrane." Membranes. 7(43) : 1-16.

[74] Mubashir, M., Yin fong, Y., Thiam Leng, C., Kok Keong, L. and Jusoh, N. 2020. "Study on the effect of process parameters on CO2/CH4 binary gas separation performance over NH_2-MIL-53(Al)/cellulose acetate hollow fiber mixed matrix membrane." Polymer Testing. 81 : 106223-106232.

[75] Noroozi, Z. and Bakhtiari, O. 2019. "Preparation of amino functionalized titanium oxide nanotubes and their incorporation within Pebax/PEG blended matrix for CO_2/CH_4separation." Chemical Engineering Research and Design. 152 : 149-164.

[76] Farashi, Z., Azizi, S., Rezaei-DashtArzhandi, M., Noroozi, Z. and Azizi, N. 2019. "Improving CO_2/CH_4 separation efficiency of Pebax-1657 membrane by adding Al_2O_3 nanoparticles in its matrix." Journal of Natural Gas Science and Engineering. 72 : 103019-103027.

Appendices

Appendix A

The calculation of carbonyl index

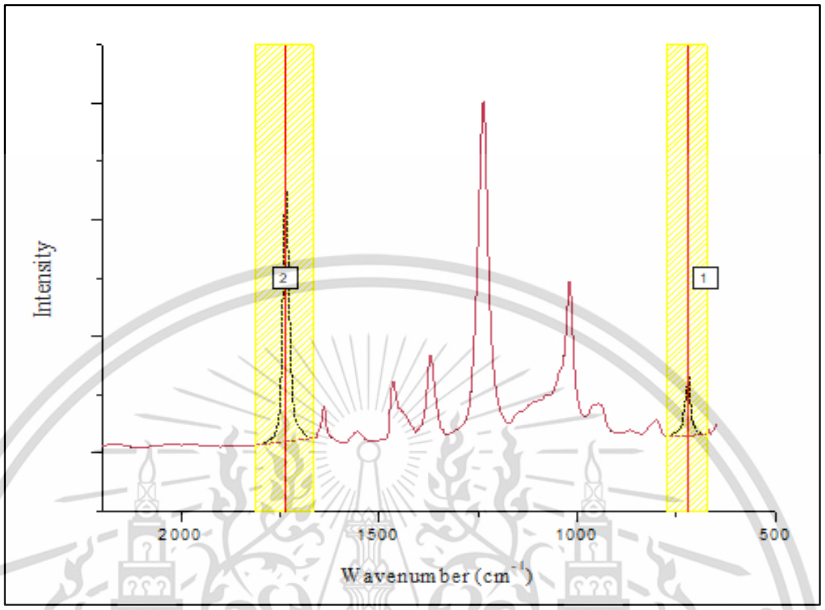

Figure A.1 Integration of the peak area of EVA for carbonyl index calculation

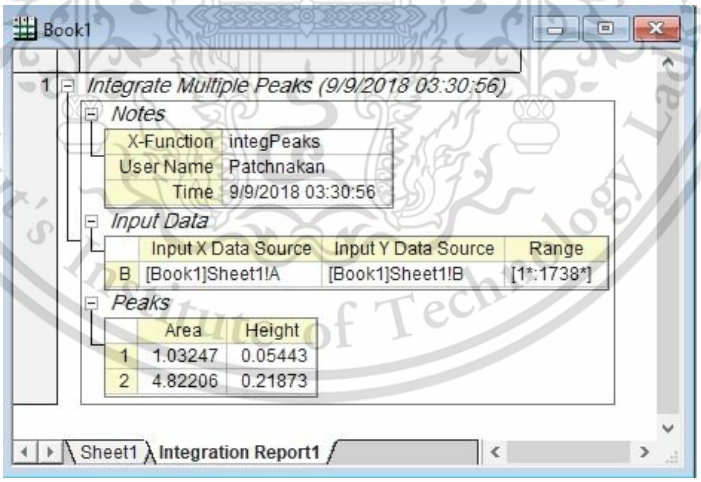

Figure A.2 Raw data of EVA for carbonyl index calculation

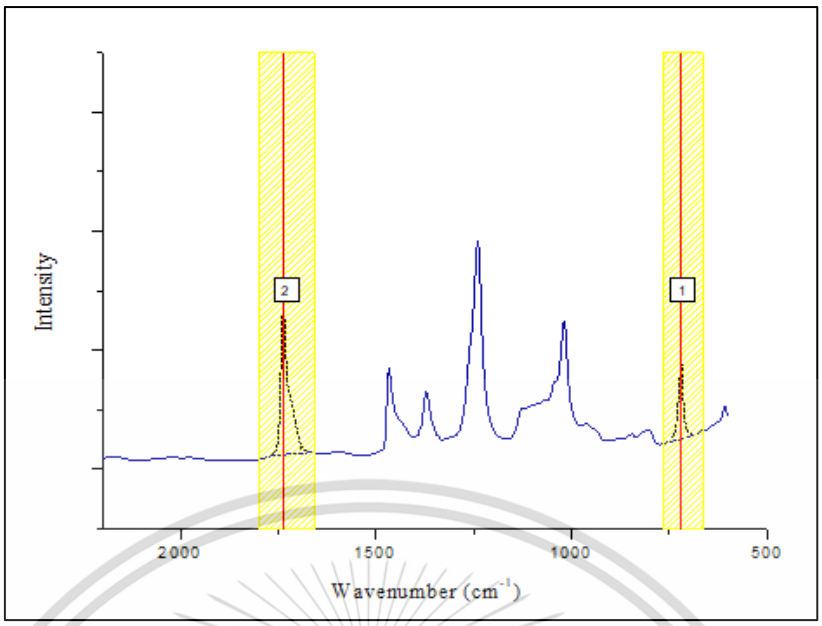

Figure A.3 Integration of the peak area of p-EVA for carbonyl index calculation

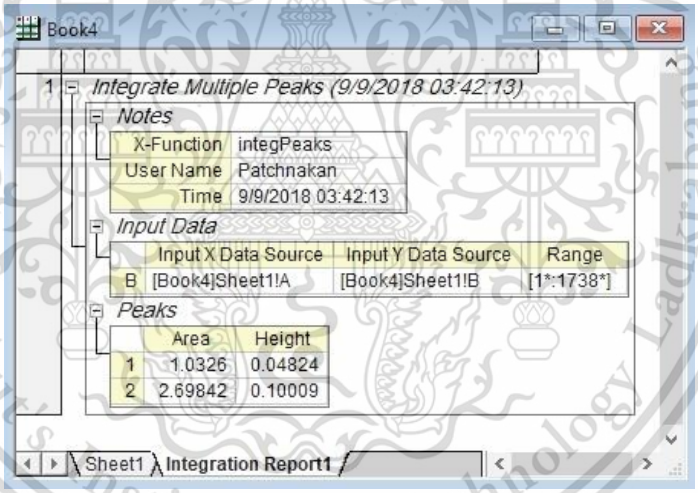

Figure A.4 Raw data of p-EVA for carbonyl index calculation

EVA

Area under carbonyl peak (C=O) = 4.82206

Area under CH_2 rocking = 1.03247

$$\text{C.I.} = \frac{\text{Carbonyl}}{CH_2 \text{ rocking}} = \frac{4.82206}{1.03247} = 4.6704$$

p-EVA

Area under carbonyl peak (C=O) = 2.69842

Area under CH_2 rocking = 1.03260

$$C.I. = \frac{\text{Carbonyl}}{CH_2 \text{ rocking}} = \frac{2.69842}{1.03260} = 2.6132$$

C.I. of EVA = 4.6704 is 100%

C.I. of p-EVA = 2.6132 is $\frac{2.6132 \times 100}{4.6704}$ = 55.95%

The residual carbonyl group (C=O) is 55.95%. Therefore, it was concluded that the C=O in EVA was transferred to be the hydroxyl groups (-OH) in p-EVA at 44.05% (which is from 100 - 55.95).

Appendix B

Carbon dioxide and methane permeations

Carbon dioxide permeation

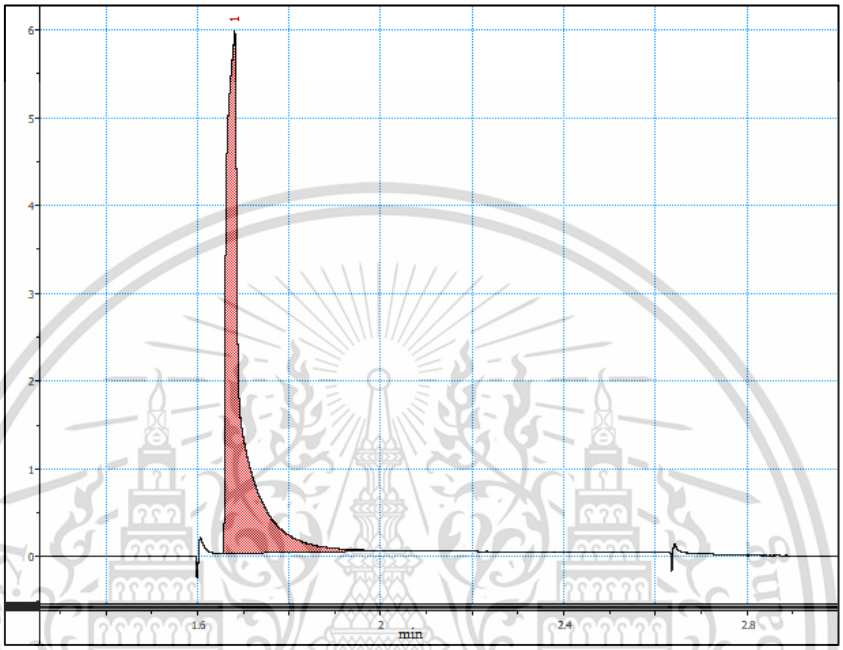

Figure B.1 TCD signal of carbon dioxide standard

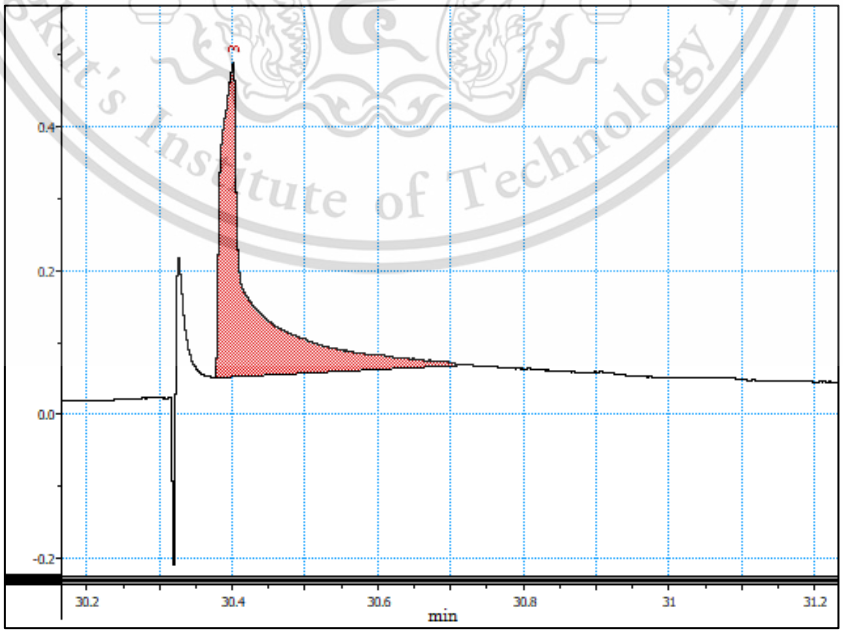

Figure B.2 TCD signal of carbon dioxide of EVA membrane

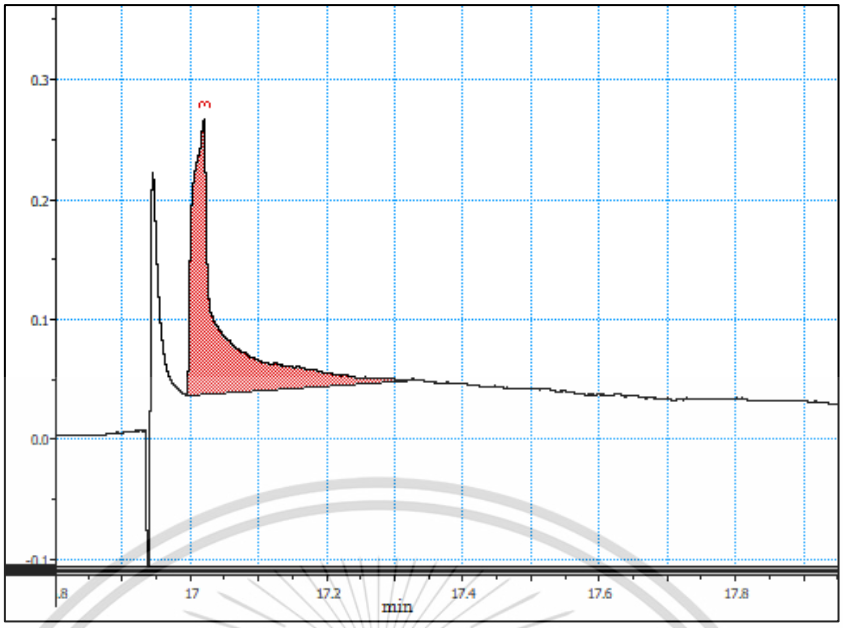

Figure B.3 TCD signal of carbon dioxide of p-EVA membrane

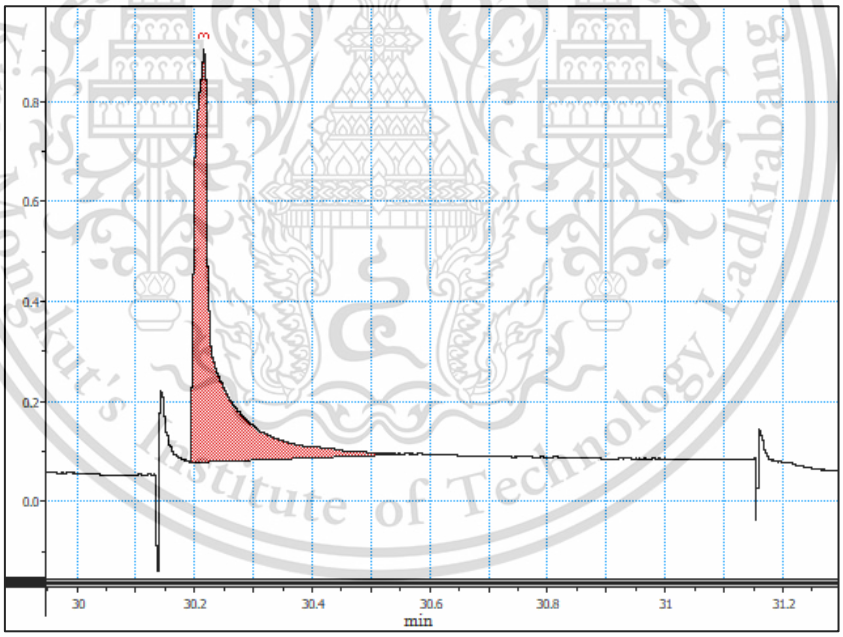

Figure B.4 TCD signal of carbon dioxide of p-EVA/5PEG400 membrane

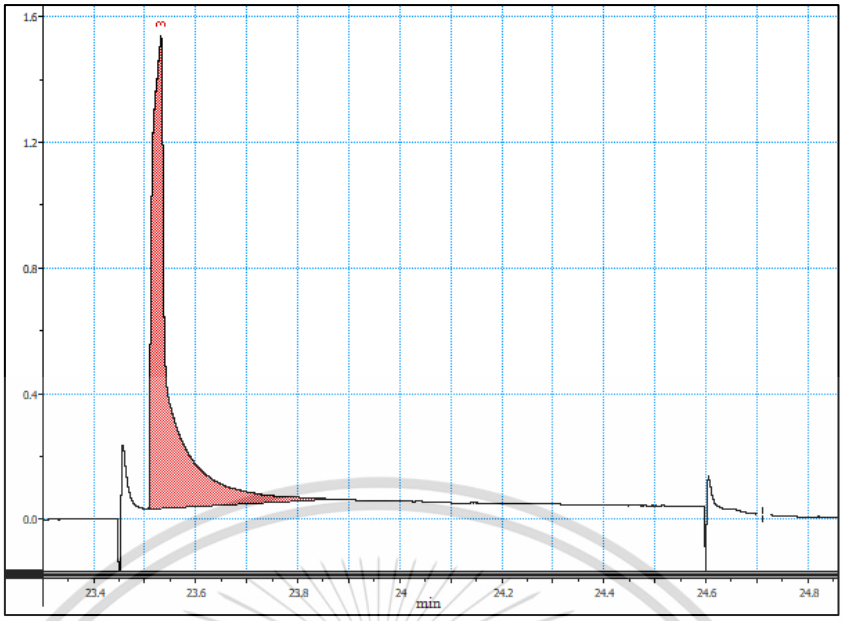

Figure B.5 TCD signal of carbon dioxide of p-EVA/10PEG400 membrane

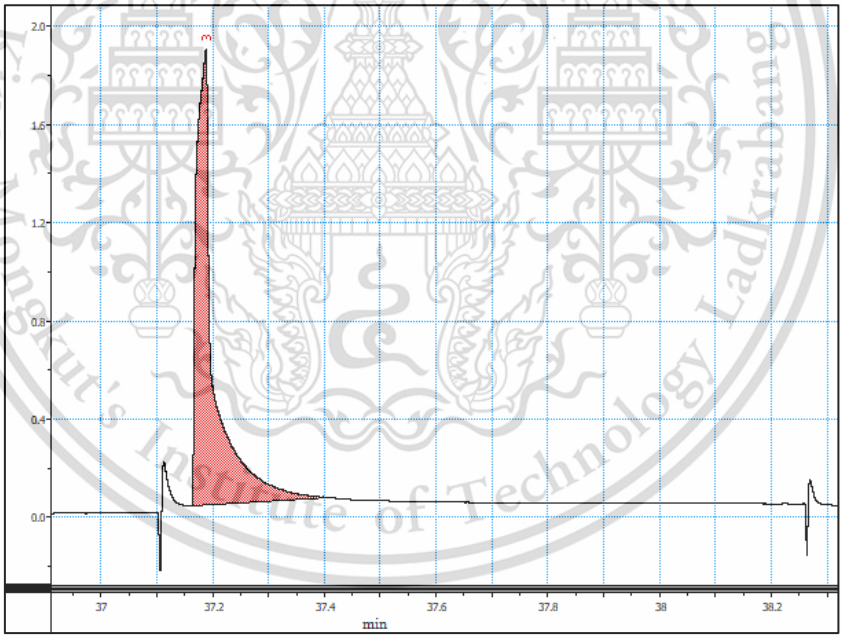

Figure B.6 TCD signal of carbon dioxide of p-EVA/15PEG400 membrane

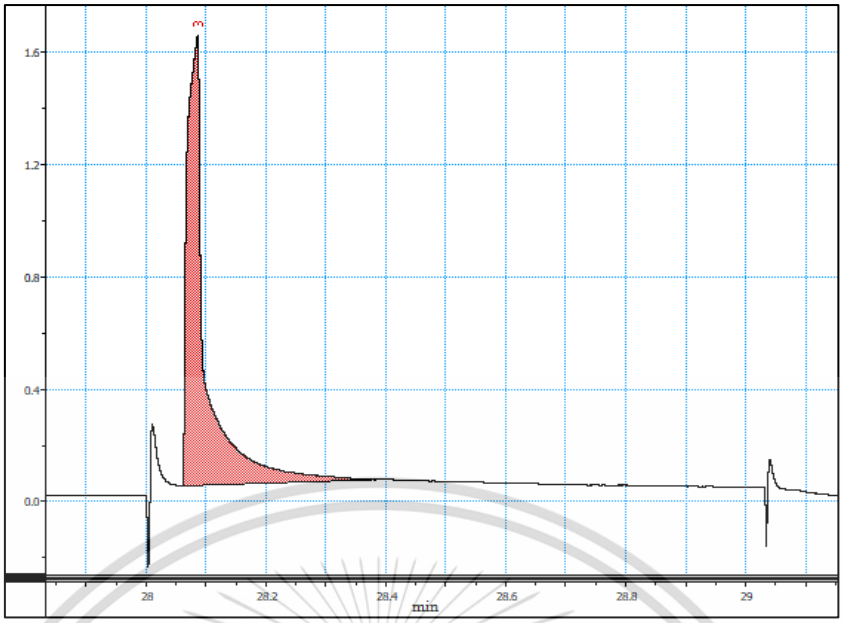

Figure B.7 TCD signal of carbon dioxide of p-EVA/5PEG1450 membrane

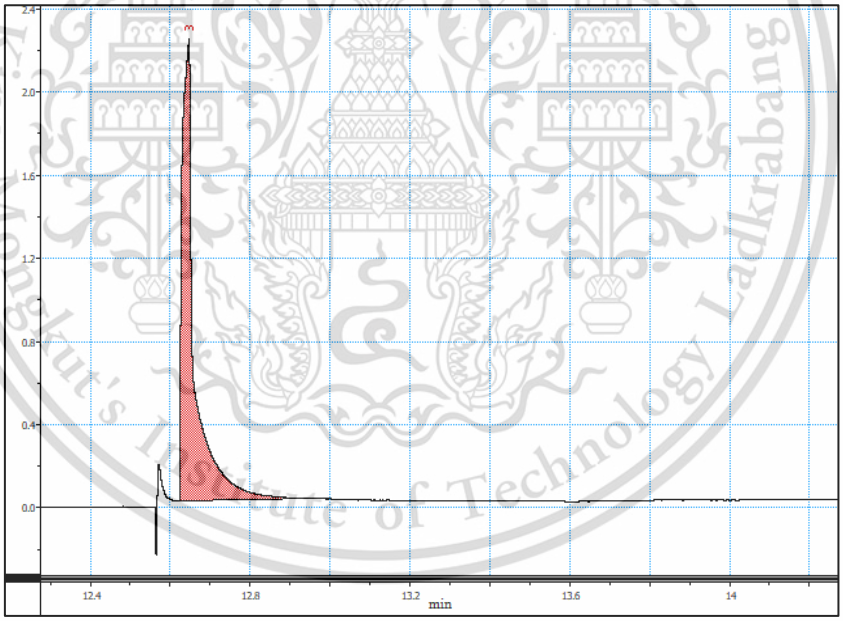

Figure B.8 TCD signal of carbon dioxide of p-EVA/10PEG1450 membrane

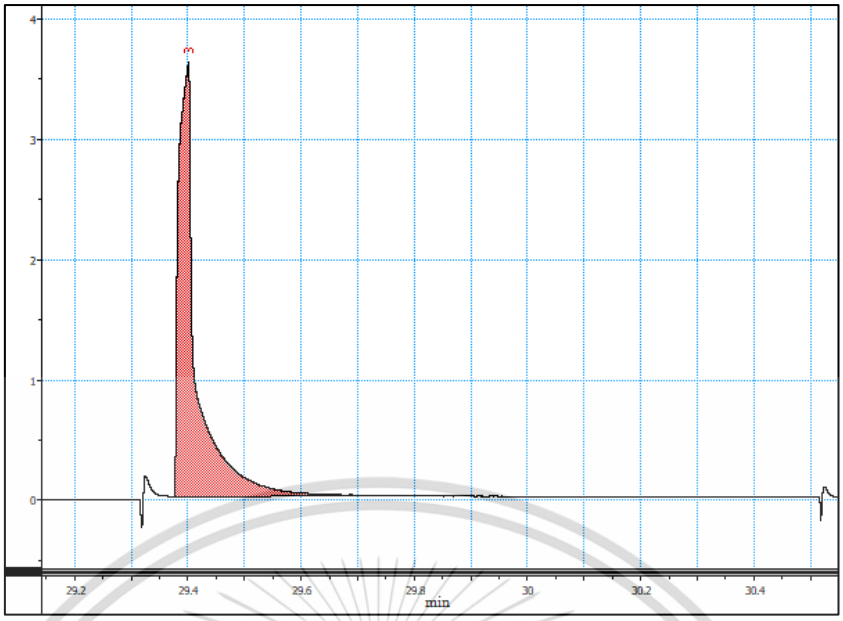

Figure B.9 TCD signal of carbon dioxide of p-EVA/15PEG1450 membrane

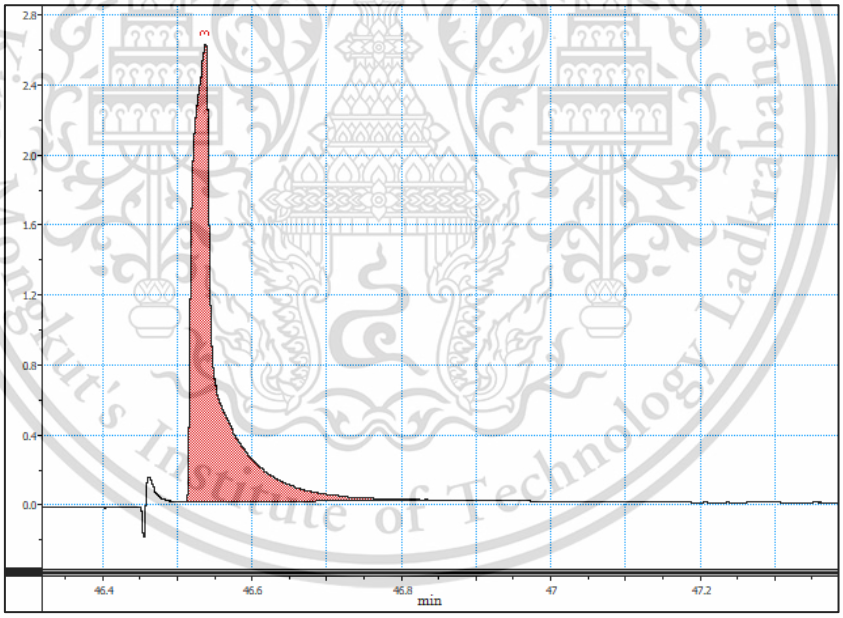

Figure B.10 TCD signal of carbon dioxide of p-EVA/15PEG400-0.3AFS membrane

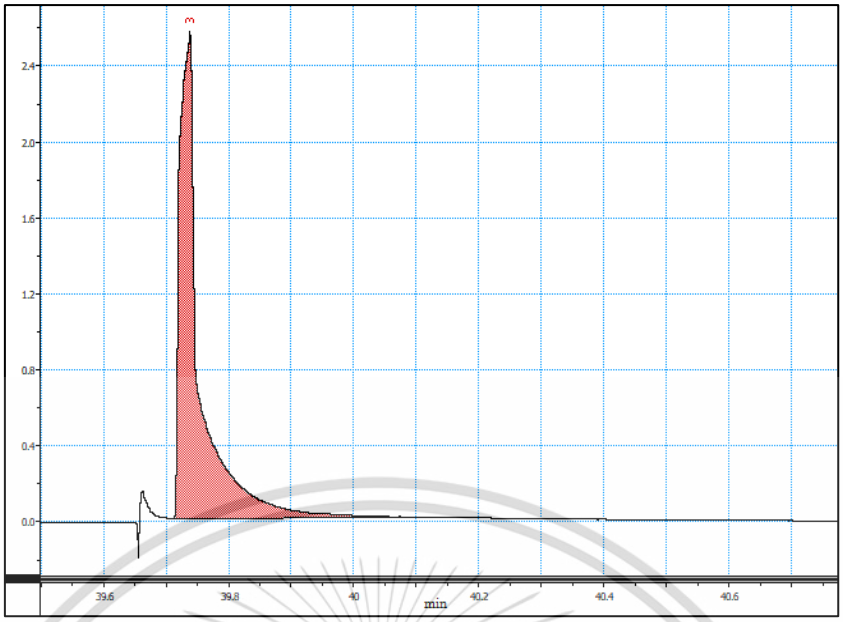

Figure B.11 TCD signal of carbon dioxide of p-EVA/15PEG400-0.6AFS membrane

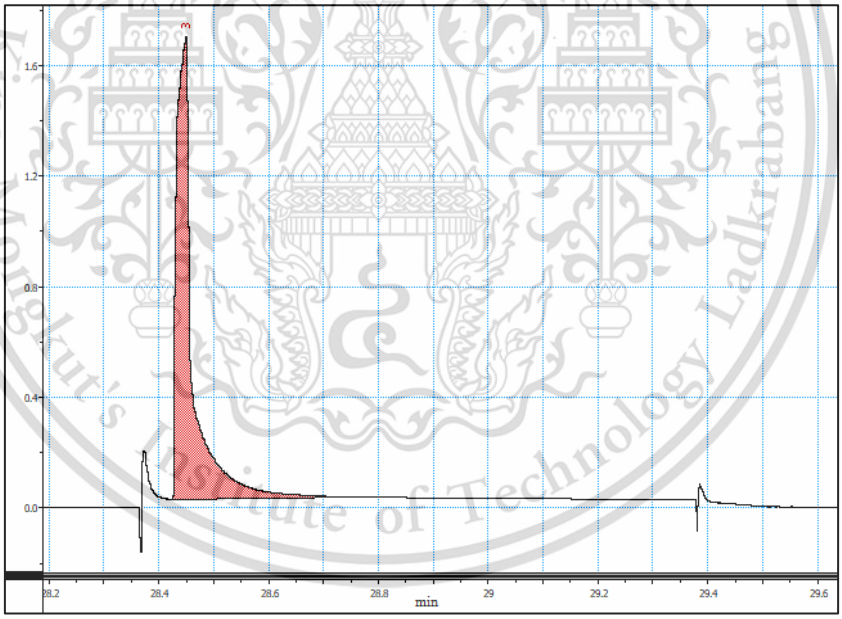

Figure B.12 TCD signal of carbon dioxide of p-EVA/15PEG400-0.9AFS membrane

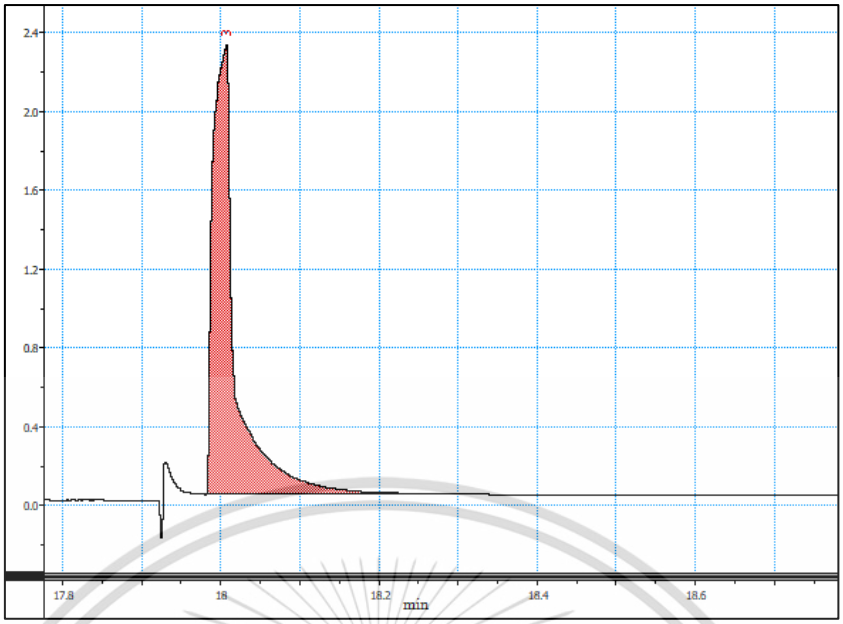

Figure B.13 TCD signal of carbon dioxide of p-EVA/15PEG1450-0.3AFS membrane

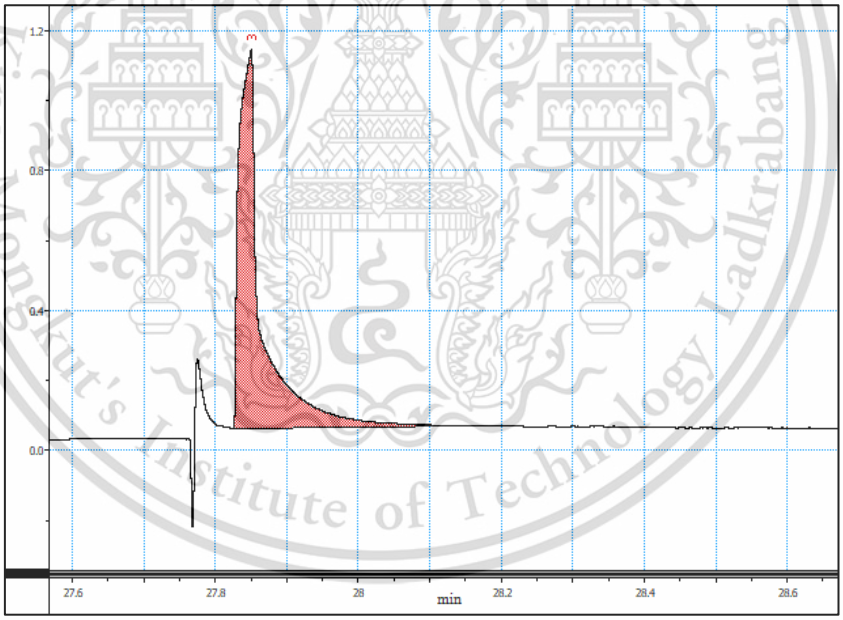

Figure B.14 TCD signal of carbon dioxide of p-EVA/15PEG1450-0.6AFS membrane

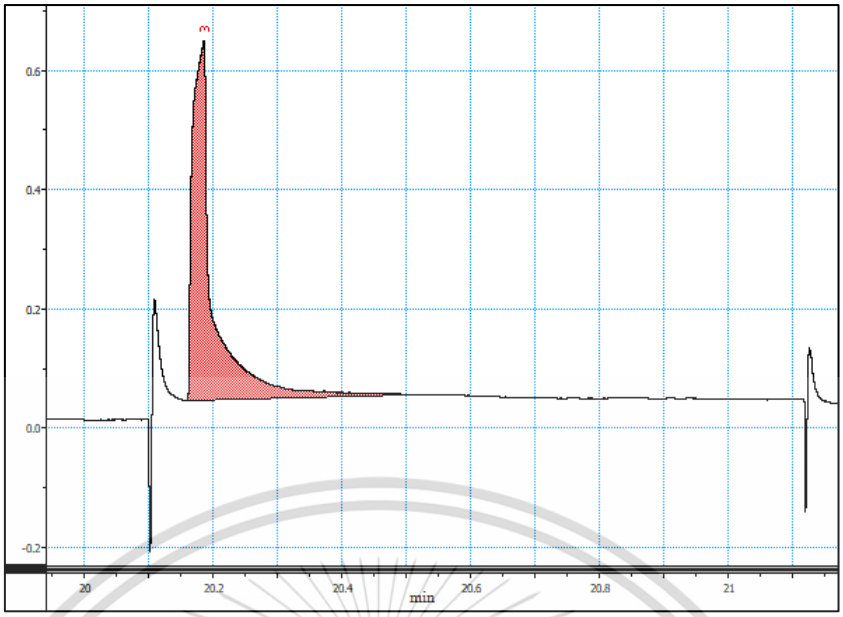

Figure B.15 TCD signal of carbon dioxide of p-EVA/15PEG1450-0.9AFS membrane

Carbon dioxide permeation calculation

Pressure drop (P_{drop})

$$P_{drop} = \frac{F}{A} = \frac{mg}{A}$$

When m = Mass of water in U-tube (kg)

g = Gravitational force (9.807 m/s^2)

A = Area of U-tube (m^2)

Mass of water in U-tube (m)

$$D = \frac{m}{V} \longrightarrow m = DV$$

$$; V = \pi r^2 h$$

$$= \pi \times (3\times10^{-3})^2 m^2 \times 6.67\times10^{-2} m$$

$$= 1.8859 \times10^{-6} m^3$$

When D = Density of water (~1 g/cm^3 or 1000 kg/m^3)

$$; m = (1000\ kg/m^3) \times (1.8859 \times10^{-6} m^3)$$

$$= 1.8859 \times10^{-3} kg$$

$$; So \quad P_{drop} = \frac{F}{A} = \frac{mg}{A} = \frac{(1.8859 \times10^{-3}\ kg)(9.807\ m/s^2)}{\pi(3\times10^{-3})^2\ m^2}$$

$$P_{drop} = 654.1276\ Pa$$

$$= 6.4557 \times10^{-3}\ atm$$

Transmission rate of CO_2 (J) (g/min)

$$PV = nRT$$

$$n = \frac{PV}{RT} \quad ; \quad V = \left(\frac{A_{CO_2}}{A_{std.}}\right) \times F_{feed} \quad ; \quad n = \frac{g}{M_w}$$

$$g = \frac{P \times \left(\frac{A_{CO_2}}{A_{std.}}\right) \times F_{feed} \times M_w}{RT}$$

When A_{CO_2} = Peak area of the permeate CO_2 (V·s)

$A_{std.}$ = Peak area of the standard CO_2 (V·s)

P = Pressure (atm)

M_w = Molecular weight of CO_2

F_f = Flow rate of the feed gas (L/min)

R = Ideal gas constant (L·atm/K·mol)

T = Temperature (K)

Example

CO_2 transmission rate of p-EVA/10PEG400 (g/min)

$$g = \frac{1.0066 \text{ atm} \times \left(\frac{3.41 \text{ V·s}}{140.16 \text{ V·s}}\right) \times 0.03 \text{ L/min} \times 44.01 \text{ g/mol}}{(0.08205 \text{ L·atm/K·mol}) \times 296 \text{ K}}$$

$$g = 1.3313 \times 10^{-3} \text{ g/min}$$

$$g = (1.3313 \times 10^{-3}) \text{ g/min} \times 1440 \text{ min/day}$$

$$g = 1.9171 \text{ g/day}$$

; So, the CO_2 transmission rate of p-EVA/10PEG400 = 1.9171 g/day

The CO_2 permeation rate (g/m^2·day)

$$\text{The } CO_2 \text{ permeation rate (g/m}^2\text{·day)} = \frac{J}{S_c}$$

When J = Transmission rate of CO_2 (g/day)

S_c = Size of permeation cell (m^2) ; ~2.5×10^{-3}m^2

$$\therefore \text{ The } CO_2 \text{ permeation rate (g/m}^2\text{·day)} = \frac{1.9171 \text{ g/day}}{2.5\times10^{-3}\text{m}^2}$$

$$= 766.84 \text{ g·m}^2\text{/day}$$

Methane permeation

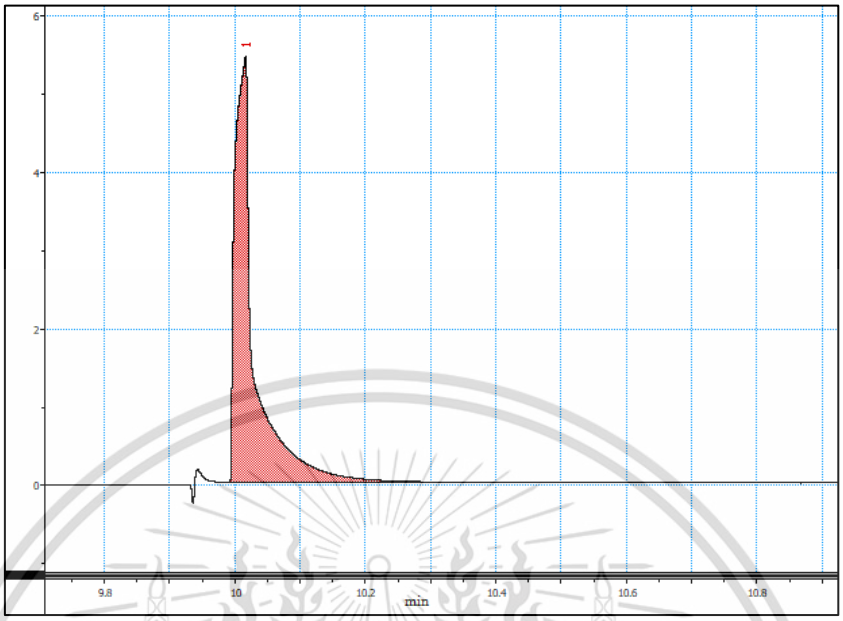

Figure B.16 TCD signal of methane standard

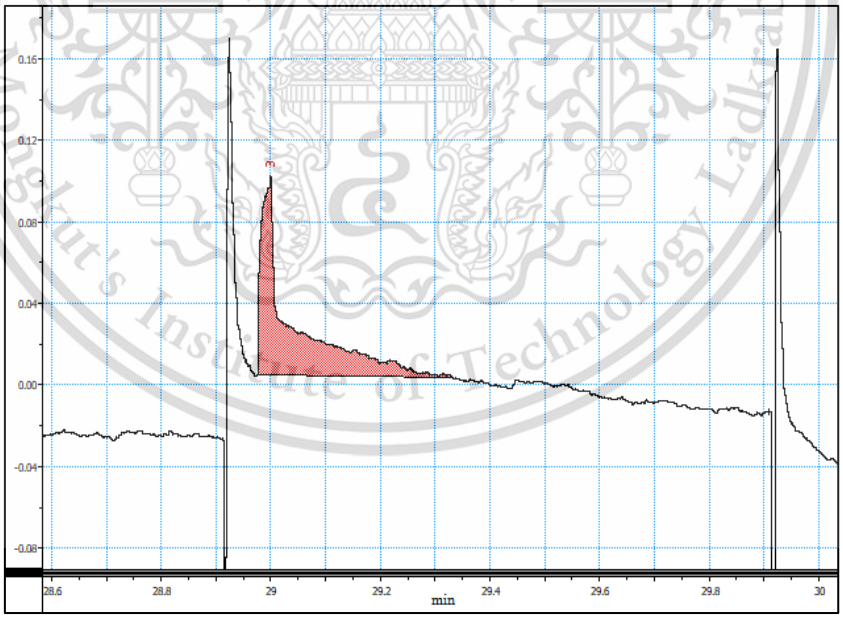

Figure B.17 TCD signal of methane of EVA membrane

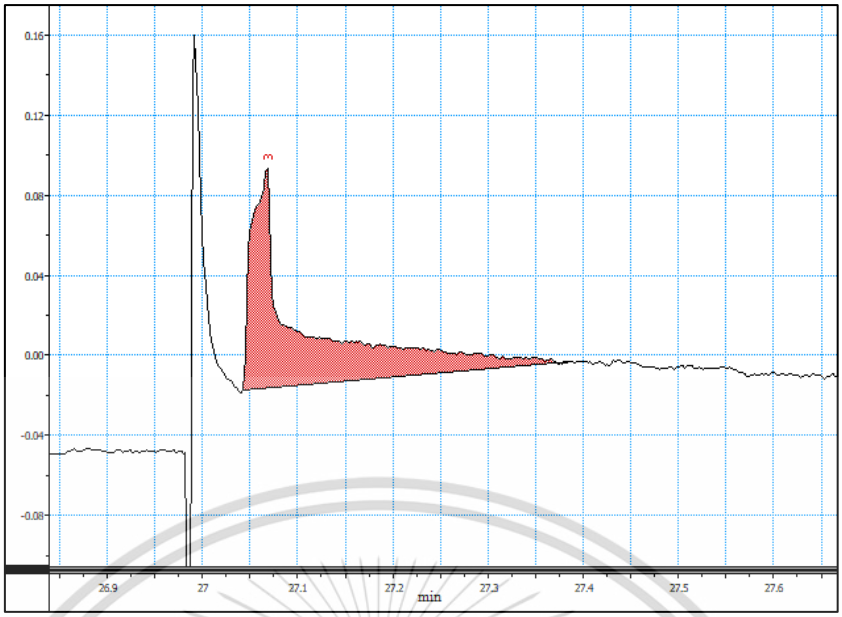

Figure B.18 TCD signal of methane of p-EVA membrane

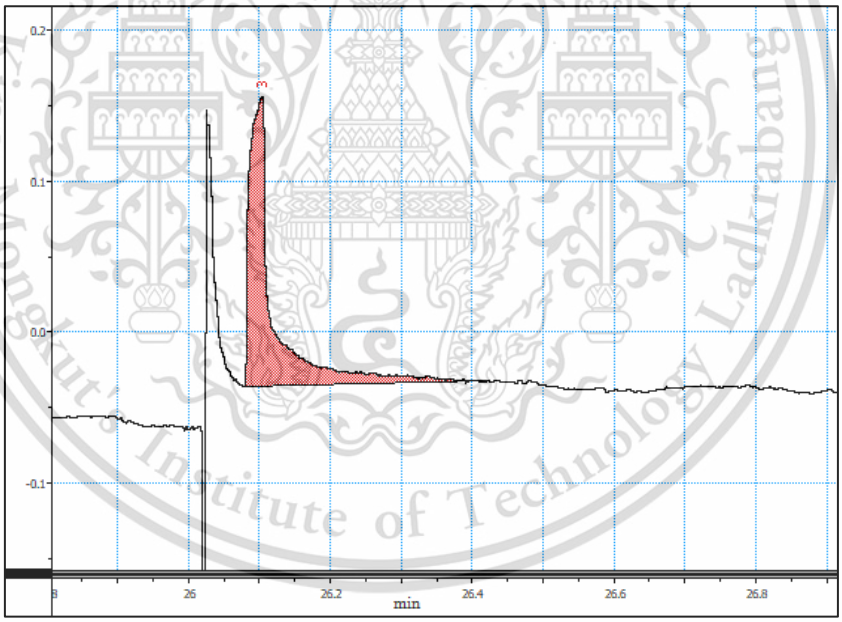

Figure B.19 TCD signal of methane of p-EVA/5PEG400 membrane

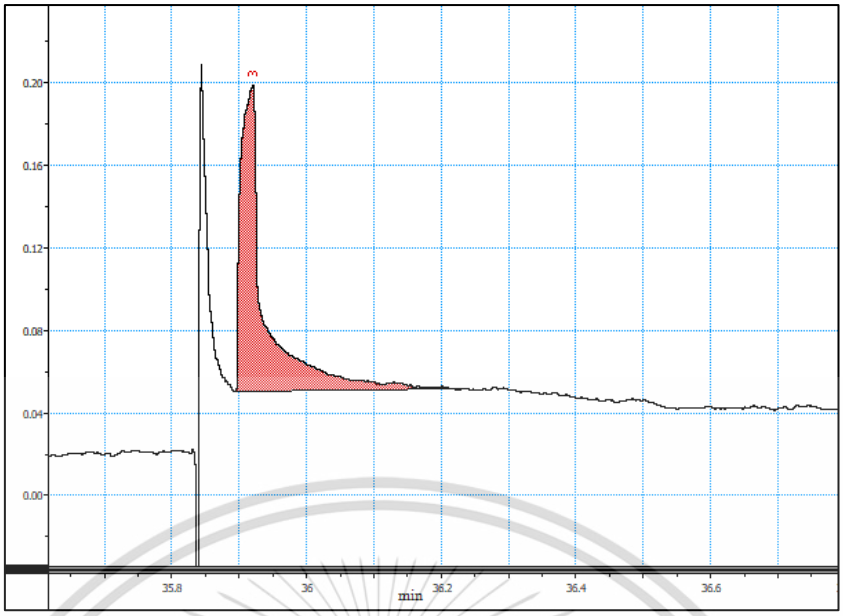

Figure B.20 TCD signal of methane of p-EVA/10PEG400 membrane

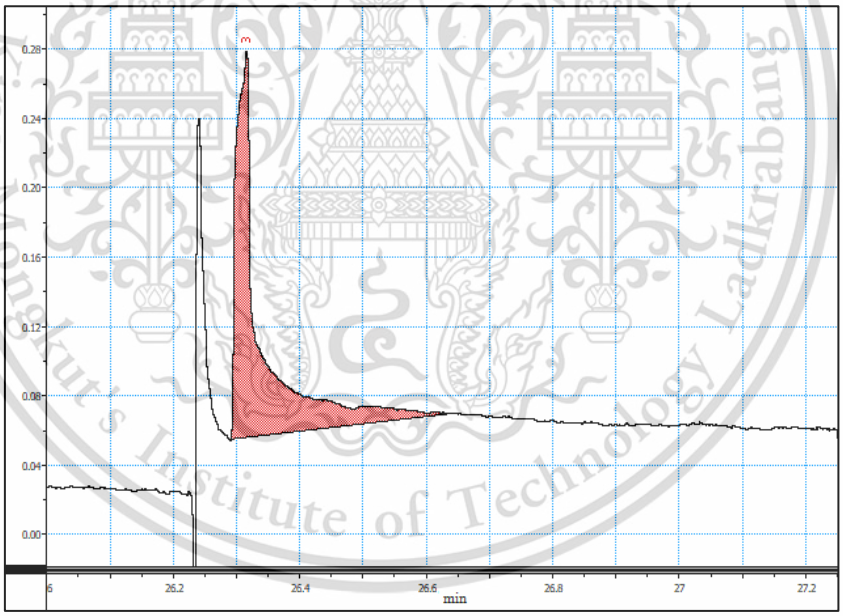

Figure B.21 TCD signal of methane of p-EVA/15PEG400 membrane

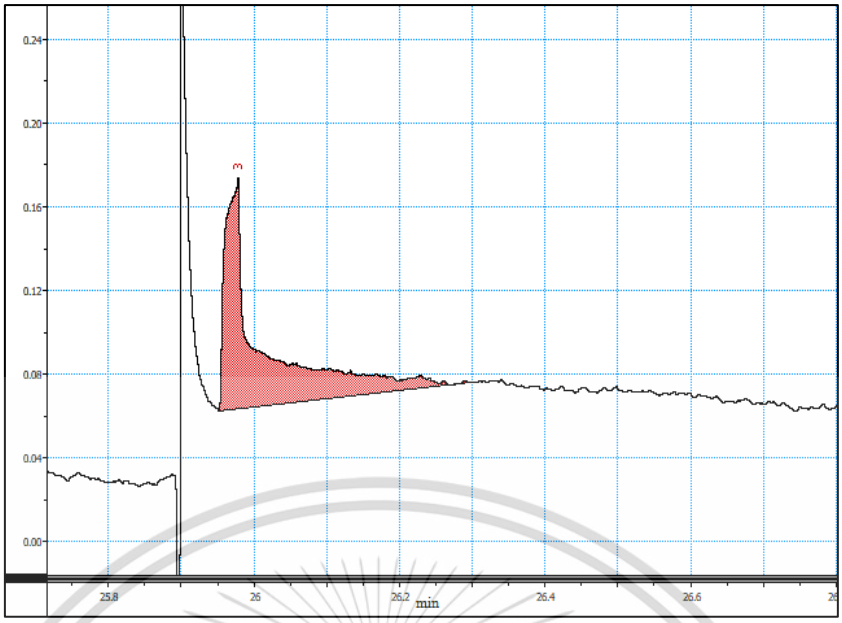

Figure B.22 TCD signal of methane of p-EVA/5PEG1450 membrane

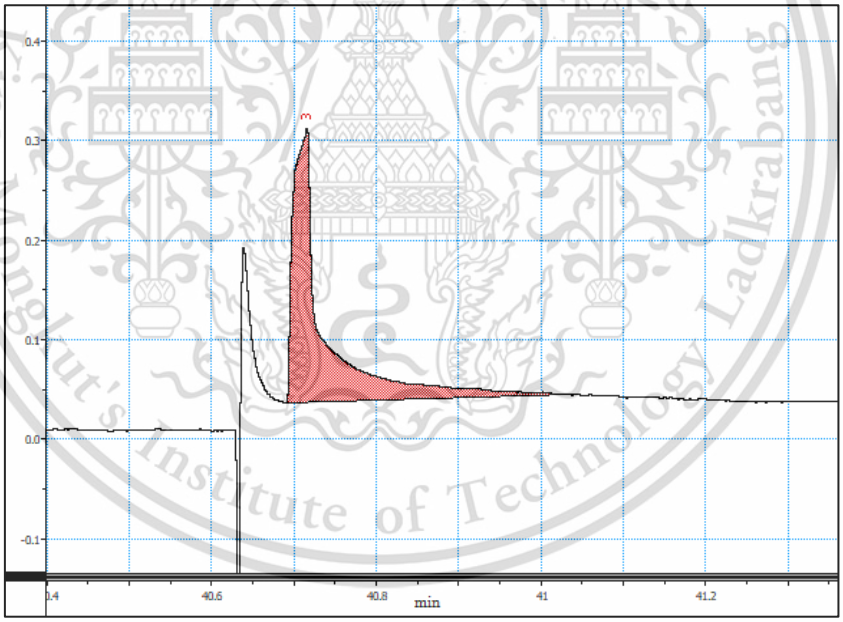

Figure B.23 TCD signal of methane of p-EVA/10PEG1450 membrane

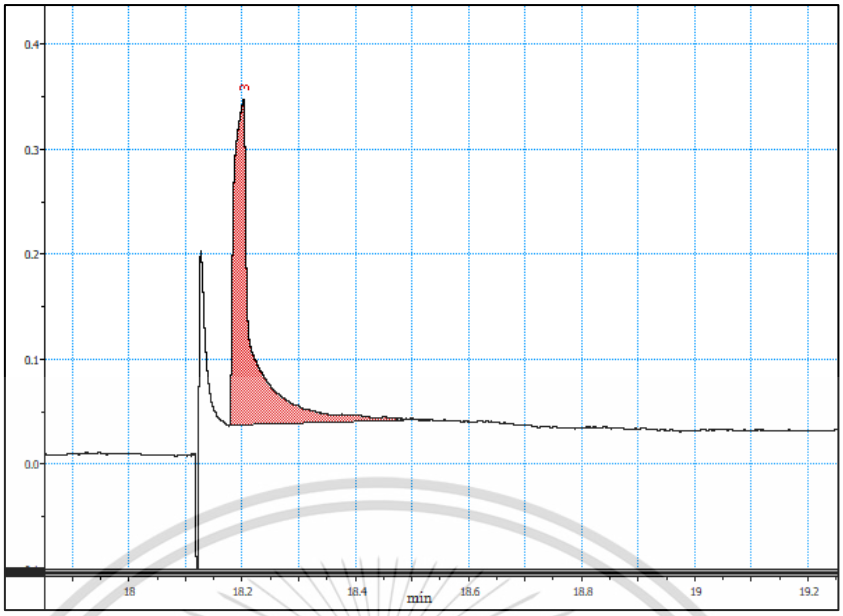

Figure B.24 TCD signal of methane of p-EVA/15PEG1450 membrane

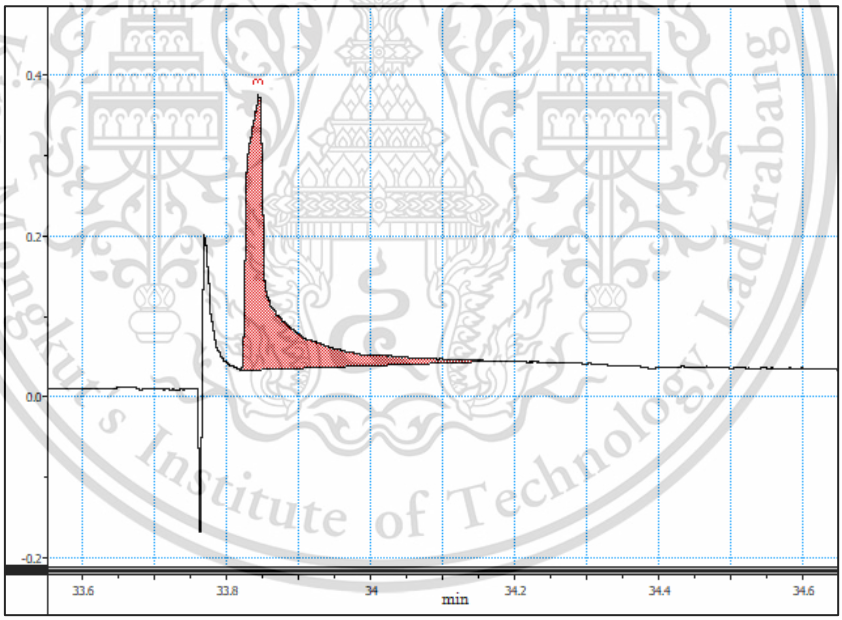

Figure B.25 TCD signal of methane of p-EVA/15PEG400-0.3AFS membrane

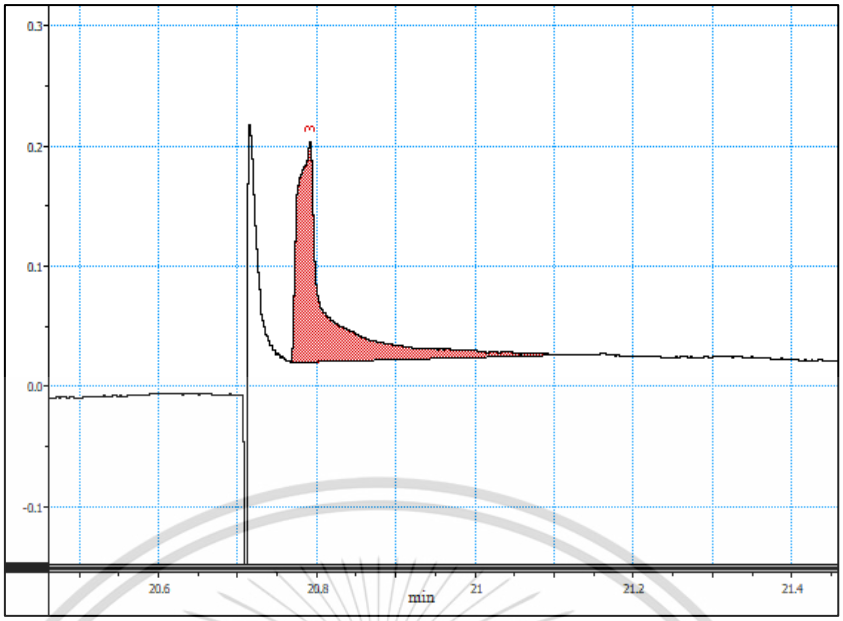

Figure B.26 TCD signal of methane of p-EVA/15PEG400-0.6AFS membrane

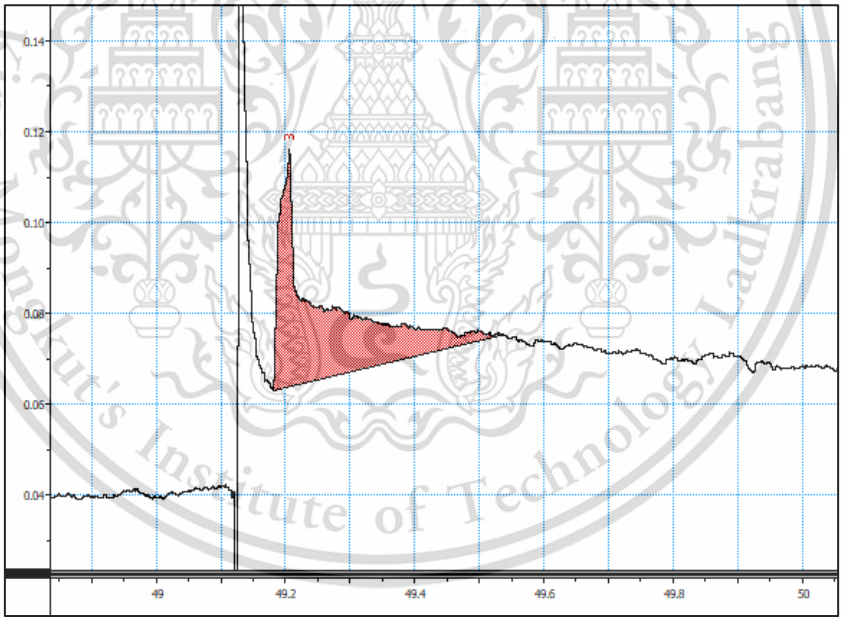

Figure B.27 TCD signal of methane of p-EVA/15PEG400-0.9AFS membrane

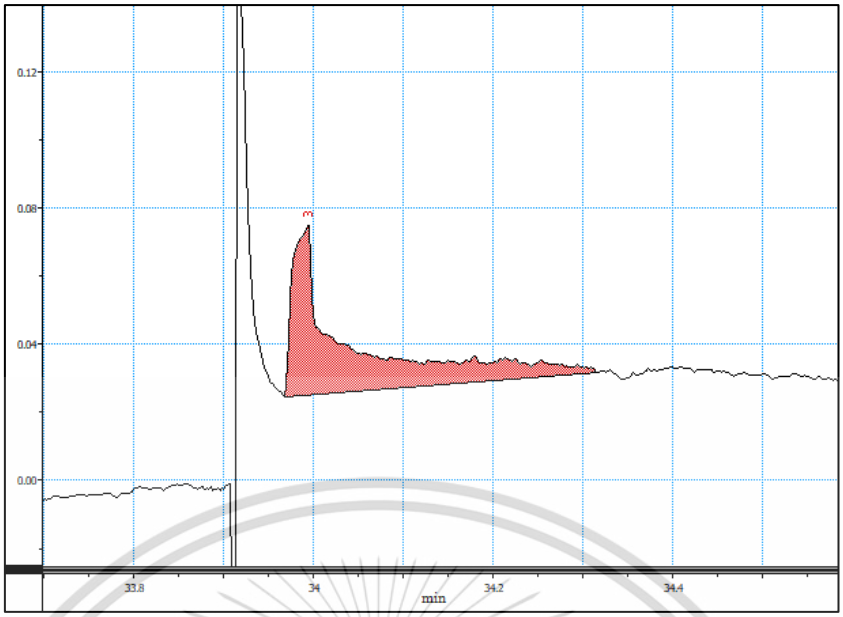

Figure B.28 TCD signal of methane of p-EVA/15PEG1450-0.3AFS membrane

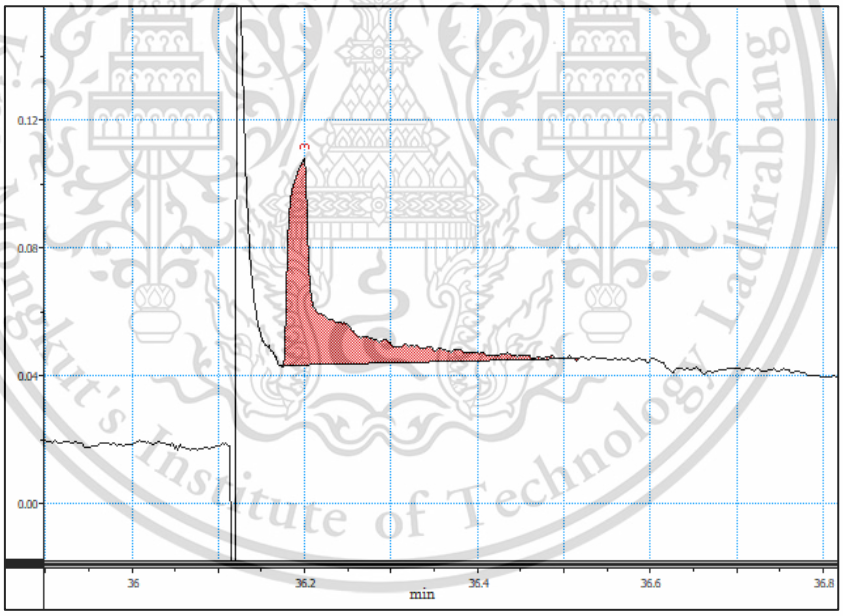

Figure B.29 TCD signal of methane of p-EVA/15PEG1450-0.6AFS membrane

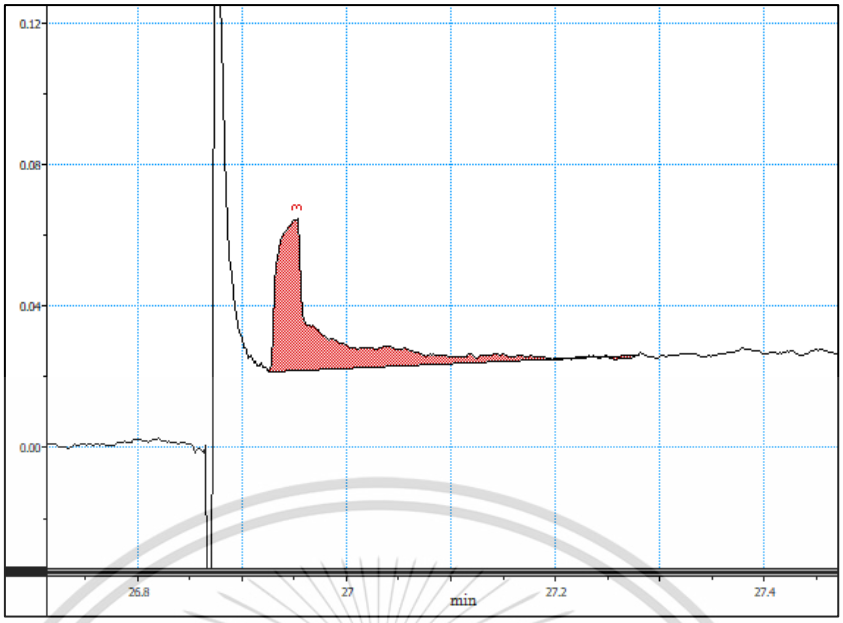

Figure B.30 TCD signal of methane of p-EVA/15PEG1450-0.9AFS membrane

Methane permeation calculation

Transmission rate of CH_4 (Q) (g/min)

$$PV = nRT$$

$$n = \frac{PV}{RT} \quad ; \quad V = \left(\frac{A_{CH_4}}{A_{std.}}\right) \times F_{feed} \quad ; \quad n = \frac{g}{M_w}$$

$$g = \frac{P \times \left(\frac{A_{CH_4}}{A_{std.}}\right) \times F_{feed} \times M_w}{RT}$$

When A_{CH_4} = Peak area of the permeate CH_4 (V·s)

$A_{std.}$ = Peak area of the standard CH_4 (V·s)

P = Pressure (atm)

M_w = Molecular weight of CH_4

F_f = Flow rate of the feed gas (L/min)

R = Ideal gas constant (L·atm/K·mol)

T = Temperature (K)

Example

CH_4 transmission rate of p-EVA/10PEG400 (g/min)

$$g = \frac{1.0066 \text{ atm} \times \left(\frac{0.89 \text{ V·s}}{110.97 \text{ V·s}}\right) \times 0.03 \text{ L/min} \times 16.0 \text{ g/mol}}{(0.08205 \text{ L·atm/K·mol}) \times 296 \text{ K}}$$

g = 1.5956×10^{-4} g/min

g = 1.5956×10^{-4} g/min × 1440 min/day

g = 0.2298 g/day

; So, the CO_2 transmission rate of p-EVA/10PEG400 = 0.2298 g/day

The CH_4 permeation rate (g/m^2·day)

$$\text{The } CH_4 \text{ permeation rate (g/m}^2\text{·day)} = \frac{Q}{S_c}$$

When Q = Transmission rate of CH_4 (g/day)

S_c = Size of permeation cell (m^2) ; ~$2.5\times10^{-3} m^2$

$$\therefore \text{ The } CH_4 \text{ permeation rate (g/m}^2\text{·day)} = \frac{0.2298 \text{ g/day}}{2.5\times10^{-3} m^2}$$

$$= 91.92 \text{ g·m}^2\text{/day}$$

So, the CO_2/CH_4 selectivity of p-EVA/10PEG400 blend membrane

$$\alpha_{CO_2/CH_{4(\text{by weight})}} = \frac{CO_2 \text{ permeation rate}}{CH_4 \text{ permeation rate}}$$

$$= \frac{766.84 \text{ g·m}^2\text{/day}}{91.92 \text{ g·m2/day}}$$

; $\alpha_{CO_2/CH_4} = 8.34$

Table B.1 The comparison of CO_2 and CH_4 permeability and CO_2/CH_4 selectivity of all membranes

Formulas	CO_2 permeability ($g/m^2 \cdot day$)	CH_4 permeability ($g/m^2 \cdot day$)	CO_2/CH_4 selectivity
1. EVA	317.0 ± 7.6	38.4 ± 2.5	8.3
2. p-EVA	149.0 ± 5.2	23.1 ± 2.2	6.5
3. p-EVA/5PEG400	500.2 ± 18.7	48.2 ± 1.1	10.4
4. p-EVA/10PEG400	784.3 ± 26.0	88.2 ± 5.1	8.9
5. p-EVA/15PEG400	985.9 ± 11.3	139.5 ± 13.7	7.1
6. p-EVA/5PEG1450	803.5 ± 8.3	43.1 ± 2.9	18.6
7. p-EVA/10PEG1450	1159.1 ± 14.0	87.8 ± 2.6	13.2
8. p-EVA/15PEG1450	1791.7 ± 20.9	161.9 ± 6.6	11.1
9. p-EVA/15PEG400-0.3AFS	1395.4 ± 43.6	112.9 ± 6.0	12.4
10. p-EVA/15PEG400-0.6AFS	1402.3 ± 37.7	62.9 ± 4.0	22.3
11. p-EVA/15PEG400-0.9AFS	752.3 ± 19.5	34.8 ± 7.6	21.6
12. p-EVA/15PEG1450-0.3AFS	957.2 ± 22.9	28.3 ± 4.6	33.8
13. p-EVA/15PEG1450-0.6AFS	684.7 ± 21.0	23.6 ± 4.2	29.0
14. p-EVA/15PEG1450-0.9AFS	312.5 ± 13.6	16.8 ± 1.7	18.6

Appendix C

DSC

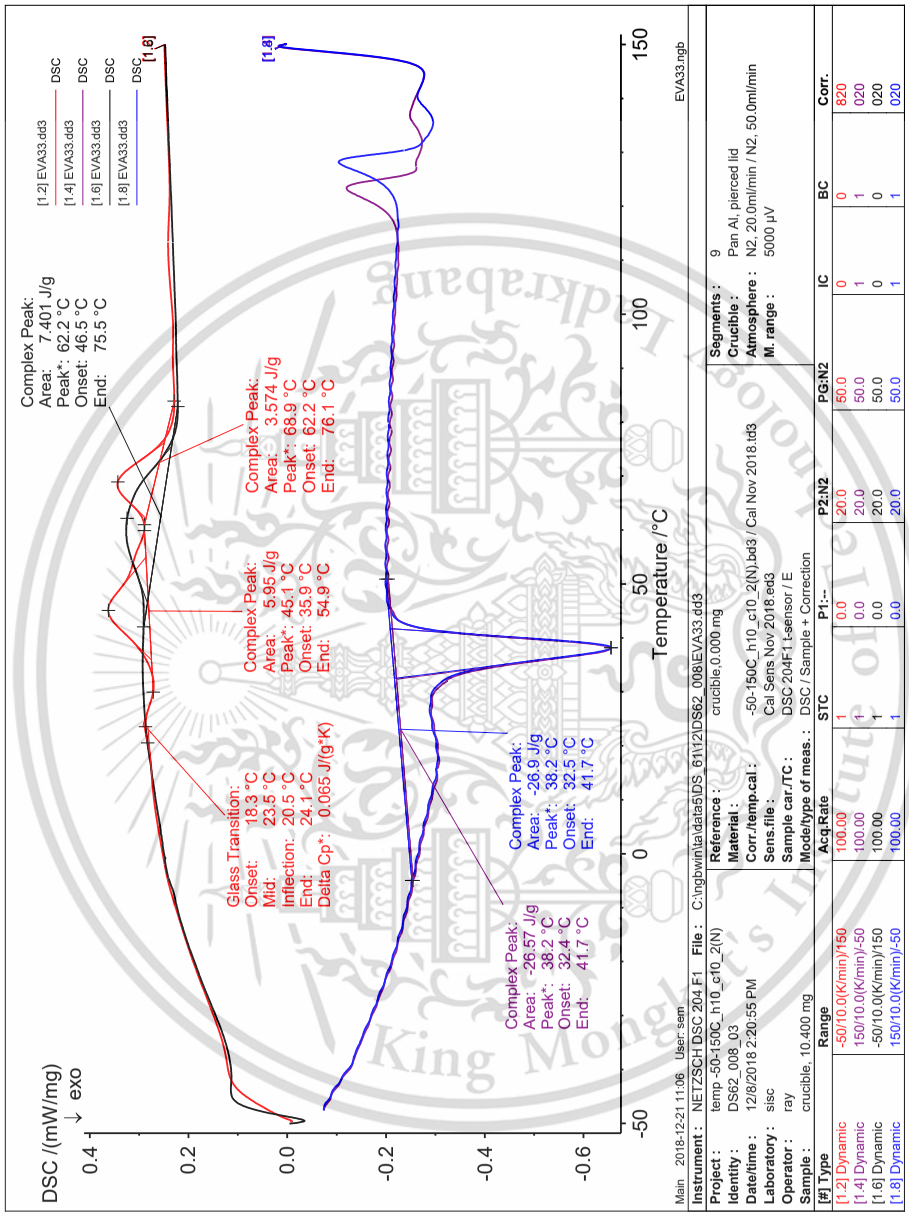

Instrument :	NETZSCH DSC 204 F1	**File :**	C:\ngbwin\data5\DS_6\1\2\DS62_008\EVA33.dd3				**Segments :**	9		
Project :	temp -50-150C_h10_c10_2(N)	**Reference :**	crucible,0.000 mg				**Crucible :**	Pan Al, pierced lid		
Identity :	DS62_008_03	**Material :**					**Atmosphere :**	N2, 20.0ml/min / N2, 50.0ml/min		
Date/time :	12/8/2018 2:20:55 PM	**Corr./temp.cal :**	-50-150C_h10_c10_2(N).bd3 / Cal Nov 2018.td3				**M. range :**	5000 µV		
Laboratory :	sisc	**Sens.file :**	Cal Sens Nov 2018.ed3							
Operator :	ray	**Sample car./TC :**	DSC 204F1 t-sensor / E							
Sample :	crucible, 10.400 mg	**Mode/type of meas. :**	DSC / Sample + Correction							
[#] Type	**Range**	**Acq.Rate**	**STC**	**P1:-**	**P2:N2**	**PG:N2**	**IC**	**BC**	**Corr.**	
[1.2] Dynamic	-50/10.0(K/min)/150	100.00	1	0.0	20.0	50.0	0	0	820	
[1.4] Dynamic	150/10.0(K/min)/-50	100.00	1	0.0	20.0	50.0	1	1	020	
[1.6] Dynamic	-50/10.0(K/min)/150	100.00	1	0.0	20.0	50.0	0	0	020	
[1.8] Dynamic	150/10.0(K/min)/-50	100.00	1	0.0	20.0	50.0	1	1	020	

Figure C.1 DSC thermogram of EVA membrane

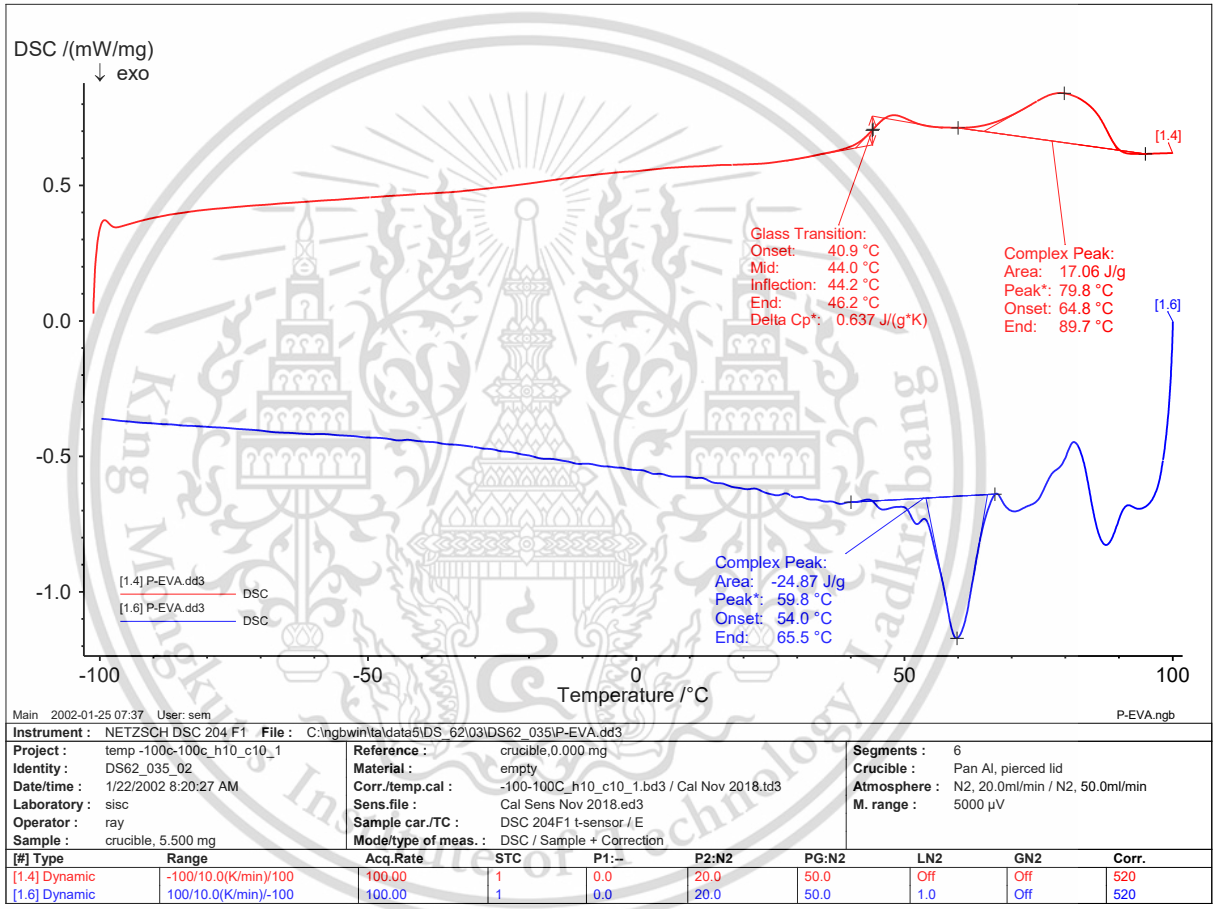

Figure C.2 DSC thermogram of p-EVA membrane

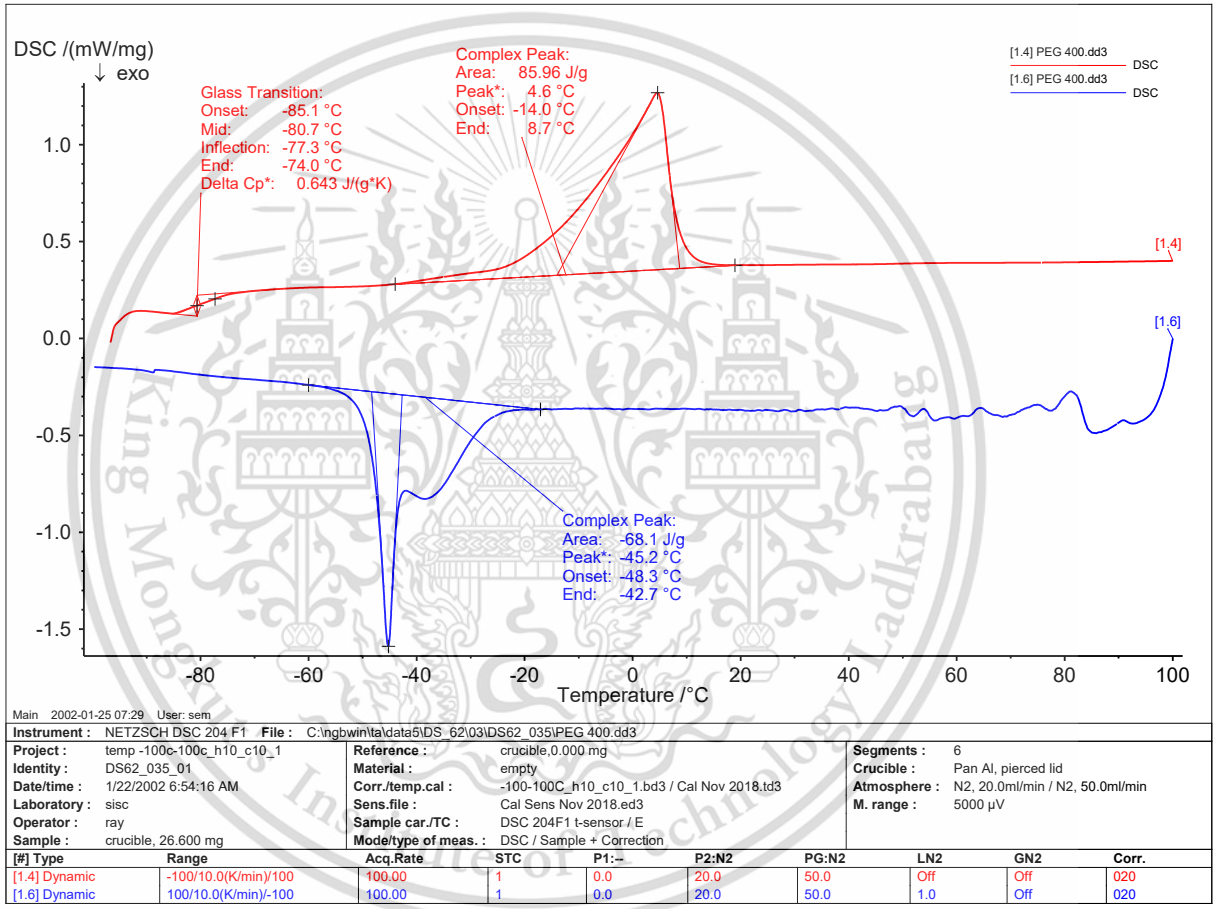

Figure C.3 DSC thermogram of PEG-400

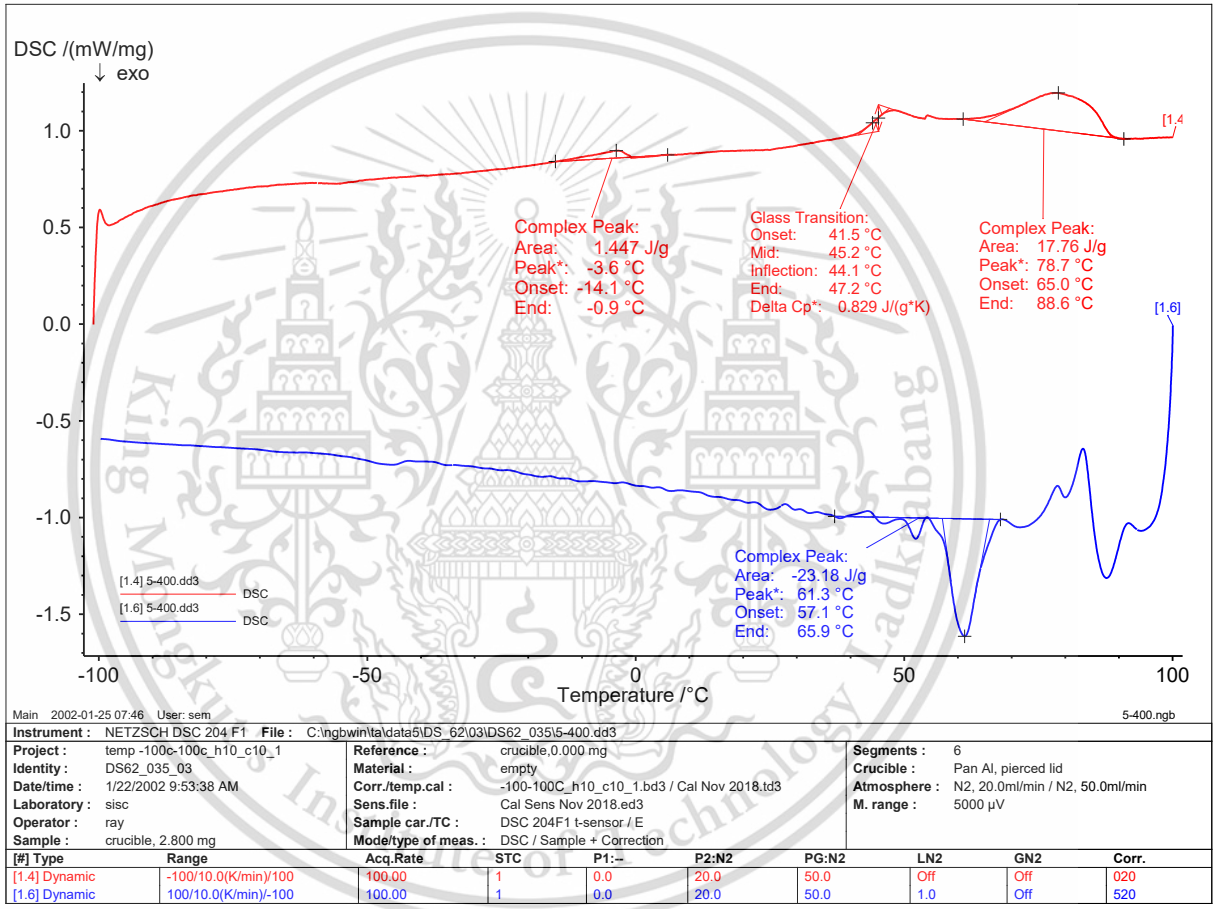

Figure C.4 DSC thermogram of p-EVA/5PEG400 membrane

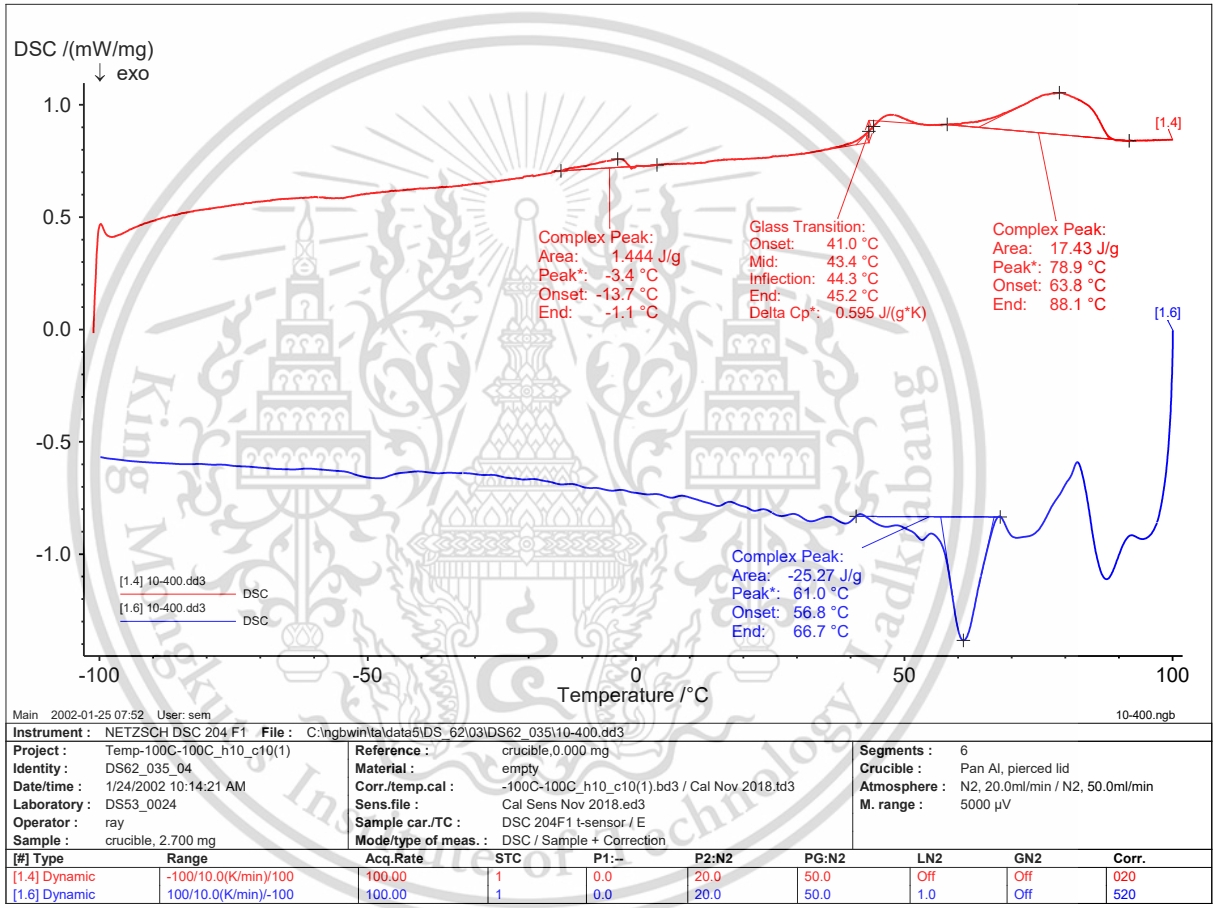

Figure C.5 DSC thermogram of p-EVA/10PEG400 membrane

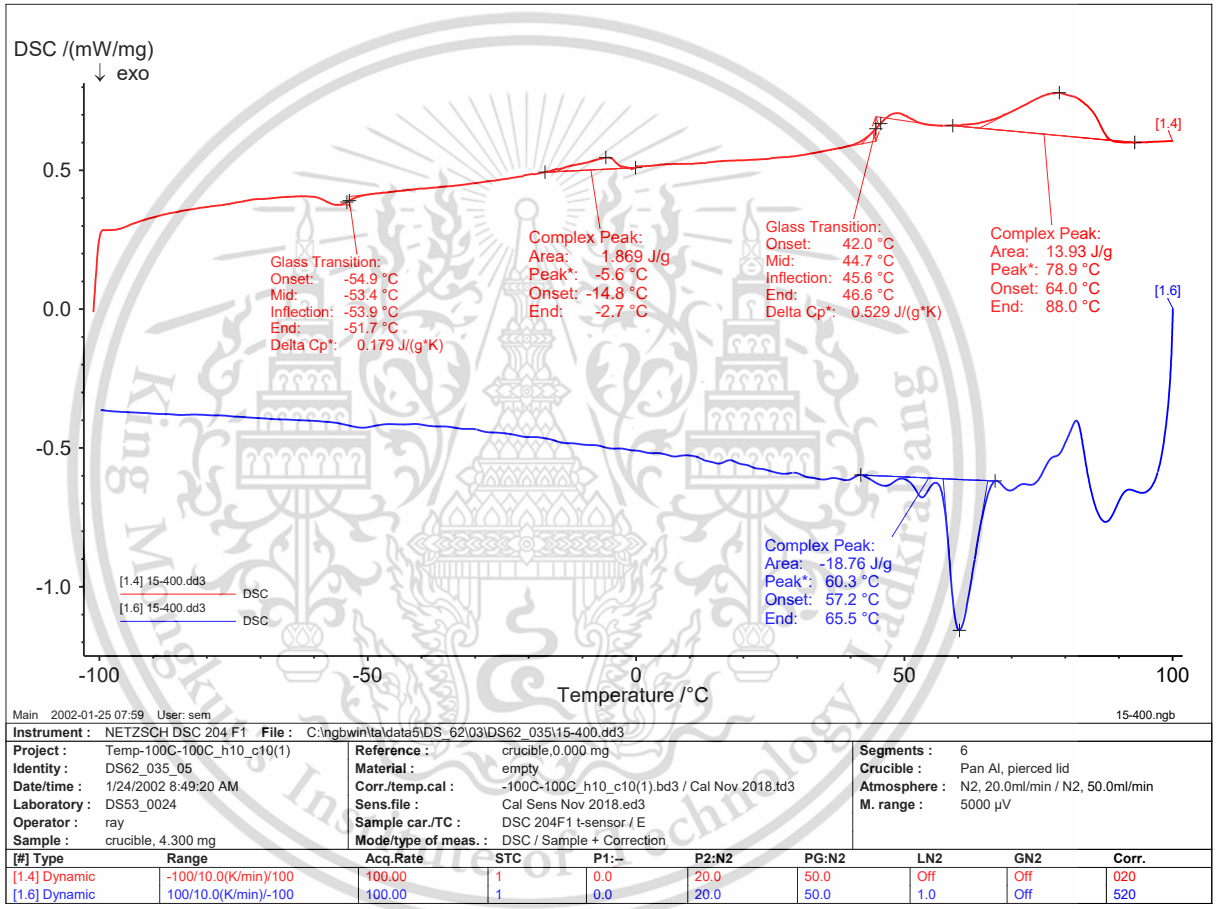

Figure C.6 DSC thermogram of p-EVA/15PEG400 membrane

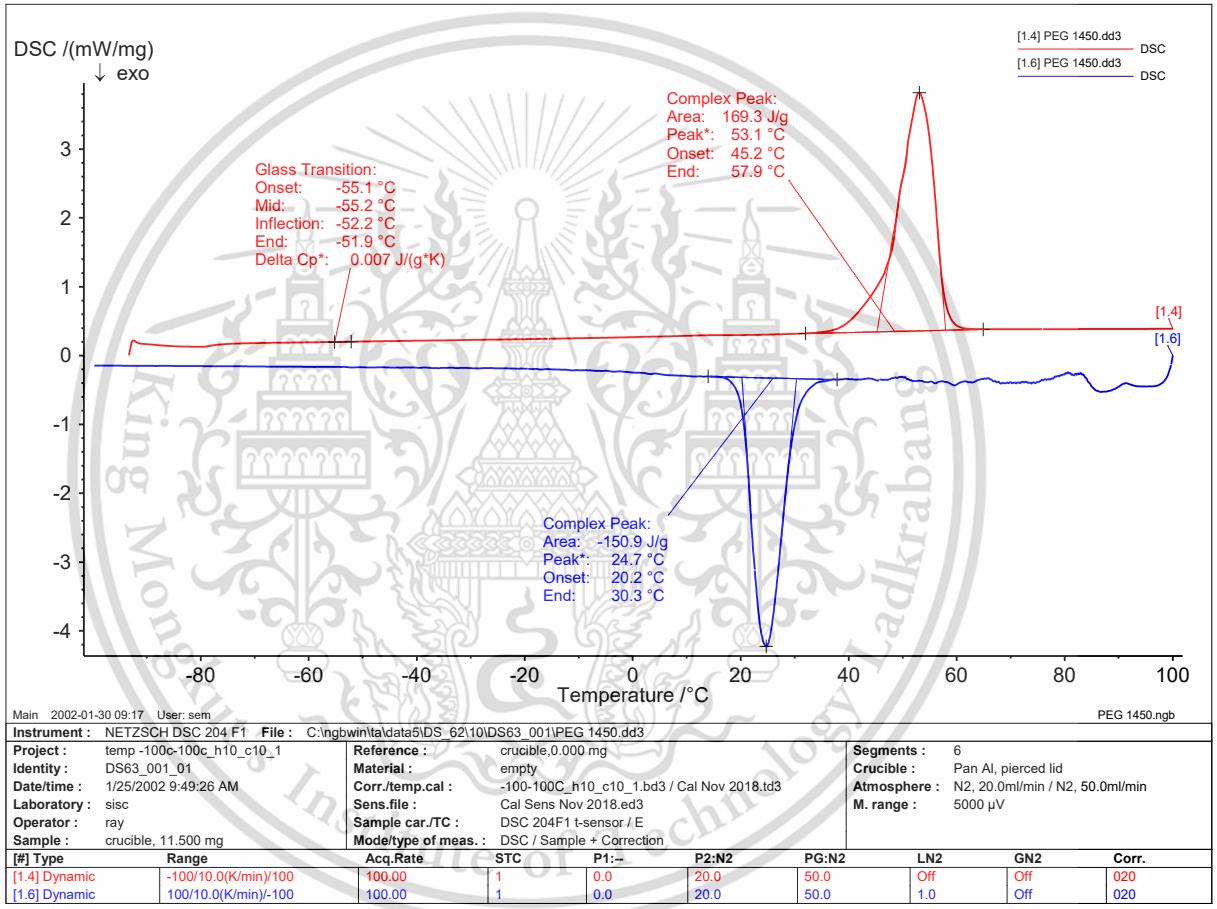

Figure C.7 DSC thermogram of PEG-1450

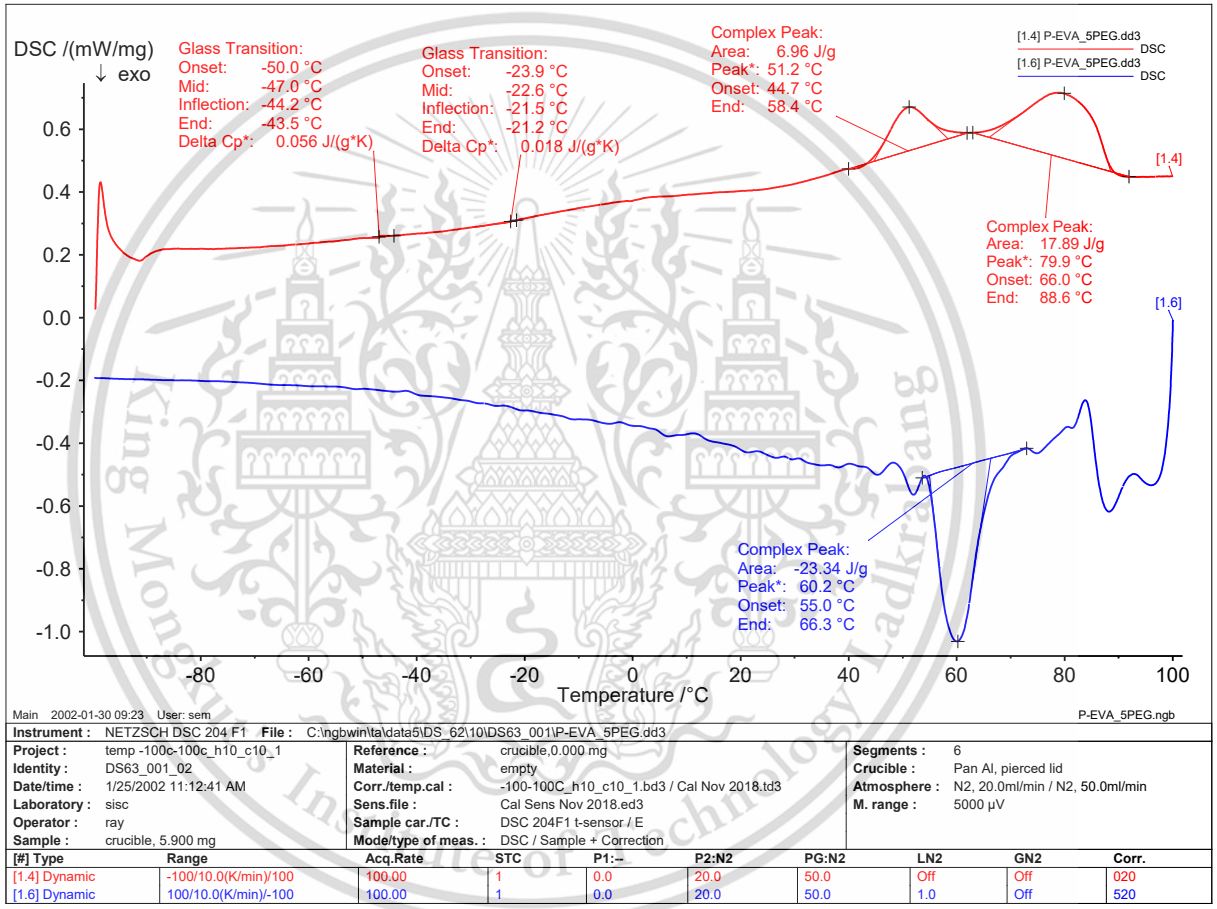

Figure C.8 DSC thermogram of p-EVA/5PEG1450 membrane

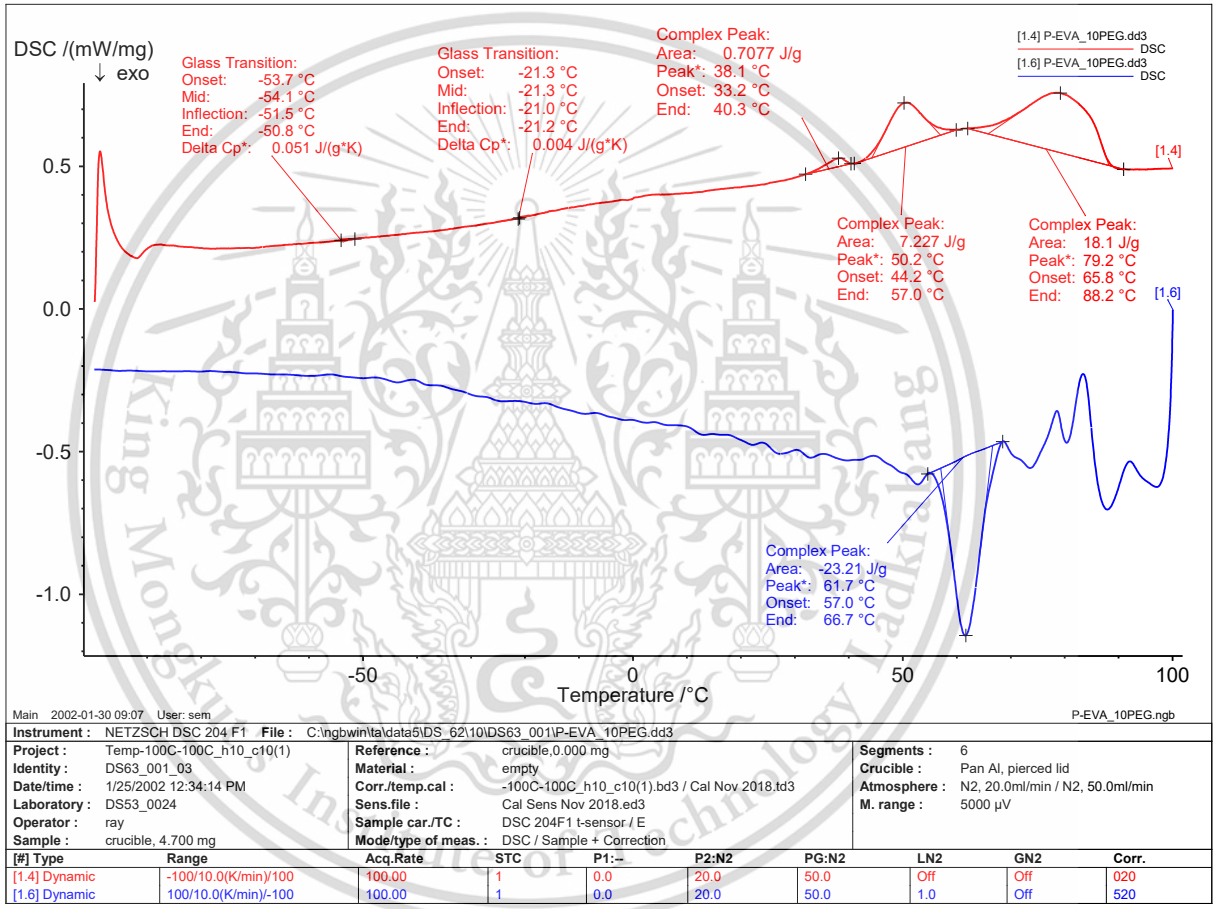

Figure C.9 DSC thermogram of p-EVA/10PEG1450 membrane

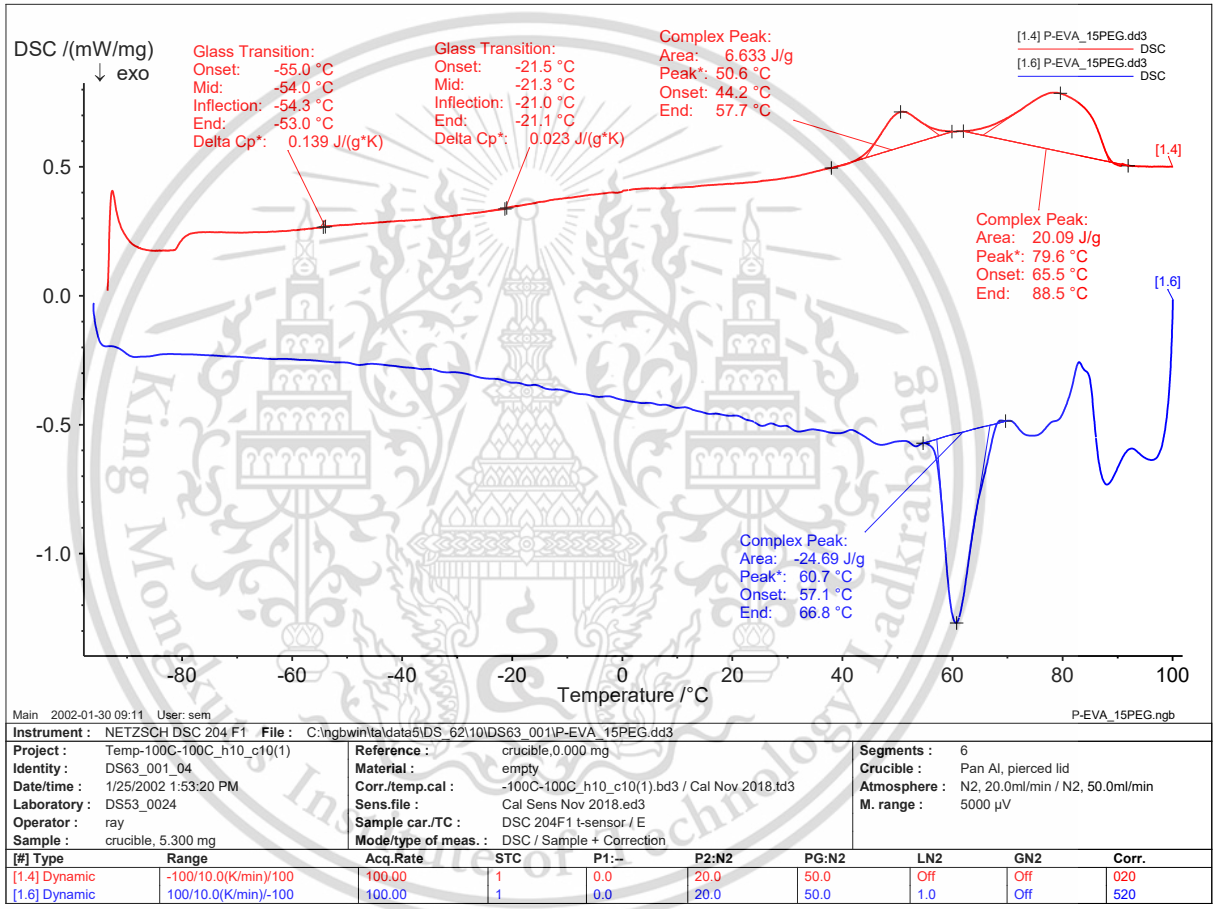

Figure C.10 DSC thermogram of p-EVA/15PEG1450 membrane

Table C.1 The percentage of crystallinity of EVA or p-EVA

Sample	EVA in membrane (%wt)	ΔH_f (J/g)	Crystallinity, X_c (%)
EVA	100	7.40	2.5
p-EVA	100	17.06	5.8
p-EVA/5PEG400	95	17.76	6.4
p-EVA/10PEG400	90	17.43	6.6
p-EVA/15PEG400	85	13.93	5.6
p-EVA/5PEG1450	95	17.89	6.4
p-EVA/10PEG1450	90	18.10	6.8
p-EVA/15PEG1450	85	20.09	6.0

$$\Delta H_f^0 \text{ (J/g)} = 293 \text{ J/g (100\% crystallinity of polyethylene) [56]}$$

$$\%\text{Crystallinity} = \left(\frac{\Delta H_f}{\Delta H_f^0} \times 100 \right) \times \frac{100}{\text{EVA or p-EVA in membrane (\%wt)}}$$

Example: %Crystallinity of p-EVA in p-EVA/5PEG400 membrane

$$= \left(\frac{17.76}{293} \times 100 \right) \times \frac{100}{95}$$

$$= 6.38\%$$

$$\approx 6.4\%$$

Appendix D

SEM

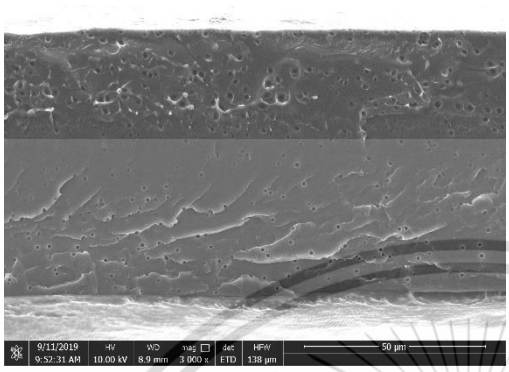

p-EVA/5PEG400 (3000X)

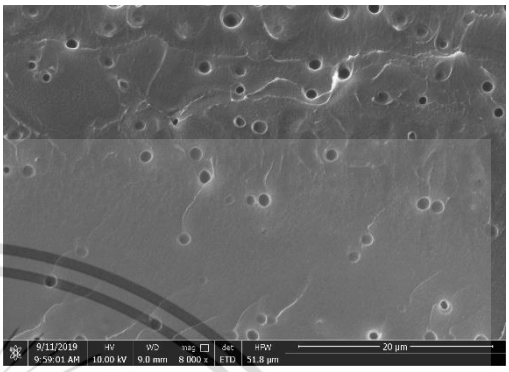

p-EVA/5PEG400 (8000X)

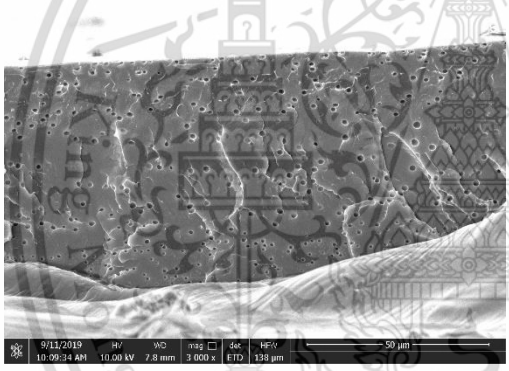

p-EVA/10PEG400 (3000X)

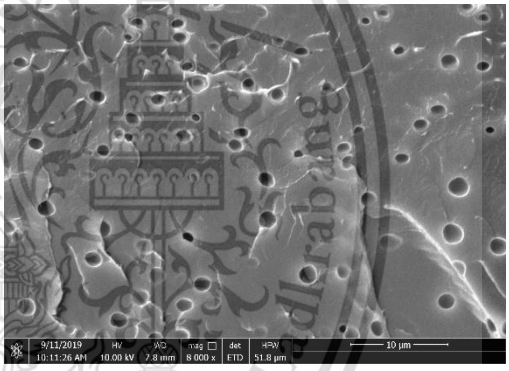

p-EVA/10PEG400 (8000X)

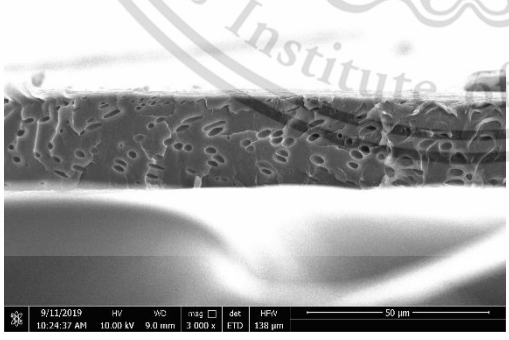

p-EVA/15PEG400 (3000X)

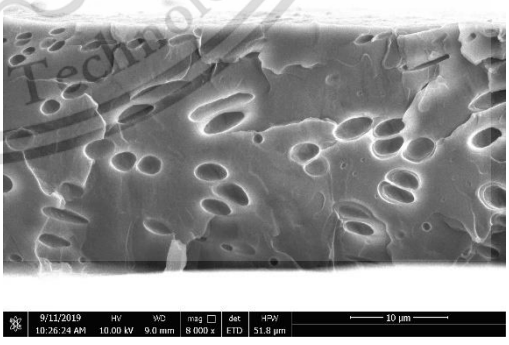

p-EVA/15PEG400 (8000X)

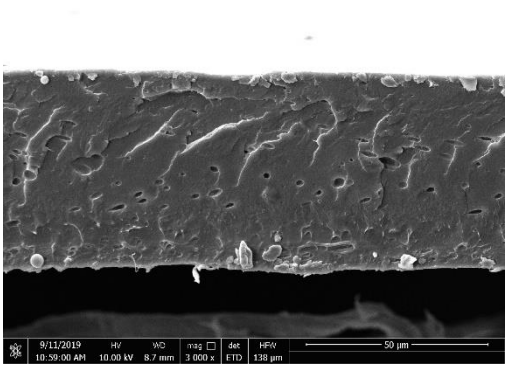

p-EVA/5PEG1450 (3000X)

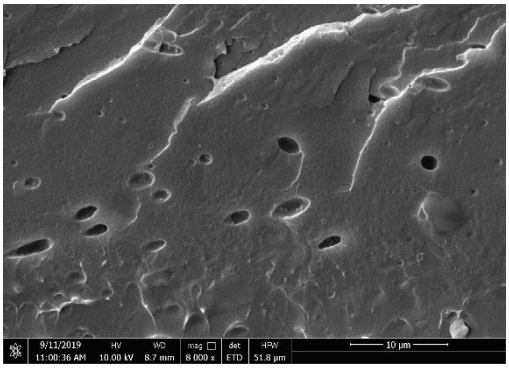

p-EVA/5PEG1450 (8000X)

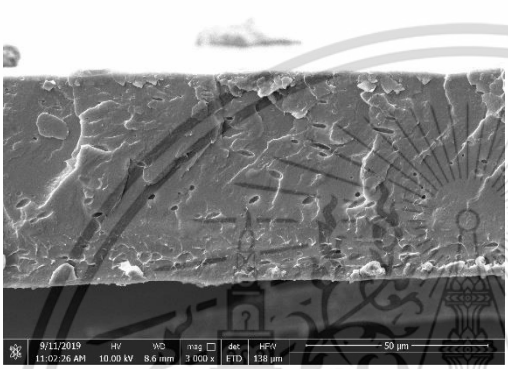

p-EVA/10PEG1450 (3000X)

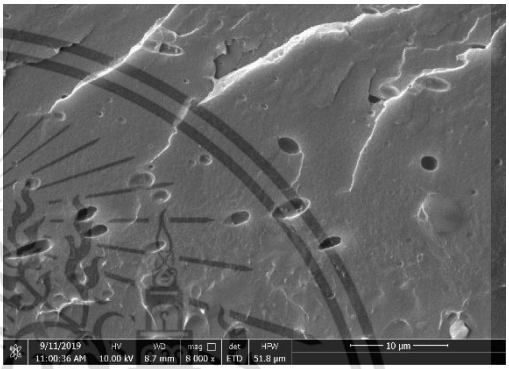

p-EVA/10PEG1450 (8000X)

p-EVA/15PEG1450 (3000X)

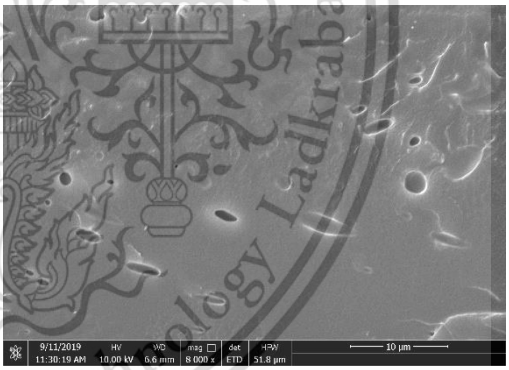

p-EVA/15PEG1450 (8000X)

Figure D.1 SEM micrographs of the p-EVA/PEG blend membranes (3000X and 8000X magnifications)

Appendix E

Tensile properties

Table E.1 Tensile properties of the membranes

Sample	Thickness (μm)	Tensile strength at break (MPa)	Elongation at break (%)	Young's modulus (MPa)
EVA	64.3±5.6	2.7±0.2	1101±61	2.4±0.2
p-EVA	67.1±7.8	10.2±0.8	770±25	17.6±0.9
p-EVA/5PEG400	62.5±2.3	9.1±1.3	820±42	18.6±0.9
p-EVA/10PEG400	61.8±7.8	8.6±0.5	873±44	16.8±0.6
p-EVA/15PEG400	62.2±.8.5	7.7±0.7	901±81	15.0±0.9
p-EVA/5PEG1450	63.8±1.2	8.4±0.9	771±42	18.2±0.6
p-EVA/10PEG1450	62.4±6.7	7.4±0.4	855±86	15.5±0.6
p-EVA/15PEG1450	61.4±5.6	7.0±0.3	781±32	12.5±0.8

Appendix F

X-ray photoelectron spectroscopy

Table F.1 The quantification report of unmodified SiO_2

Peak	Position BE (eV)	FWHM (eV)	Raw Area (cps eV)	RSF	Atomic Mass	Atomic Conc %	Mass Conc %
C 1s	285.4	3.013	10800.0	0.278	12.011	3.23	2.00
N 1s	399.0	0.764	25.0	0.477	14.007	0.00	0.00
O 1s	533.2	2.970	598630.0	0.780	15.999	68.17	56.43
Si 2p	104.0	2.949	122630.0	0.328	28.086	28.60	41.56

Table F.2 The quantification report of amine-functionalized SiO_2

Peak	Position BE (eV)	FWHM (eV)	Raw Area (cps eV)	RSF	Atomic Mass	Atomic Conc %	Mass Conc %
C 1s	284.8	3.513	94690.0	0.278	12.011	30.13	21.05
N 1s	400.4	3.709	17765.0	0.477	14.007	3.39	2.77
O 1s	531.9	2.979	380190.0	0.780	15.999	46.12	42.92
Si 2p	102.6	2.842	81980.0	0.328	28.086	20.36	33.26

Author biography

Name	Miss Patchnakan Wisatsuvan
Date of Birth	2nd January 1995
Address	15 Mitsampan R. Banpuek Dist. Mueng, Chonburi, 20130
Education	(2017) Bachelor of Science in Industrial Chemistry GPA 3.33 King Mongkut's Institute of Technology Ladkrabang
	(2020) Master of Science in Polymer Technology GPA 3.87 King Mongkut's Institute of Technology Ladkrabang
Scholarship	1. Tuition fee scholarship from Faculty of Science, King Mongkut's Institute of Technology Ladkrabang
	2. Scholarship from King Mongkut's Institute of Technology Ladkrabang for poster presentation of International Polymer Conference of Thailand 2019 (PCT-9)
	3. Financial support from Taiwan government for research collaboration (2019-2020 TEEP@AsiaPlus Program) at Department of Chemistry, Tamkang University (TKU)
Academic Publication	Wisatsuvan P., Sooknoi T., Rukchonlatee S., and Ritvirulh C. 2019. "Effect of Polyethylene Glycol on CO_2 Permeation in the Partially Hydrolyzed Ethylene Vinyl Acetate Membrane." *The proceedings of International Polymer Conference of Thailand 2019* (PCT-9), Amari Watergate Bangkok Hotel, June 13-14, Bangkok, Thailand, pp. 163-168.